

**MOHAMMED V UNIVERSITY, UM5**  
**Faculty of Sciences in Rabat, FSR**

Laboratory of High Energy Physics, Modeling & Simulation (LPHE-MS)

## Master Dissertation

Submitted in fulfillment of the requirement of:

### Master's Degree in Mathematical Physics

By

**Rafik ER-RABIT<sup>(1)</sup>**

supervised by: Pr. Mohammed GOUIGHRI

---

Search for a  $Z'$ , a New Heavy Gauge Boson  
Beyond the Standard Model, as a Resonance  
Within a  $t\bar{t}t\bar{t}$  Event in a Fully-Hadronic Decay  
Channel, With the ATLAS Detector

---

Defended on the 23<sup>rd</sup> of November 2020, in front of the jury:

Pr. Driss BENCHEKROUN	PES, Faculty of Sciences Aïn Chock, Casablanca	Chair
Pr. El Hassan SAIDI	PES, Faculty of Sciences, Rabat	Member of the jury
Pr. Mohammed GOUIGHRI	PES, Faculty of Sciences, Kénitra	Thesis supervisor
Pr. Rachid Ahl LAAMARA	PES, Faculty of Sciences, Rabat	Member of the jury
Pr. Yahya TAYALATI	PES, Faculty of Sciences, Rabat	Member of the jury

---

<sup>1</sup> [rafik.errabit@um5r.ac.ma](mailto:rafik.errabit@um5r.ac.ma) | [rafik.errabit@cern.ch](mailto:rafik.errabit@cern.ch)



# Acknowledgments

A wise philosopher said once: "*knowledge is in the end based on acknowledgment*". This humble work would never have been written without the existence of numerous people who have positively impacted me, either professionally or personally, and shaped me as I am today. A few paragraphs would certainly not be enough to mention everyone by his name, but to you all, I am deeply indebted and grateful!

Foremost, I would like to thank my supervisor, Pr. Mohammed Gouighri, for his continuous support, enlightening advices, endless tolerance, and confidence in my abilities throughout the preparation of this master thesis. Pr. M. Gouighri is a model of the exemplary advisor, under his charge I never felt minor, he defended me on my attitudes whenever he felt they were lucid, and in an unoffending way showed me the flaws in my mistaken thoughts. Despite this year's special conditions due to the worldwide Covid-19 pandemic, Pr. M. Gouighri assisted me remotely and constantly, making the entire journey, an appealing experience, and I would be very blessed if we can be together in future work.

This work is realized within the LPHE-MS lab at the Faculty of Sciences in Rabat (FSR), headed by Pr. El Hassan Saidi. Being part of the first high energy physics lab in Morocco is a crown on my head, and I am heavily thankful to each professor that has assisted us in our two years adventure. I would like to express my sincere gratitude to Pr. Rachid Ahl Laamara, who managed our master's class since the entrance examination up to this point. Besides accompanying us in Lie Algebra and Supersymmetry introductory courses, Pr. R. A. Laamara was the one we headed on whenever we came across an issue, we have met him the first time with a businesslike tone, later we discovered how careful he is about our goodness, and for this, I am very grateful. I wish also to thank Dr. Mohammed Amin Loualidi, who assisted us in the Standard Model introductory course, where I prepared, along with other colleagues, multiple talks about topics from his suggestions, topics that helped me a lot while writing the first part of this manuscript.

I owe huge amounts of thanks to the *BSM4 Tops ATLAS analysis team* for all the Friday talks. I sincerely thank Pr. Mark Kruse from DUKE, Dr. Alexandra Nedaa Asbah from Harvard for helping me with running the top-xaod code, and gently adding me to their skype chat group, Dr. Li Xingguo for his aid with the configuration file, and all other members of the analysis team.

I cannot forget to thank my classmates, the students of PM\_2018/2020 class, a.k.a. the greatest PM class of all time, for all the memorable moments, all the laughs, and for those organized trips. While I cannot cite everyone's name here, I find myself obliged to mention El Abbassi Abderrazaq and Belfakir Mohammed who have worked on topics similar to mine, I thank them for all the late at night Zoom meetings. Also, our delegate Erramah Abdellatif, as well as Ribag Khalil and Mouloudi Aziz who have

made my residence on the campus a pleasing one. Finally, I warmly thank those to whom I found myself spiritually connected; Assia, Aziz, Ez-Zaili, Mbark, Nadia, Nouhaila, Soukayna, and Sarra.

I must extend a special thanks to the jury members for accepting to review this document.

To close, I would like to express my deepest recognition to my beloved family, to whom I am eternally indebted. I thank my mother Zahra for all the prayers and coffee cups prepared with love. I thank my father, the real hero who has worked tens of kilometers underground to keep our heads raised above the skies, and who has started working at the age of 16 so that his son today continues his postgraduate studies at the age of 24. My immense thanks to my siblings, Fatima, Jawad, and Zobair for their love and support.

# Abstract

The Standard Model of particle physics is the ultimate cumulation of many theories and experimental results aiming to describe the elementary particles constructing the universe around us at its most fundamental level, and to define the interactions perceived by these tiny building blocks. Despite being one of the greatest achievements in modern physics, the SM, like any other model, has some limitations and shortcomings, for this reason, many approaches beyond the standard model (BSM) attempted to overcome these flaws. All these BSM approaches suggest new particles outside the contents of the SM, and the discovery of these particles is mandatory for their approval. In this Master thesis, we were interested in probing the observation of a new heavy gauge boson outside of the SM framework, as a resonance state within a very rare event predicted by the SM, the four top-quarks  $t\bar{t}t\bar{t}$ , using the ATLAS detector. Such a boson, called  $Z'$ , is predicted by several BSM propositions, namely the Sequential Standard Model (SSM), the Left-Right Symmetric Model (LRM), and the Grand Unified Theories (GUTs).

After introducing the SM, its limitations, and the requirement for BSM representations, we exposed different production and decay modes of the top quark within and beyond the SM. Next, we presented the experimental setup, specifically, the Large Hadron Collider (LHC), its acceleration chain, and the ATLAS detector. The process of translating the electrical signals from the detector to identified objects and reconstructed paths is mentioned for the physic objects used in this work, i.e. electrons, muons, and jets. Finally, we have proceeded with a fully hadronic event selection, using `top-xaod`, the main `AnalysisTop` program.

Accomplishing a full and complete analysis was further on than this manuscript's scope, taking into consideration the limited abilities of a master's student, and the research tight timeframe. However, in addition to the bibliography mentioned above, there were two main tasks addressed throughout this study journey. On the theoretical side, we re-calculated the BRs of the 12 deferent decay channels of a  $t\bar{t}t\bar{t}$  event, and on the analysis side, we adapted the configuration file used as input for the main program in `AnalysisTop`, the `top-xaod`, to suit a fully-hadronic decay channel. The former task revealed results tunning to the ones we received, moreover, the sum of BRs we have calculated was **1.0001**, while it was **0.996** in the given document, and this is due to us considering two digits after decimal instead of just one taken in the same document. As for the latter task, the configuration file was tested for different MC samples; MC16a, MC16d, MC16f, and MC16e, as well as data samples, and it did run with only some warnings but without any errors. However, we only presented in the last section of the last chapter some results from the output file we have obtained using the MC16e sample, and this is because it was the one with the greatest number of entries, so the plots are quite satisfying.

# Table of Contents

<b>Acknowledgements</b>	i
<b>Abstract</b>	iii
<b>Table of Contents</b>	iv
<b>List of Abbreviations</b>	vii
<b>List of Figures</b>	ix
<b>List of Tables</b>	xiv
<b>Chapter 1 To the Standard Model and Beyond</b>	1
1.1 Matter Particles and Force Carriers.....	2
1.1.1 From Atoms to Quarks.....	3
1.1.1.1 The Particle Zoo .....	5
1.1.1.2 Conservation of Quantum Numbers.....	8
1.1.1.3 The Eightfold Way .....	9
1.1.1.4 The Quark Model.....	11
1.1.1.5 The Charge of Color .....	14
1.1.1.6 Charm, Bottom, and Top .....	15
1.1.2 The Forces and their Mediators .....	16
1.1.2.1 Quantum Electrodynamics (QED).....	17
1.1.2.2 Quantum Flavor Dynamics (QFD).....	18
1.1.2.3 Quantum Chromodynamics (QCD) .....	20
1.2 The Standard Model Lagrangian.....	22
1.2.1 Gauge Symmetry Group .....	22
1.2.2 Quarks and Leptons Fields' Labels .....	23
1.2.3 The Famous Lagrangian $\mathcal{L}_{SM}$ .....	24
1.3 Successes and Weaknesses of the Standard Model .....	28
1.3.1 The Higgs Boson Discovery .....	28
1.3.2 No Gravity!.....	29
1.3.3 Masses of Neutrinos .....	29
1.3.4 Matter Anti-matter Asymmetry .....	30

1.3.5	Hierarchy Problem.....	30
1.3.6	Dark Matter and Dark Energy .....	31
1.3.7	So Many Free Parameters .....	31
1.3.8	The Holy Grail of Unification.....	31
1.4	Beyond the Standard Model (BSM).....	32
<b>Chapter 2 Top Quark (New)Physics</b>		<b>34</b>
2.1	Top Quark Production.....	35
2.1.1	Top Quark Pair Cross Section $\sigma_{t\bar{t}}$ .....	35
2.1.2	Production of Four-Top Quarks $t\bar{t}t\bar{t}$ in the SM .....	39
2.1.3	Production of Four-Top Quarks $t\bar{t}t\bar{t}$ BSM.....	40
2.2	Top Quark decay .....	43
2.2.1	Single Top Decay.....	43
2.2.2	$t\bar{t}$ Quark Pair Decay.....	44
2.2.3	$t\bar{t}t\bar{t}$ Four-Top Quarks Decay.....	45
<b>Chapter 3 LHC and the ATLAS Detector</b>		<b>50</b>
3.1	The Large Hadron Collider (LHC).....	51
3.1.1	From Hydrogen Bottle to Interaction Point .....	52
3.1.2	Notion of Luminosity.....	53
3.2	The Giant ATLAS Detector.....	54
3.2.1	ATLAS Coordinate System .....	54
3.2.2	Inner Detector .....	55
3.2.2.1	Pixel and SCT Detectors .....	56
3.2.2.2	Transition Radiation Tracker .....	57
3.2.3	The ATLAS Calorimeters.....	58
3.2.4	The Muon Spectrometer .....	59
3.2.5	Trigger System and Data Acquisition.....	60
<b>Chapter 4 ATLAS Physics Objects: Reconstruction &amp; Identification</b>		<b>62</b>
4.1	Tracking and Vertexing .....	62
4.1.1	Tracking .....	63
4.1.2	Vertexing.....	65
4.2	Electrons .....	66
4.2.1	Electron Reconstruction .....	66
4.2.2	Electron Identification .....	66
4.3	Muons .....	67
4.3.1	Muon Reconstruction in the MS.....	67
4.3.2	Muon Identification .....	68
4.4	Jets.....	69
4.4.1	Jets Reconstruction .....	69
4.4.2	b-jets.....	70
<b>Chapter 5 Search for a Top-Philic Resonance BSM: A First Step</b>		<b>73</b>
5.1	BSM- $t\bar{t}t\bar{t}$ Backgrounds in the SM.....	74

5.2 Top Analysis .....	76
5.2.1 Configuration File Options .....	77
5.2.2 Local Running .....	80
5.2.2.1 MC16e Sample .....	81
5.2.2.2 Results .....	81
<b>Concluding Remarks</b>	<b>86</b>
<b>Bibliography</b>	<b>90</b>

# List of Abbreviations

2HDM	Two Higgs Doublet Model
ATLAS	A Toroidal LHC ApparatuS
AD	Antiproton Decelerator
AMI	ATLAS Metadata Interface
BEH	Brout-Englert-Higgs
BR	Branching Ratio
BSM	Beyond the Standard Model
CB	Combined
CERN	European Organization for Nuclear Research
CKM	Cabibbo-Kobayashi-Maskawa
CLI	Command Line Interface
CM	Center of Momentum
CMS	Compact Muon Solenoid
CP	Charge-Parity / Combined Performance
CSC	Cathode Strip Chambers
CT	Calorimeters-tagged
DE	Dark Energy
DM	Dark Mater
EF	Event Filter
EM	Electromagnetic
EWS	Electroweak Symmetry
EWSB	Electroweak Symmetry Breaking
FCNC	Flavor-Changing Neutral Currents
GIM	Glashow Iliopoulos Maiani
GRL	Good Run List
GUT	Grand Unified Theory
GWS	Glashow Weinberg Salam
h.c.	hermitian conjugate
HLT	High-Level Trigger
IBL	Insertable B-Layer
ICHEP	International Conference on High Energy Physics
ID	Inner Detector
IP	Interaction Point
ISS	International Space Station
JVF	Jet Vertex Fraction

L1	Level 1
LAr	Liquid Argon
LEP	Large Electron-Positron collider
LH	Likelihood
LHC	Large Hadron Collider
LHCP	Large Hadron Collider Physics
LINAC	Linear Accelerator
LO	Leading Order
LRM	Left-Right Symmetric Model
lxplus	LinuX Public Login User Service
MC	Monte Carlo
MDT	Monitored Drift Tubes
ME	Extrapolated muons
MS	Muon Spectrometer
NLO	Next to Leading Order
NNLO	Next to Next to Leading Order
NP	New Physics
OS	Opposite Sign
PDF	Parton Distribution Function
pp	Proton-Proton
PS	Proton Synchrotron
PSB	Proton Synchrotron Booster
PV	Primary Vertex
QCD	Quantum Chromodynamics
QED	Quantum Electrodynamics
QFD	Quantum Flavor Dynamics
QFT	Quantum Field Theory
QGP	Quark-Gluon Plasma
RCJ	Re-clustered Jet
RF	radiofrequency
RPC	Resistive Plate Chambers
SCT	Semiconductor Tracker
SLAC	Stanford Linear Accelerator Center
SM	Standard Model
SPS	Super Proton Synchrotron
SS	Same Sign
SSM	Sequential Standard Model
ST	Segment-tagged
TGC	Thin Gap Chambers
ToF	Theory of Everything
TRT	Transition Radiation Tracker
WP	Working Point

# List of Figures

<b>Figure 1-1:</b> The elementary particles of the SM. At the first glance, it might seem like if there are only 30 elementary particles in the SM, while (as we shall see later) this table presents more than a hundred! (retrieved from Wikimedia, credit to Cush, copyright-free).	2
<b>Figure 1-2:</b> A representation of the cathode ray tube used by J.J. Thomson to discover the electron. The cathode-anode cellule is subject to a high voltage, to extract electrons from the cathode and direct them to the end of the tube through the anode. The beam of electrons, shown in yellow, is reflected using charged plates and magnets, and the amount of deflection is related to the mass of the electrons and their charge. (Credit to “Kurzon”)	4
<b>Figure 1-3:</b> The Plum-Pudding model of the Atom	4
<b>Figure 1-4:</b> The Eightfold Way supermultiplets. (a) the baryons octet, (b) the mesons octet. In both figures, hadrons in same line have the same strangeness, while those lying along the same diagonal hold the same electric charge.	9
<b>Figure 1-5:</b> The vector mesons nonet	10
<b>Figure 1-6:</b> Baryon decuplet. As always, baryons of the same line have the same hypercharge (and the same strangeness since they are all baryons) and baryons of the same electric charge happen to be in the same diagonal. The four levels (lines) are separated with the same amount of energy.	10
<b>Figure 1-7:</b> representations of quarks (a) and antiquarks (b) Eightfold Way style	11
<b>Figure 1-8:</b> the primary vertex of the QED. The straight lines with an arrow pointing towards the direction of time is an electrically charged particle, while curvy line represents the photon. This diagram can be read as: a particle emits or absorbs a photon	17
<b>Figure 1-9:</b> The annihilation process of a particle and its antiparticle. The line between the two vertices is a virtual particle (off mass-shell). As we can see, this diagram is nothing but a combination of the 5 <sup>th</sup> and 2 <sup>nd</sup> diagrams in <a href="#">Table 1-9</a> .	18
<b>Figure 1-10:</b> the direct coupling of $W^\pm$ and $Z^0$	19
<b>Figure 1-11:</b> Cartoon of the jet formation process. This representation shows four stages, the p-p collision gives rise to an energetic quark, the fragmentation of the quark making a parton shower, the hadronization of partons into two jets, and finally the detection of the final state particles (Credit to Eric M. Metodiev ©).	21

<b>Figure 1-12:</b> plots of the BEH potential in function of $\phi^2$ in both cases, before and after the EWSB. In (a) $\mu^2 > 0$ and the EW symmetry is intact since the $v \neq 0$ . In (b), $\mu^2 < 0$ , the $v \neq 0$ and chosen to be $+v$ breaking the EW symmetry. ....	28
<b>Figure 1-13:</b> The discovery of the Higgs boson by the ATLAS detector at an energy of 126.5 GeV, decayed into two energetic photons. (Credit to ATLAS collaboration/CERN) .....	29
<b>Figure 1-14:</b> the contribution of the Top-quark loop to the effective Higgs mass.....	30
<b>Figure 1-15:</b> the evolution of the inverse of coupling constants of the three fundamental forces described by the SM in function of the energy levels. The couplings do not all meet at high energies. (credit to Victor Blacus) .....	32
<b>Figure 2-1:</b> Feynman Diagrams of the Leading-Order (LO) production mechanisms of the $t\bar{t}$ pairs. The given proportions are for pp collisions with an energy of $\sqrt{s} = 14 \text{ TeV}$ . .....	35
<b>Figure 2-2:</b> Theoretical spectrum of $t\bar{t}$ pair mass in different frameworks. The “QCD only” plot refers to the SM predictions. At a mass of 2 TeV, models with additional colorless gauge boson $Z'$ present a bump. So, if data shows such a bump it would be evidence for a new particle discovery. figure taken from [82, p. 18] .....	36
<b>Figure 2-3:</b> theoretical predictions for $t\bar{t}$ pair production with different NNLO approximations. Predictions are done for pp collisions at $\sqrt{s} = 7 \text{ TeV}$ . Figure taken from [81, p. 17].....	38
<b>Figure 2-4:</b> Measurements and predictions of $\sigma_{t\bar{t}}$ in function of $\sqrt{s}$ for $m_{top} = 172.5 \text{ GeV}$ . CDF and DØ measurements are taken from [90], [91] for $\sqrt{s} = 1.8 \text{ TeV}$ and from [92]–[94] for $\sqrt{s} = 1.96 \text{ TeV}$ , ATLAS and CMS data points are taken from [95]–[98], while those of LHCb are extracted from [99]. Finally, the theoretical predictions are based on [100]. Figure taken from [101, p. 743] .....	38
<b>Figure 2-5:</b> Examples of tree-level diagrams of $gg \rightarrow t\bar{t}t\bar{t}$ in the SM. [103, p. 7].....	39
<b>Figure 2-6:</b> Examples of one-loop diagrams of $gg \rightarrow t\bar{t}t\bar{t}$ in the SM. [103, p. 7].....	39
<b>Figure 2-7:</b> Event display of a candidate four-top-quark event in a semi-leptonic final state, where two of the top quarks decay leptonically (giving birth to a muon in red and one electron in green), while two others decay hadronically. This is the heaviest particle final state ever seen at the LHC, with almost 700 GeV in total. (Credit to <i>ATLAS Experiment</i> © CERN) .....	40
<b>Figure 2-8:</b> A four-top quark production process beyond the SM. The $V_1$ is a color singlet (so that the color charge is conserved at the two vertices) vector boson BSM. .....	41
<b>Figure 2-9:</b> (a) The transverse momentum spectra of the four-top quarks for a resonance mass of 1.5 TeV and coupling constant $c_t = 2.0$ . We notice that the first hardest top has a peak at almost $M_{V_1}/2$ , the second hardest top peaks at a little lower value, and while the first spectator top peaks at a value	

slightly higher than the  $m_t \approx 173 \text{ GeV}$  the other spectator has a peak at a value slightly lower than  $m_t$ .  
(b) The pseudo-rapidity presents a symmetry as supposed. Figures taken from [109, p. 3] .....42

**Figure 2-10:** Pie chart displaying the BRs of a single top quark decay processes. .....44

**Figure 2-11:** Pie chart showing the different decay channels of a  $t\bar{t}$  pair, as well as their BRs. .....45

**Figure 2-12:** illustration of three examples of the decay channels of a  $t\bar{t}t\bar{t}$  four-top quarks. (a) all hadronic channel. (b) semi-leptonic channel. (c) same-sign-dilepton channel.....46

**Figure 2-13:** Pie chart of the different decay channels of  $t\bar{t}t\bar{t}$  along with their branching ratios. We notice that the single lepton channel has the largest BR, but in fact, if we take the decay of  $\tau$  in considerations, the full hadronic channel will take the lead. .....49

**Figure 3-1:** Sketch of the CERN Accelerator Complex. In the next run, Hydrogen anions will be accelerated to 160 MeV by the linear accelerator 4 (LINAC 4), replacing the LINAC 2 after the current Long Shutdown (LS) 2019/2020, and then after extracting the two electrons, the protons are injected into the LHC injection chain, following this path: BOOSTER  $\leftrightarrow$  PS  $\leftrightarrow$  SPS  $\leftrightarrow$  LHC, before they collide at the heart of ATLAS. (credit to CERN).....51

**Figure 3-2:** The main LHC dipole bending magnet. (a) A two-dimensional cut showing the main parts of an LHC dipole, the protons are accelerated inside the Beam Pipes. (b) Map of the magnetic flux bending the proton beams inside the pipes. (Credit to CERN).....52

**Figure 3-3:** General cut-away view of the ATLAS detector, indicating its dimensions as well as its multiple subdetectors. (Credit to *ATLAS Experiment* © CERN) .....54

**Figure 3-4:** Representation of the Cartesian and the cylindrical coordinate systems. The half side of ATLAS where  $z > 0$  is called ‘A’ side, while the other half is referred to as the ‘C’ side. Figure taken from [130, p. 72] .....55

**Figure 3-5:** cut-away view of the Inner Detector. The dimensions of the detector in addition to its subdetectors either barrel or end-cap modules are shown. (Credit to *ATLAS Experiment* © CERN) ..56

**Figure 3-6:** A perspective cut-away view of the pixel detector laying at the heart of the ID. The four layers of barrel modules and the three disks of one end-cap are shown. (Credit to *ATLAS Experiment* © CERN) .....56

**Figure 3-7:** visualization of a particle detection using a straw tube (Credit to LHCb at CERN) .....57

**Figure 3-8:** a sketch of the barrel section of the ID. The three subdetectors are shown, with  $r$  reflecting the distance of each layer from the beam-pipe. The orientation of the TRT straws is well presented. The figure is taken from [131] .....58

**Figure 3-9:** A skeleton of ATLAS calorimeters. The LAr calorimeter consists of a barrel, forward calorimeter (FCal), EM, and hadronic end caps. The tile calorimeter has a central barrel weighing 20,000

kg and two extended others, each weighs 9,600 kg. The ID is shown covered by the calorimeters. (Credit to *ATLAS Experiment* © CERN) ..... 59

**Figure 3-10:** the magnetic system of the ATLAS detector. The figure is taken from [132] ..... 59

**Figure 3-11:** A perspective cut-away view of the Muon Spectrometer chambers. Both Barrel and end-cap toroid magnets are shown. The MS makes the major part of ATLAS and the MDT forward wheels are placed at the extreme end of the UX15 cavern. (Credit to *ATLAS Experiment* © CERN) ..... 60

**Figure 4-1:** Sketch illustrating the five parameters characterizing a track.  $d_0$  and  $z_0$  are defined with respect to the primary vertex, which is (0,0,0) in this case.  $\phi$  et  $\theta$  are respectively the azimuthal and polar angles of the track at the point defined by  $d_0$  and  $z_0$ .  $q/p$  is deduced from the curvature of the track, while the side to which it is bent reflects the sign of the electrical charge. [61, p. 71], [80, p. 60] ..... 63

**Figure 4-2:** Collision event at 7 TeV with 2 pile up vertices. The event display at the top right corner shows the curvature of tracks in the xy-plane [139]. ..... 65

**Figure 4-3:** Sketch illustrating the reconstruction of an electron trajectory. From its creation to its absorption, the electron (red line) has 12 silicon hits, 1 with IBL, 3 with the 3 pixel-layers, and 8 with the SCT (2 with each side of the four layers), and 73 hits with the 73 layers of the TRT. The electron ends up depositing the totality of its energy along the four layers of the EM calorimeter. ..... 66

**Figure 4-4:** the reconstruction efficiency of muons as a function of the pseudo-rapidity  $\eta$  for a Medium selection as well as the loose one for  $\eta < 0.1$ , measured lying on  $Z \rightarrow \mu\mu$  event. We see from this results that Muons are reconstructed in ATLAS with an efficiency of nearly 100%. Figure taken from [142, p. 13]. ..... 68

**Figure 4-5:** Illustration of the results of the anti- $k_T$  algorithm for  $R = 1$ . The colored circles in the ( $y - \phi$ ) plane are related to the R parameter. Figure taken from [148, p. 4] ..... 70

**Figure 4-6:** cartoon displaying the decay of a b quark to b-hadrons forming a secondary vertex (SV). The distance from the PV to the SV is the decay length (in the range of few millimeters). The dashed lines between the PV and SV represent the transverse and longitudinal components of the momentum vector (c.f. eq. (4-1)), and they determine the Track Impact Parameter used to distinguish different flavor-jets. Figure taken from [149, p. 2]. ..... 71

**Figure 4-7:** Sketch showing interactions of different particles with the barrel section of the detector, the cut is taken in the  $r - \phi$  plane. In the ID, we can see that negatively charged particles  $\mu^-$  and  $e^-$  are bent to the right with different angles (so they have different momenta), the positively charged proton is deviated to the left, while the electrically neutral particles are not affected by the central solenoid magnet, hence cannot be tracked by the ID. The electron and photon are absorbed within the EMC while the hadrons ( $p^+$  and  $n^0$ ) are not stopped until the Hadronic Calorimeter, giving birth to a spectacular showering. The muon and the neutrino are the only particles capable to reach the outermost subdetector, the MS, with the former can be tracked while the latter is completely invisible to ATLAS. (Credit to *ATLAS Experiment* © CERN) ..... 72

**Figure 5-1:** fully-hadronic decay products of the  $t\bar{t}t\bar{t}$ . Represented in, four b-jets (pink circles) two from the spectator tops, and two others from the hardest tops within the two re-cluster jets (RCJs, blue rectangles), and four jets outside of the RC (called additional jets, yellow hexagons). ..... 74

**Figure 5-2:** the reconstructed mass of the  $Z'$  prime resonance from those of the hardest top jets. As we can notice, the backgrounds are significantly huge. The reconstructed resonance peaks at 1.5 TeV. Figure from [109] ..... 75

**Figure 5-3:** The cutflow of our `BSM_alljets_DL1_RCJ` selection. Veto cuts did not reduce the size of the sample, i.e. all the events pass the veto cuts, trigger decision cut takes away most of the events, only 11331 events did survive this cut, 6200 events did not respect the requirements of the b-tagging cuts, so they were rejected and only 5131 events are remaining, the three RCJ cuts leave us with 3982 events, and after excluding four events presenting electrons or muons, the final number of events passing our selection is 3978 events ..... 82

**Figure 5-4:** The pseudo-rapidity of jets after applying different cuts.  $L_i$  refers to different levels of our `BSM_alljets_DL1_RCJ` selection (c.f. Sect. 5.2.1). We notice that  $\eta$  has a normal distribution (as it should be) with  $|\eta_{jet}| < 2.5$ , and the only difference between the different cut levels is the number of entries getting smaller and smaller for each cut added. ..... 82

**Figure 5-5:** Jets' parameters of interest for different cuts. (Top) the azimuthal angle  $\phi$ , (down right) the transvers momenta  $p_T$ , (down left) the masses  $M_{jet}$  that shows hundreds of energetic jets with masses in the range of TeV. The two latter are plotted on a logarithmic scale. ..... 83

**Figure 5-6:** Parameters of interest for RCJs. (Top)  $\eta_{RCJ}$ , it keeps the previous shape, except that it peaks with 800 RC jets instead of 4000 jets, which gives an insight about how few RCJs are. (Down Left)  $p_T^{RCJ}$ , we notice that after applying the RCJ cuts, the histograms peak at a  $p_T^{RCJ} > 500 \text{ GeV}$ . (Down Right) range of the RCJs masses, after applying all cuts in our selection, the  $n_{RCJ}$  peaks at  $0.5 \text{ TeV} < M_{RCJ} < 1 \text{ TeV}$ , which makes the mass of a  $Z'$  candidate in the range of [1 TeV, 2 TeV].] ..... 84

**Figure 5-7:** Transverse momenta of truth tops. This histogram is similar to the previous one ( $p_T^{RCJ}$ ), where after all cuts are applied, the histogram peaks a bit above 500 GeV with almost 600 jets, which confirms that RCJ cuts are distinguishing the top-tagged jets from other flavor-tagged jets. ..... 85

**Figure 5-8:** Truth top-quarks masses. After all cuts are applied, the  $M_T$  peaks at a value around 0.75 TeV, so if two of such massive tops were originated from the same vertex, it might suggest a 1.5 TeV  $Z'$  resonance ..... 85

# List of Tables

<b>Table 1-1:</b> Properties of mesons of spin-zero, called <i>pseudo-scalar mesons</i> .....	6
<b>Table 1-2:</b> Properties of baryons of spin 1/2, called <i>low-mass baryons</i> .....	7
<b>Table 1-3:</b> Properties of baryons of spin 3/2, called <i>baryon resonances</i> .....	7
<b>Table 1-4:</b> Properties of mesons of spin 1, called <i>vector mesons</i> . ....	8
<b>Table 1-5:</b> properties of the flavors of quarks.....	11
<b>Table 1-6:</b> the ten possible combinations of three quarks. The 2 <sup>nd</sup> and 3 <sup>rd</sup> columns are filled taking into consideration that Q and S are additional quantum numbers. The corresponding baryons are deduced from <a href="#">Table 1-3</a> and <a href="#">Table 1-2</a> , judging from their strangeness and electric charge. ....	12
<b>Table 1-7:</b> the nine possible combinations of a quark and an antiquark. The corresponding mesons are deduced from <a href="#">Table 1-1</a> and <a href="#">Table 1-4</a> , judging from their strangeness and electric charge. Except that the combinations <i>uu</i> , <i>dd</i> and <i>ss</i> are identical and there is no way to differentiate between the three of them, hence, $\pi^0$ , $\eta^0$ and $\eta'^0$ are different superpositions of the three states, and the same goes for $\omega^0$ , $\phi^0$ and $\rho'^0$ .....	13
<b>Table 1-8:</b> the four fundamental interactions and their properties.....	16
<b>Table 1-9:</b> primitive vertices of the QED. The green arrow indicates the direction of time, straight lines with an arrow pointing towards the direction of time are electrically charged particles, while those with an arrow directing at the opposite direction of time are antiparticles .....	17
<b>Table 1-10:</b> Neutral vector and axial-vector couplings in the GWS model. [19] .....	20
<b>Table 1-11:</b> the particle content of the Standard Model. ....	22
<b>Table 1-12:</b> the contents of the SM fields, and their transformation under the three gauge symmetry groups.....	24
<b>Table 5-1:</b> simulated cross sections for different backgrounds. Values taken from [109, p. 8] .....	75
<b>Table 5-2:</b> Basic and Ditop selections for the fully hadronic channel. $N_{fj}$ and $P_T^{fj}$ are respectively the number and transvers momentum of “fat jets”, which are jet with a radius parameter of 0.7 and they can be any flavor-tagged. $N_t$ is the number of top-tagged jets.....	75

# Chapter 1

## To the Standard Model and Beyond

*If we want to claim an understanding of the physical world that we see, we need at least three kinds of knowledge; the particles everything is made of, the interactions (forces) that form our world from these particles, and the rules for calculating the resulting world.*

— Gordon Kane, *Modern Elementary Particle Physics*.

*Essentially, all models are wrong, but some are useful.*

— George E.P. Box

The standard model of particle physics (SM) is the ultimate cumulation of many previous theories and efforts to describe on one hand the elementary particles at the most fundamental level, and on the other hand, the interactions perceived by these building bricks of the Universe.

The SM is indeed one of the most successful achievements of humankind, and a giant leap in the eternal pursuit of understanding the nature of the cosmos. However, as any other model, the SM suffers from some limitations and open questions that we cannot explain in its framework, namely the existence of Dark Matter (DM) and Dark Energy (DE), the massive neutrinos, the flavors issue, the hierarchy problem, the gravity that is not included in addition to the so many free parameters introduced by hand in the model.

In this chapter, we are going to follow the first quote above and chronologically introduce the SM, in order to understand how did we arrive at the current picture of the elementary particles and forces governing their behaviors. Then, we will expose the famous Lagrangian of the SM, explaining the aim of each term (sector) before sealing this chapter with the limitations and the shortcomings of the SM and the requirement of models Beyond the Standard Model (BSM).

## 1.1 Matter Particles and Force Carriers

In the frame of the SM, the building blocks of the Universe can be classified into two major types, *fermions*, which are  $spin \sim \frac{1}{2}$  particles that form matter, and *bosons*, which have an integer spin value, like the vector gauge bosons responsible for carrying forces between particles, and the famous scalar Higgs boson that is an excitation of the Higgs field to blame for breaking the electroweak symmetry (EWS) and slowing down some particles gaining them some mass.[1], [2]

in the light of their sensitivity to different forces, which are to the best of our knowledge four fundamental forces, fermions can be divided into six *quarks* and six *leptons*. While quarks are sensitive to all the three forces (strong, weak, and electromagnetic) leptons do not perceive the strong interaction (hence we say that they do not carry color charge), and the three of them that are not affected by the electromagnetic interaction are three generations of the *neutrinos*, while the remaining three are the three generations of the electrically charged particle, the *electron*.[3]

In a point-like-particles world, the contents of the SM can be summarized in the following well-known *periodic table*:

three generations of matter (elementary fermions)			three generations of antimatter (elementary antifermions)			interactions / force carriers (elementary bosons)		
	I	II	III	I	II	III		
QUARKS	mass $\approx 2.2 \text{ MeV}/c^2$ $\frac{2}{3}$ charge $\frac{1}{3}$ spin $\frac{1}{2}$	<b>u</b> up	<b>c</b> charm	<b>t</b> top	<b>ū</b> antiup	<b>cc̄</b> anticharm	<b>tt̄</b> antitop	0 0 1
	$\approx 4.7 \text{ MeV}/c^2$ $-\frac{1}{3}$ $\frac{1}{2}$	<b>d</b> down	<b>s</b> strange	<b>b</b> bottom	<b>đ</b> antidown	<b>đđ̄</b> antistrange	<b>đđ̄</b> antibottom	<b>g</b> gluon
	$\approx 0.511 \text{ MeV}/c^2$ $-1$ $\frac{1}{2}$	<b>e</b> electron	<b>μ</b> muon	<b>τ</b> tau	<b>e<sup>+</sup></b> positron	<b>μ̄</b> antimuon	<b>τ̄</b> antitau	$\approx 124.97 \text{ GeV}/c^2$ 0 0 0
	$<2.2 \text{ eV}/c^2$ 0 $\frac{1}{2}$	<b>ν<sub>e</sub></b> electron neutrino	<b>ν<sub>μ</sub></b> muon neutrino	<b>ν<sub>τ</sub></b> tau neutrino	<b>ν̄<sub>e</sub></b> electron antineutrino	<b>ν̄<sub>μ</sub></b> muon antineutrino	<b>ν̄<sub>τ</sub></b> tau antineutrino	<b>H</b> higgs
	$\approx 105.66 \text{ MeV}/c^2$ $-1$ $\frac{1}{2}$							<b>γ</b> photon
	$\approx 1.7768 \text{ GeV}/c^2$ $-1$ $\frac{1}{2}$							<b>Z<sup>0</sup> boson</b> GAUGE BOSONS VECTOR BOSONS
	$\approx 0.511 \text{ MeV}/c^2$ $1$ $\frac{1}{2}$							<b>W<sup>+</sup> boson</b> W <sup>-</sup> boson
	$\approx 105.66 \text{ MeV}/c^2$ $1$ $\frac{1}{2}$							
	$\approx 1.7768 \text{ GeV}/c^2$ $1$ $\frac{1}{2}$							

*Figure 1-1: The elementary particles of the SM. At the first glance, it might seem like if there are only 30 elementary particles in the SM, while (as we shall see later) this table presents more than a hundred! (retrieved from Wikimedia, credit to Cush, copyright-free).*

The questions that spring immediately to mind are, how did we get this specific picture of the Universe? Were these particles required by theories or theorized after their experimental discoveries? What secret (if any) lies behind the existence of three, or only three, generations of matter and antimatter?

As we shall see next, some of these particles were first discovered experimentally either in intention or by accident, others were required by theory to explain some phenomena, while some were introduced based on philosophical thoughts or even personal believes. However, the whole collection has been observed and their existence is experimentally confirmed by the discovery of the last piece of the puzzle, the Higgs boson, on 4 July 2012. [4]

### 1.1.1 From Atomos to Quarks

The atomic theory assuming that everything is made of little, microscopic, and indivisible objects, is initiated in the 5<sup>th</sup> century B.C, by the Greek philosopher *Leucippus* along with his student *Democritus*, and they called them *atoms* from the Greek word *atomos* that means *indivisible* [5]. However, the modern concept of the atom is believed to start with the English chemist *John Dalton* [6], who was the first to suggest different symbols for atoms constituting different elements, and in 1805, he was able to determine the atomic weight of 21 different elements. [7]

In 1865, another English chemist, named *John A.R. Newlands*, noticed a periodic pattern laying behind the physical and chemical characteristics of elements. Arranging elements according to their atomic weights, he observed that after a period of seven elements we find one with similar properties, and this is what he called the *Law of Octaves*. [8]

Four years later, the Russian chemist *Dimitri Mendeleev* used the Law of octaves to organize all the known elements at the time, in a periodic table according to their atomic weight, where elements in the same columns are found to have similar properties. Nonetheless, Mendeleev's table was not complete, and it had some gaps interpreted as yet to be discovered elements, that he called eka-aluminum, eka-boron, and eka-silicon, and from their positions in the table, he could predict their atomic weights and their chemical properties. It took 15 years to discover all the three predicted elements that were named gallium, scandium, and germanium, which proved the validity of the periodic table.[9] However, the reasons behind the Law of octaves remained a secret, because, at the time, the atoms were considered elementary and indivisible particles, a standpoint that will be questioned by the discovery of radioactivity later.<sup>2</sup>

In 1896, the French physicist *Henri Becquerel* discovered, by accident, the spontaneous radioactivity of uranium. Becquerel realized that the uranium salts were able to emit some radiations without being exposed to sunlight (so it can be neither fluorescence nor phosphorescence), these radiations are electrically charged, since they can be bent by an electric or magnetic field [10, p. 12]. Shortly, *Ernest Rutherford* classified the new radiations into three types, *alpha*, *beta*, and *gamma* [11]. The name radioactivity was coined by *Marie Curie* who, along with her husband *Pierre Curie*, was able to calculate the intensity of radioactivity and shared the 1903 Nobel Prize with Becquerel for their contributions to radioactivity [12]. By this discovery, the indivisibility of atoms started to fall under suspicion, and it was only a matter of time before a subatomic particle will be discovered.

A year later, in 1897, *J.J. Thomson* discovered the first subatomic particle. A negatively charged *corpuscle*, 2000 times lighter than an atom of hydrogen, the *electron*<sup>3</sup>. Thomson used the cathode ray tubes ([Figure 1-2](#)) to prove the existence of a tiny charged particle, along with some magnets to deduce the electron's mass judging from its deviation by the magnetic field.[13]

---

<sup>2</sup> I might be the first high energy physics student to introduce chemists in his manuscript, but the reason behind this will come clear later with the *Eightfold Way* and the quark model.

<sup>3</sup> The term “*electron*” actually proposed earlier by *G.J. Stoney* as the particle making electricity, Thomson called his particles the *corpuscles* before realizing that his corpuscle is actually the electron.

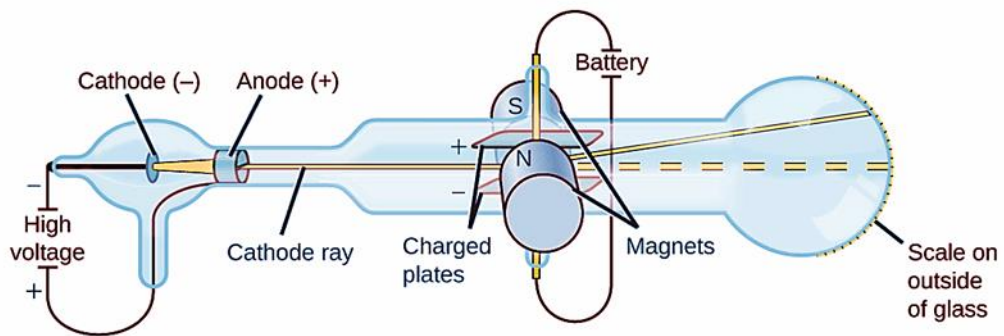


**Figure 1-2:** A representation of the cathode ray tube used by J.J. Thomson to discover the electron. The cathode-anode cellule is subject to a high voltage, to extract electrons from the cathode and direct them to the end of the tube through the anode. The beam of electrons, shown in yellow, is reflected using charged plates and magnets, and the amount of deflection is related to the mass of the electrons and their charge. (Credit to "Kurzon")

To explain the neutrality of atoms, after discovering negatively charged electrons inside of it, Thomson suggested that an atom is a positively charged ball surrounding the negatively charged electrons ([Figure 1-3](#)). This model, called the *Plum-Pudding Model*, was the first one representing the substructure of atoms. [\[14\]](#) However, it failed to explain some phenomena, namely the Rutherford scattering of alpha particles across a gold plate.

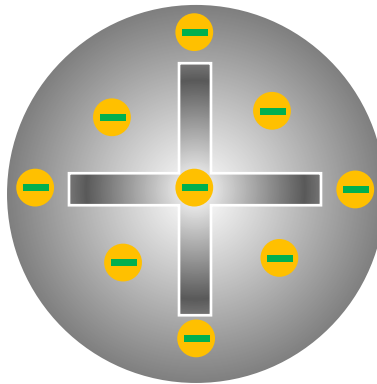


**Figure 1-3:** The Plum-Pudding model of the Atom

In 1911, the British physicist *Ernest Rutherford* came with a new atomic model consisting of a heavy positively charged nucleus surrounded by orbits determining the trajectories of electrons [\[15\]](#), [\[16, p. 377\]](#), it is something like the solar system and probably the picture that pops into everyone's mind whenever they heard the term *atom*. This model replaced the Plum-Pudding model, but according to such model, electrons, as electrically charged particles moving in the electric field created by the nucleus, had no reason to remain in orbits and will keep radiating getting closer to the heart of the atom, to eventually end up falling into the nucleus catastrophically<sup>4</sup>.

In 1913, the Danish physicist *Niels Bohr* used the *quantas* of *Max Planck*, and his constant, to quantify the orbital momentum of electrons, the thing that allowed them only to orbit around quantified distances from the nucleus, preventing them from falling into it [\[17\]](#).

---

<sup>4</sup> We would finish with a Universe of neutron stars, or even worse!

Up to this point, the only elementary particle discovered is the electron, while each atom had a different nucleus. However, Rutherford was convinced that the nucleus has a substructure and was determined to split it!

In 1919, Rutherford discovered the *proton*, and later in 1932, the English physicist *James Chadwick* discovered the last subatomic particle, the *neutron* [18]. So, by this time, the building blocks of the Universe elegantly sum up to the electron, the proton, and the neutron<sup>5</sup>.

Away from the atom, and in a try to explain the missing energy in radioactive beta decay, *Wolfgang Pauli* hypothesized the existence of a neutral particle that cannot be detected, holding the missing energy so that the energy conservation principle can be saved, an idea that will help *Enrico Fermi* to introduce a theory for  $\beta$  decay in 1934, contriving the name *neutrino* for Pauli's particle [19, p. 24]. In 1956, Pauli received a telegram from *Clyde Cowan* and *Frederick Reines* informing him that they succeeded in discovering the neutrino, actually an *antineutrino* [20], [21, p. 38].

In 1936, the Japanese physicist *Yukawa Hideki* suggested that the protons and neutrons are bound with the strong force through what he called *pions* [22]. A year later, *Carl D. Anderson* and *Seth Neddermeyer* discovered, in cosmic rays, a particle that seems like the electron except that it is 207 times heavier and unstable, the *muon*  $\mu$ ! At first, they thought it was the Yukawa's pion, but since it doesn't perceive the strong force, this idea was rejected [23].

Since the processes involving a neutrino always accompanied by an electron, several hypotheses suggested the existence of a second neutrino by the discovery of the *muon*. Such a neutrino, called the *muon neutrino*  $\nu_\mu$ , was discovered by *Leon Lederman*, *Melvin Schwartz*, and *Jack Steinberger* in 1962 [24].

The electron family will get bigger by the discovery of another chubby cousin by a team in *SLAC*, led by *Martin Perl* who named it *tau* particle  $\tau$ , as it is the first letter in the word “*τρίτος*” which refers to “*third*” in Greek [25]. And yes! This discovery triggered the hunt of the tau neutrino  $\nu_\tau$ , a goal achieved and announced in 2000 by the Donut collaboration [26]. By this accomplishment, the list of leptons is completed, and since then, no other lepton has been neither discovered experimentally nor theorized in the frame of the SM.

### 1.1.1.1 The Particle Zoo

Many years before the discovery of  $\nu_\tau$ , precisely in 1947, the  $\pi^+$  pion was discovered in cosmic rays. Later, two particles were identified to behave just like  $\pi^+$  but with different electric charges, one is neutral  $\pi^0$ , and the other is negatively charged  $\pi^-$ . At the same year, and always in cosmic rays, the neutral *Kaon*  $K^0$  was discovered. Next, similar particles but electrically charged were discovered and the family of *Kaons* widened to contain four particles. *Kaons* were strange, they could easily be produced and take a relatively long time to decay as if they were busy doing something between these two processes. To explain this behavior, *M. Gell-Mann* [27], *T. Nakano*, and *K. Nishijima* independently suggested a new quantum number, called *strangeness*  $S$ , which is non-zero only for the strange particles.

---

<sup>5</sup> In addition to the particle of light, the *photon*, and the first antiparticle to be discovered in the same year by Carl Anderson, the *positron*.

This quantum number is conserved in strong and electromagnetic processes, but not in the weak one [19, pp. 28–33].

The jungle of elementary particles kept growing, especially after the development of accelerators. And by the 60s we had, besides already mentioned particles, the *lambda*  $\Lambda^0$ , *Xis*  $\Xi$ , *Sigmas*  $\Sigma$ , *Epsilons*  $\varepsilon$ , and *deltas*  $\Delta$ ,... This particle zoo, as called, was so annoying for physicists, it surely breaks no law of physics, yet it seemed so wrong that all these particles are elementary, besides, it did not look like it is going to stop getting more crowded anytime soon, because, as accelerators achieved higher and higher energies, new particles popped out. In his Nobel Prize lecture, *Willis Lamb* said: “*I have heard it said that the finder of a new elementary particle used to be rewarded by a Nobel Prize. But such a discovery now ought to be punished by a 10.000\$*”.

Physicists always tried to organize the elementary particles, they noticed that the families of electrons and neutrinos weren’t sensitive to the strong force, while all the other particles are. Hence, they name the 6 former with *leptons*, while the others are labeled as *hadrons*. The latter, which were numerous, fell into two categories; those who decay into protons, such as the neutron, lambda, sigmas, and they<sup>6</sup> are called *baryons*, and those who do not, which the term *mesons* is coined for them.

While all the leptons were of spin  $\frac{1}{2}$ , the hadrons come with different spin values, zero,  $\frac{1}{2}$ , 1 and  $\frac{3}{2}$ . And always in a try to order the messy jungle of hadrons and transform it into a tidy garden, all the discovered hadrons (at the time) can be classified in the four following tables.

Name	Symbol	Charge	Isospin	Isospin's 3rd component	Strangeness	Rest Mass
		(Q)	(T)	( $T_3$ )	(S)	(MeV/ $C^2$ )
Pions	$\pi^+$	+1		+1		140
	$\pi^0$	0	1	0	0	135
	$\pi^-$	-1		-1		140
Kaons	$K^+$	+1		$+\frac{1}{2}$	+1	494
	$K^0$	0	$\frac{1}{2}$	$-\frac{1}{2}$	+1	498
	$K^-$	-1	$-\frac{1}{2}$	-1	-1	494
	$\bar{K}^0$	0		$+\frac{1}{2}$	-1	498
Eta	$\eta^0$	0	0	0	0	548

*Table 1-1: Properties of mesons of spin-zero, called pseudo-scalar mesons.*

---

<sup>6</sup> The proton included.

Name	Symbol	Charge (Q)	Isospin (T)	Isospin's 3rd component ( $T_3$ )	Strangeness (S)	Rest Mass (MeV/ $C^2$ )
Nucleons	$p^+$	+1	$\frac{1}{2}$	$+\frac{1}{2}$	0	938
	$n^0$	0	$\frac{1}{2}$	$-\frac{1}{2}$		940
Lambda	$\Lambda^0$	0	0	0	-1	1116
	$\Sigma^+$	+1		+1		1189
Sigmas	$\Sigma^0$	0	1	0	-1	1193
	$\Sigma^-$	-1		-1		1197
Xis	$\Xi^0$	0	$\frac{1}{2}$	$+\frac{1}{2}$	-2	1315
	$\Xi^-$	-1	$\frac{1}{2}$	$-\frac{1}{2}$		1322

Table 1-2: Properties of baryons of spin 1/2, called low-mass baryons

Name	Symbol	Charge (Q)	Isospin (T)	Isospin's 3rd component ( $T_3$ )	Strangeness (S)	Rest Mass (MeV/ $C^2$ )
Deltas	$\Delta^{++}$	+2		$+\frac{3}{2}$		
	$\Delta^+$	+1		$+\frac{1}{2}$	0	1232
	$\Delta^0$	0	$\frac{3}{2}$	$-\frac{1}{2}$		
	$\Delta^-$	-1		$-\frac{3}{2}$		
Sigmas resonances	$\Sigma^{*+}$	+1		+1		
	$\Sigma^{*0}$	0	1	0	-1	1385
	$\Sigma^{*-}$	-1		-1		
Xis resonances	$\Xi^{*0}$	0	$\frac{1}{2}$	$+\frac{1}{2}$	-2	1530
	$\Xi^{*-}$	-1	$\frac{1}{2}$	$-\frac{1}{2}$		

Table 1-3: Properties of baryons of spin 3/2, called baryon resonances.

Name	Symbol	Charge (Q)	Isospin (T)	Isospin's 3rd component ( $T_3$ )	Strangeness (S)	Rest Mass (MeV/ $C^2$ )
Rho	$\rho^+$	+1		+1		140
	$\rho^0$	0	1	0	0	135
	$\rho^-$	-1		-1		140
Kaon resonances	$K^{*+}$	+1		$+\frac{1}{2}$	+1	892
	$K^{*0}$	0		$-\frac{1}{2}$	+1	896
	$K^{*-}$	-1	$\frac{1}{2}$	$-\frac{1}{2}$	-1	892
	$\bar{K}^{*0}$	0		$+\frac{1}{2}$	-1	896
Omega	$\omega^0$	0	0	0	0	783
Phi	$\phi^0$	0	0	0	0	1019

Table 1-4: Properties of mesons of spin 1, called vector mesons.

### 1.1.1.2 Conservation of Quantum Numbers

To explain why some processes are never observed in experiments even if they conserve the electric charge, e.g.  $p^+ \not\Rightarrow e^+ + \gamma$  scientists introduced new quantum numbers, such as the *baryonic number*  $B$ , taking the value +1 for a baryon, -1 for an anti-baryon, and zero for other particles (i.e. mesons and leptons). In the light of the above, for the previous process, we have  $B=1$  on the left while it is zero on the right, so the baryon number is not conserved, and (fortunately) the decaying process of protons is not allowed <sup>7</sup>.

Another quantum number to conserve in any process is the *lepton number*  $L$ , which is equal to +1 for leptons, -1 for anti-leptons and zero for all the hadrons, the conservation of this number explains why we never observe the following process,  $\pi^- \not\Rightarrow e^- + \gamma$  even if it conserves the electric charge and the baryonic number. Yet, there is another issue with leptons, the muon is heavier than the electron, so why it is never observed to decay to an electron and a photon?

$$\mu^- \not\Rightarrow e^- + \gamma$$

Even if it conserves all the known numbers, including the lepton number  $L$ .

	$\mu^-$	$\not\Rightarrow$	$e^- + \gamma$
$L$	1		$1 + 0 = 1$
$B$	0		0
$Q$	-1		-1

<sup>7</sup> At least not in the Standard Model.

The answer was to separate the lepton number into three numbers,  $L = L_e + L_\mu + L_\tau$  where  $L_e = +1$  for the electron and the electron neutrino  $\nu_e$ ,  $L_e = -1$  for  $e^+$  and  $\bar{\nu}_e$  and zero for any other particle (including the two other generations of leptons), the same for  $L_\mu$  and  $L_\tau$ ,  $L_\mu = +1$  for  $\mu^-$  and  $\nu_\mu$ ,  $L_\mu = -1$  for  $\mu^+$  and  $\bar{\nu}_\mu$  otherwise, it equals zero,  $L_\tau = +1$  for  $\tau^-$  and  $\nu_\tau$ ,  $L_\tau = -1$  for  $\tau^+$  and  $\bar{\nu}_\tau$  and zero elsewhere. The conservation of each number separately is mandatory.

Back to the previous process, both  $L_\mu$  and  $L_e$  are not conserved, preventing the given process from occurring.

### 1.1.1.3 The Eightfold Way

While leptons constructed a beautiful and tidy garden, the hadrons were a messy and chaotic jungle, with new hadrons pop into existence every time accelerators reach higher energies. Hadron physics needed its periodic table to organize this mess in an elegant scheme, and the new *Mendeleev* was *Murray Gell-Mann* with his *Eightfold Way* introduced in 1961 [28].<sup>8</sup>

According to their strangeness and electric charge, M. Gell-Mann arranged all the hadrons in a non-orthogonal frame, forming what so-called the *Eightfold Way supermultiplets*. The 8 low mass baryons of spin 1/2 ([Table 1-2](#)) constructed a supermultiplet called *the baryon octet* ([Figure 1-4](#) (a)), and the same pattern is filled by the pseudo-scalar mesons ([Table 1-1](#)) as shown in [Figure 1-4](#) (b).

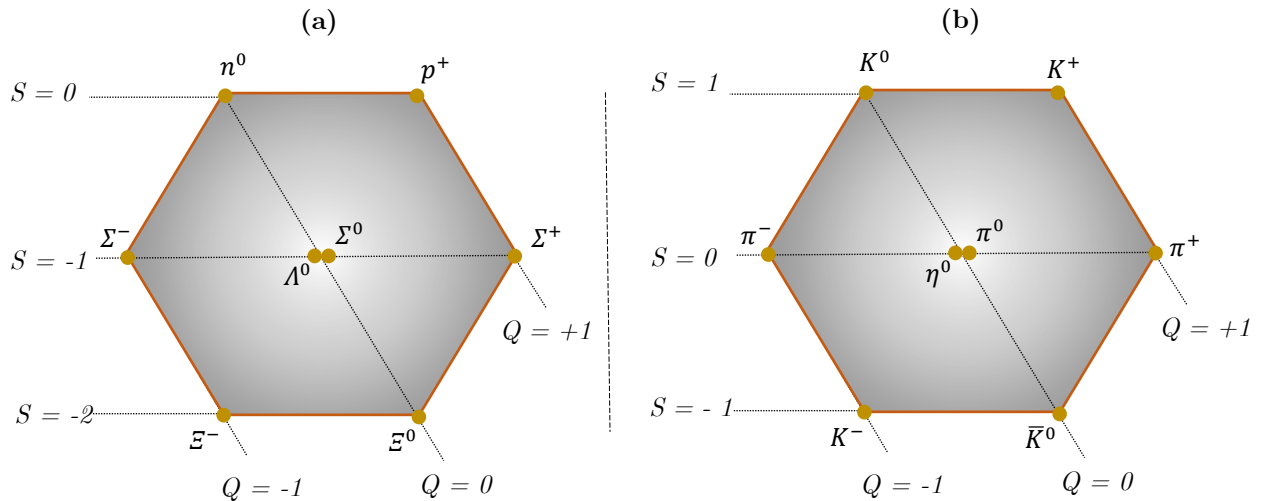


**Figure 1-4:** The Eightfold Way supermultiplets. (a) the baryons octet, (b) the mesons octet. In both figures, hadrons in same line have the same strangeness, while those lying along the same diagonal hold the same electric charge.

The only difference between the above supermultiplets is the strangeness level, wherein (a) the middle line is of strangeness (-1), while in (b) it is of strangeness zero. Introducing a new charge, named the hypercharge, as:

$$Y = B + S \quad (1-1)$$

So that for the baryons  $Y = S + 1$ , while  $Y = S$  for mesons. This way, the middle line of both octets will be of hypercharge  $Y = 0$ .

<sup>8</sup> The same work was done independently by Ne'eman.

The vector mesons of spin 1 also fill the same pattern, but with 3 particles at the center, forming the *meson nonet* (Figure 1-5).

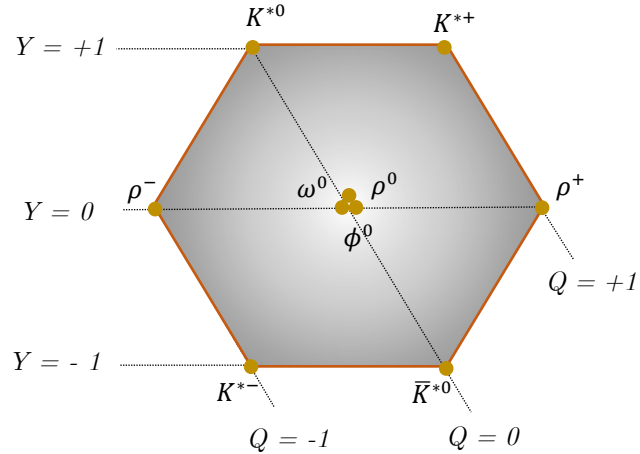


*Figure 1-5: The vector mesons nonet.*

However, the heavier baryons (baryon resonances) of spin 3/2 (Table 1-3) come in a different shape. Instead of a hexagonal, they form a triangle with a baryon in its center (Figure 1-6).

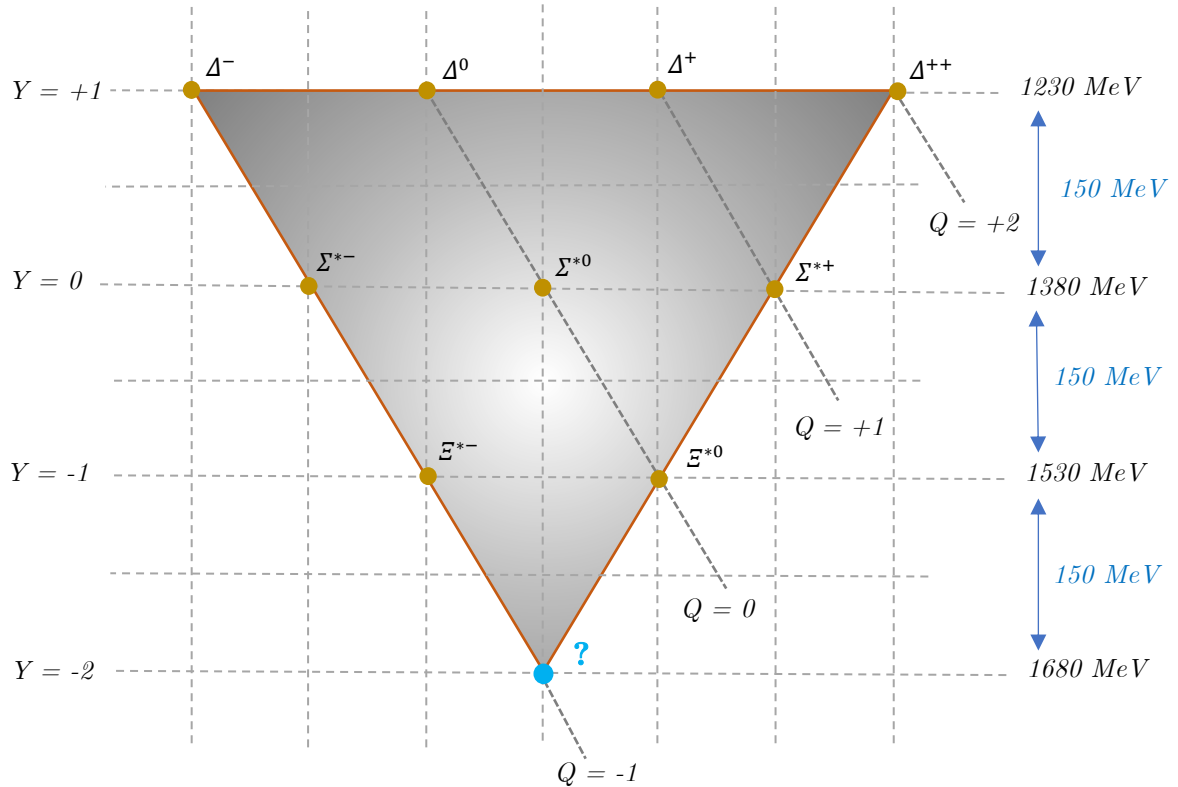


*Figure 1-6: Baryon decuplet. As always, baryons of the same line have the same hypercharge (and the same strangeness since they are all baryons) and baryons of the same electric charge happen to be in the same diagonal. The four levels (lines) are separated with the same amount of energy.*

Exactly as happened with Mendeleev's periodic table<sup>9</sup>, Gell-Mann's decuplet presents a gap, a particle of electric charge  $Q=-1$  and a hypercharge  $Y=-2$  (the blue spot in Figure 1-6), and just as Mendeleev did, Gell-Mann interpreted this gap as a yet to be discovered baryon, and from its place in the supermultiplet he could precisely predict its mass, its charge, and its lifetime. He named this particle *omega-minus*  $\Omega^-$ . The predicted particle was discovered in 1964 [29], and since then, the scientific community was convinced that the Eightfold Way is the right way to go.

#### 1.1.1.4 The Quark Model

Early at the beginnings of the atomic model and the periodic table of elements, the reasons behind the periodicity in Mendeleev's table was a secret, since atoms were considered elementary. Now we know they are not, and the answer to why atoms of the same column were found to have the same chemical properties, was that they had the same number of valence electrons. Taking this “*substructure*” idea into consideration and trying to unveil the secret behind the weird patterns of the supermultiplets, Gell-Mann proposed in 1964 that none of the hadrons is actually an elementary particle, but a combination of much smaller and elementary particles [30].

The same proposition was given independently by the CERN scientist *Career Zweig* [31] with two differences, the first is that Zweig suggested four particles<sup>10</sup>, while Gell-Mann proposed three flavors, and the second difference was the name, while Zweig coined the name “*aces*” for the elementary particles, Gell-Mann went with the term “*quarks*”, which we are using nowadays.

M. Gell-Mann dubbed the 3 flavors of quarks *up*, *down* and *strange*, labeling them  $u$ ,  $d$ , and  $s$  respectively. The electric charge (in units of the proton's), and the strangeness of the three quarks are given in **Table 1-5**.

	$u$	$d$	$s$
$Q$	$+\frac{2}{3}$	$-\frac{1}{3}$	$-\frac{1}{3}$
$S$	0	0	-1

*Table 1-5: properties of the flavors of quarks.*

And of course, their antiparticles (antiquarks) carry the opposite charges. Also, we can represent them in an Eightfold Way pattern (Figure 1-7).

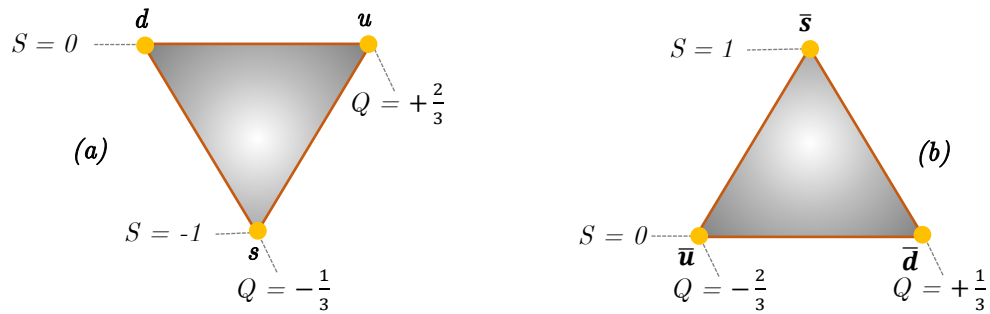


*Figure 1-7: representations of quarks (a) and antiquarks (b) Eightfold Way style.*

<sup>9</sup> And this was the main goal of introducing it at the beginning (related to the first footnote 2)

<sup>10</sup> Since at the time only four leptons were discovered ( $e, \nu_e, \mu$  and  $\nu_\mu$ ), and the idea of having quarks as many as leptons sounded good.

Since  $u$  and  $d$  quarks have no strangeness ( $S = 0$ ), the origin of strangeness observed in the hadrons is the strange quark  $s$ .

To construct all the baryons, Gell-Mann combined three quarks, the antibaryons are formed from three antiquarks, while mesons are a combination of a quark and an antiquark. So, how many hadrons someone can construct from these three quarks?

If we have  $n$  objects to choose from, and we choose  $r$  of them, the order does not matter and we can repeat, then the number of possible combinations is given by:

$$C_r^{n+r-1} = \binom{n+r-1}{r} = \frac{(n+r-1)!}{r!(n-1)!} \quad (1-2)$$

For baryons, we have  $n = 3$  quarks to choose from and we choose three, we can repeat and of course, the order does not matter, in this case, the number of possible combinations is:

$$C_3^{3+3-1} = C_3^5 = \frac{5!}{3!2!} = 10 \quad (1-3)$$

Which suggests the baryon decuplet. Explicitly, the ten combinations are:

Possible combinations	Electric charge	Strangeness	Baryon resonances	Low-mass baryons
	(Q)	(S)	spin (3/2)	spin (1/2)
$uuu$	2	0	$\Delta^{++}$	None
$uud$	1	0	$\Delta^+$	$p^+$
$udd$	0	0	$\Delta^0$	$n^0$
$ddd$	-1	0	$\Delta^-$	None
$uus$	1	-1	$\Sigma^{*+}$	$\Sigma^+$
$uds$	0	-1	$\Sigma^{*0}$	$\Lambda^0$ and $\Sigma^0$
$dds$	-1	-1	$\Sigma^{*-}$	$\Xi^-$
$uss$	0	-2	$\Xi^{*0}$	$\Xi^0$
$dss$	-1	-2	$\Xi^{*-}$	$\Xi^-$
$sss$	-1	-3	Predicted $\Omega^-$	None

**Table 1-6:** the ten possible combinations of three quarks. The 2<sup>nd</sup> and 3<sup>rd</sup> columns are filled taking into consideration that  $Q$  and  $S$  are additional quantum numbers. The corresponding baryons are deduced from [Table 1-3](#) and [Table 1-2](#), judging from their strangeness and electric charge.

To construct baryons of spins 1/2 and 3/2 the quarks must be of spin 1/2, wherein baryon resonances all the three quarks of each baryon have aligned spins<sup>11</sup>, while in low mass baryons one quark should always have the opposite spin alignment of the other two, so that the resulting baryon (such as  $p^+$  or  $n^0$ ) is of spin 1/2.

<sup>11</sup> This definitely violates the Pauli exclusion principle for all the combinations except  $uds$  combination. But we will come to this problem later.

One may ask why there is no particle of spin 1/2 that contains three quarks, like uuu, ddd, or sss? Well, the answer will be that we can never construct a symmetric combination of three quarks of the same flavor which has a total spin of 1/2 without violating the Pauli exclusion principle [19, pp. 183–188], but we need to introduce the charge of colors first, so I will just leave this question for later.

For the formation of mesons, the rule says that you combine a quark with an antiquark, and this leaves us with how many possibilities exactly?

We have 6 particles to choose from, 3 quarks and three antiquarks, we choose two of them, we can't repeat, i.e. we are not allowed to choose two quarks or two antiquarks, and surely the order does not matter. Hence, the number of possible combinations will be:

$$C_r^{n+r-1} - 2C_r^{m+r-1} = \frac{(n+r-1)!}{r!(n-1)!} - 2 \frac{(m+r-1)!}{r!(m-1)!} \quad (1-4)$$

Where  $n = 6$ ,  $r = 2$  and  $m = 3$

Hence, the number of possible  $q\bar{q}$  combinations is:

$$\frac{7!}{2!5!} - 2 * \frac{4!}{2!2!} = 21 - 12 = 9 \quad (1-5)$$

And explicitly, these possibilities are:

Possible combinations	Electric charge		Strangeness	Pseudo scalar mesons	Vector mesons
	(Q)	(S)		spin (0)	spin (1)
$u\bar{u}$	0	0		$\pi^0, \eta^0$ and $\eta'^0$	$\omega^0, \phi^0$ and $\rho'^0$
$u\bar{d}$	+1	0		$\pi^+$	$\rho^+$
$d\bar{u}$	-1	0		$\pi^-$	$\rho^-$
$d\bar{d}$	0	0		$\pi^0, \eta^0$ and $\eta'^0$	$\omega^0, \phi^0$ and $\rho'^0$
$u\bar{s}$	+1	+1		$K^+$	$K^{*+}$
$d\bar{s}$	0	+1		$K^0$	$K^{*0}$
$s\bar{u}$	-1	-1		$K^-$	$K^{*-}$
$s\bar{d}$	0	-1		$\bar{K}^0$	$\bar{K}^{*0}$
$s\bar{s}$	0	0		$\pi^0, \eta^0$ and $\eta'^0$	$\omega^0, \phi^0$ and $\rho'^0$

**Table 1-7:** the nine possible combinations of a quark and an antiquark. The corresponding mesons are deduced from Table 1-1 and Table 1-4, judging from their strangeness and electric charge. Except that the combinations  $u\bar{u}$ ,  $d\bar{d}$  and  $s\bar{s}$  are identical and there is no way to differentiate between the three of them, hence,  $\pi^0$ ,  $\eta^0$  and  $\eta'^0$  are different superpositions of the three states, and the same goes for  $\omega^0$ ,  $\phi^0$  and  $\rho'^0$ .

And just like magic, this simple quark model constructed all the existed hadrons, predicted the existence of others, and forbade the presence of some particles which we cannot form from the three flavors of quarks, e.g. a meson holding an electric charge of +2 is impossible, no  $q\bar{q}$  combination can exceed an electric charge of +1. However, this model, as any other model, suffered from some weak points, most of the scientists at the time did not like the fractional electric charge, also, why we have never observed

an individual quark? In the end, a particle with a fractional electric charge would be very distinguishable. Another flaw of this model is that it seems to violate the Pauli exclusion principle, e.g. the  $\Delta^{++}$  particle is constructed from three up quarks, all with the same spin alignment, which is an intense breach of Pauli's principle, taking into consideration the fermionic nature of quarks.

### 1.1.1.5 The Charge of Color

To overcome the exclusion principle problem, O. W. Greenberg proposed in 1964 a new quantum charge [32], with three possible values, held by the quarks, this charge is called the *color*<sup>12</sup> and its possible values are *red*, *green*, and *blue*. So, the 3 up quarks of  $\Delta^{++}$  are different,  $\Delta^{++}$  is a combination of a red up quark, green up quark, and a blue up quark, hence, it respects the exclusion principle.

It worth mentioning that while flavor charge is symmetric (i.e. the order of flavors does not matter, *uud* baryon is exactly *udu*), the color charge is not, it is antisymmetric, e.g.  $u_b d_g d_r$  is different from  $u_g d_b d_r$ , and for this reason, any combination of  $q_b q_g q_r$  cannot have a spin 1/2 without violating the exclusion principle, and that is why the lightest baryons come in an octet instead of a decuplet ([Table 1-6](#)).

As for the issue of observing individual quarks, it got (instead of an explanation) a new name, *the quark confinement*, since, for some reason, quarks exist only in combined states (as mesons or baryons) but never alone. One possible way to introduce this is to say that colored states can never be observed, all detected particles are either colorless (leptons) or white, and by white, we actually mean that red, blue, and green are present with equal quantities for baryons, and for mesons, the antiquark holds exactly the anticolor of the one held by the quark, i.e.  $q_c \bar{q}'_{\bar{c}}$ . Another way to announce this, the one I prefer, is that in terms of color charge, all particles should be neutral.

This color rule, nicely answers why there are no states of four quarks, or two quarks and an antiquark and a whole bunch of other possibilities, including a single quark. However, a four-quark meson (actually two quarks and two antiquarks), called tetraquark, has been declared to be discovered in 2003 at KEK in Japan [33], later, it seemed much likely to be a two mesons *molecule* rather than a new exotic particle. Earlier this year (2020), the LHCb collaboration at CERN posted two papers [34], [35] claiming that they have observed a true tetraquark called X(2900), which is made of two charm quarks and their antiparticles.

If states of single quarks do not exist, how can we prove their existence? As mentioned before, Rutherford concluded that there is a nucleus in the center of gold atoms just by firing a plat of gold with alpha particles, in what so-called *Rutherford inelastic scattering*, so why not doing it with the proton? Such a study was happening at the *Stanford Linear Accelerator Center* (SLAC) back in 1968, protons as targets were fired by high energy electrons in what so-called the *deep inelastic scattering*<sup>13</sup>. This study revealed that indeed at the heart of the proton exist three charged bunches, which they called *partons*<sup>14</sup> [36], and

---

<sup>12</sup> Of course, it has no link with the real meaning of the word.

<sup>13</sup> What I found amazing about the Eightfold Way and the quark model is that it seems mimicking the steps that happened with the atoms model; the classification, the gaps and predictions, the secret behind the patterns hiding in a substructure, and finally, the experimental proof of the existence of this substructure.

<sup>14</sup> Nowadays, the term partons is used to refer to quarks and gluons.

that was before the confirmation of the quark model and admitting that the partons are eventually the two up quarks and a down quark.

### 1.1.1.6 Charm, Bottom, and Top

In a paper received by Physics Letters on 19 June 1964 [37], *B.J. Bjorken and S. L. Glashow* suggested a new quantum number, *the charm C*, held by a fourth quark called charm, labeled  $c$  and violated only by the weak interaction<sup>15</sup>. 6 years later, Glashow will get back to this idea, along with *J. Iliopoulos* and *L. Maiani*, while they were working on the *Flavor-Changing Neutral Currents (FCNC)* they suggested a mechanism, called *GIM mechanism* [38] that requires the existence of the charm quark.

In November 1974, two groups, one at SLAC and the other at Brookhaven published independently and simultaneously a discovery of a new hadron, named  $\psi$  by the first team [39] and  $J$  by the second [40]. This  $\psi/J$  particle was a heavy meson with a relatively long lifetime of  $10^{-20}s$  formed of a charm quark and its antiquark, hence, its *charmness* is nullified (or hidden). The first *charmed* particle to be discovered was the charmed lambda  $\Lambda_c^+$  baryon ( $\Lambda_c^+ = udc$ ) [41], and plenty of other charmed particles were observed later, confirming the existence of the charm quark and the quark model.

In 1973, *M. Kobayashi and T. Maskawa* theorized the existence of two other quarks to explain the CP symmetry violation [42]. These quarks will be named *top* and *bottom* in 1975 by *Haim Harari* [43]. I should mention that in this same year, the term “*standard model*” was originated for the very first time by *Abraham Pais* and *Sam Treiman* in liaison to the electroweak theory with u, d, s, and c quarks [44, p. 320].

In 1977, a new heavy meson called upsilon  $\Upsilon$  was discovered at Fermilab, later, it has been defined recognized as a *bottomonium* (i.e. formed from a bottom quark and its antiquark  $\Upsilon = b\bar{b}$ ) [45], [46]. However, the first discovered particle with a naked bottom quark was the bottom lambda  $\Lambda_b^0 = udb$  in the '80s, followed by other bottom baryons discoveries over the years.

As mentioned, the first discoveries of particles carrying the new quarks were the *charmonium*  $J/\psi(c\bar{c})$  and the *bottomonium*  $\Upsilon(b\bar{b})$ , and that is why someone will guess that a *toponium* heavy meson would soon be observed, but this never happened at all, neither a baryon with a naked top quark was found. The reason why this never results is that the top quark's lifetime is way shorter than its hadronization time, i.e. it decays before it can form a hadron [47]. However, being the most important particle in the SM<sup>16</sup>, we will reserve the next chapter to discuss the special properties of the top quark.

An evidence for the existence of the top flavor of quarks will have to wait until 1995 to be revealed by the biggest accelerator at the time, the 6.28 Km circular synchrotron at Fermilab, *The Tevatron!* [48], [49] Indeed, the top quark cannot form a baryon, but this does not mean we cannot find evidence for its existence. We can identify the top quark by analyzing its decay products, and that is what CDF [48] and DØ [49] experiments exactly did, using  $67 \text{ pb}^{-1}$  of data by the former and  $50 \text{ pb}^{-1}$  of data by the latter.

<sup>15</sup> Just like *strangeness*.

<sup>16</sup> I cannot be more biased, can I?

After this remarkable discovery, no other quarks have been theorized neither experimentally discovered, and the family of elementary fermions of the standard model reached its final form with 6 flavors of quarks and 6 leptons.

### 1.1.2 The Forces and their Mediators

In classical physics, a force can be defined as a push or a pull, and it is either a contact force like spring force, or an action at a distance force like the gravitational force.

At the fundamental level, a force is a process through which elementary particles affect each other. However, this effect cannot be limited to a push or a pull, hence, the term interaction is more accurate. And unlike the classical forces, there is no spooky action at a distance force.

To the extent of our knowledge, there are only four<sup>17</sup> witnessed forces in nature, and whatsoever interaction someone can have in mind, observed with the naked eye or not, is one or composition of the following fundamental interactions: *strong*, *electromagnetic*, *weak*, and *gravitational*.

The SM inherits H. Yukawa's vision of a force as an exchange of a *messenger* between the two particles in interaction. Each interaction of the four has its force-carriers, which are *vector bosons* (i.e. bosons of spin 1) except for gravity. in the frame of the SM the gravitational interaction is carried by a *tensor boson* (i.e. boson of spin 2) called the *graviton*  $G$ , such a boson was never observed in experiments, hence, we say that the SM does not describe the gravity! However, its strength can be neglected in the elementary particles' world<sup>18</sup>, and in this section, we will only introduce the first three forces.

The four forces have different strengths and different ranges. Taking a particle that is sensitive to all the four forces, the proton, for example, we can calculate the strength of each force relative to the others ([Table 1-8](#)).

Force	Theory	Mediator	Strength <sup>19</sup>	Range
<i>Strong</i>	Chromodynamics (QCD)	Gluons ( $g_{c\bar{c}}$ )	1	$\infty, < 10^{-15}$ m
<i>Electromagnetic</i>	Electrodynamics (QED)	Photon ( $\gamma$ )	$10^{-2}$	$\infty$
<i>Weak</i>	Flavordynamics (QFD)	$W^\pm$ and $Z^0$	$10^{-13}$	$10^{-18}$
<i>Gravitational</i>	Geometrodynamics	graviton (g)	$10^{-38}$	$\infty$

*Table 1-8: the four fundamental interactions and their properties.*

<sup>17</sup> In the current energy level to be precise, since as we shall see, the weak and electromagnetic interactions are only two different manifestations of the same force, the electroweak force. So, at higher energy, there are only three fundamental interactions instead of four.

<sup>18</sup> Although, scientist in the LHC have to account for the phases of the Moon when adjusting the protons beam!

<sup>19</sup> The strength of a force is relative to many factors, but if in a p-p interaction the strength of the strong force was 1, then the strengths of other forces are as shown in the table.

### 1.1.2.1 Quantum Electrodynamics (QED)

The QED is the theory describing the electromagnetic phenomena, and the first quantum field theory (QFT), formulated by *Freeman Dyson* [50], [51], *Julian Schwinger* [52], [53], *Richard Feynman* [54]–[56], and *Shinichiro Tomonaga* [57] back in the ‘60s.

All electromagnetic processes that introduce electrically charged matter and light, can be described using the elementary process of the QED in [Figure 1-8](#), this type of figure is called a *Feynman diagram*, which is a purely symbolic<sup>20</sup> way to represent graphically the interactions between elementary particles.

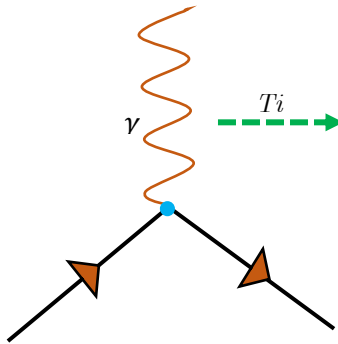
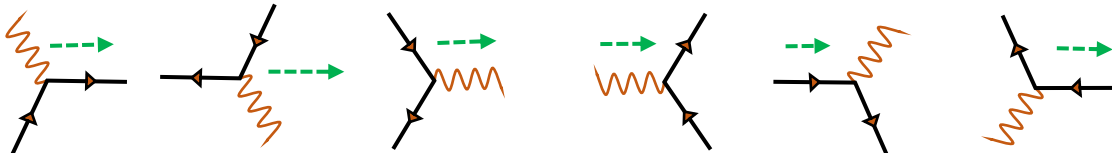


**Figure 1-8:** the primary vertex of the QED. The straight lines with an arrow pointing towards the direction of time is an electrically charged particle, while curvy line represents the photon. This diagram can be read as: a particle emits or absorbs a photon.

Rotating this diagram in time, we can have six different elementary diagrams ([Table 1-9](#)), then all the electromagnetic processes can be represented by combining these primitive vertices.



A charged particle absorbs a photon and exits	A charged antiparticle emits a photon and exits	Annihilation of a particle and its antiparticle	Creation of a particle and its antiparticle	A charged particle emits a photon and exits	A charged antiparticle absorbs a photon and exits
---	---	---	---	---	---

**Table 1-9:** primitive vertices of the QED. The green arrow indicates the direction of time, straight lines with an arrow pointing towards the direction of time are electrically charged particles, while those with an arrow directing at the opposite direction of time are antiparticles<sup>21</sup>.

It worth mentioning that none of the above primitive vertices represents a physical process by itself, but only when it is combined whit another diagram.

<sup>20</sup> By purely symbolic we mean that the lines do not represent the real trajectories of the particles.

<sup>21</sup> Because n Feynman’s interpretation, an antiparticle is a particle traveling backwards in time.

Taking the annihilation process, for example, it might seem evident that an electron and a positron can annihilate to a photon, but in fact, this is kinematically forbidden! In the center-of-momentum frame (CM) of the  $e - e^+$  system (before vertex), the total momentum is zero. However, after the vertex, we only have one photon which its momentum  $\vec{p} = \hbar\vec{k}$  cannot be zero, and this violates the law of conservation of momentum and shreds the space translation symmetry. A particle and its antiparticle can only annihilate to two photons (Figure 1-9), but not one.

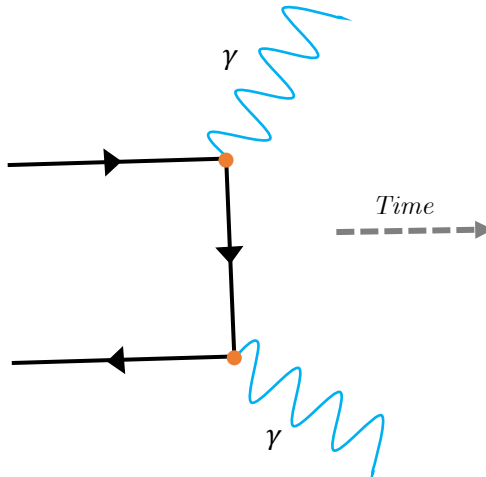


**Figure 1-9:** The annihilation process of a particle and its antiparticle. The line between the two vertices is a virtual particle (off mass-shell). As we can see, this diagram is nothing but a combination of the 5<sup>th</sup> and 2<sup>nd</sup> diagrams in Table 1-9.

In a given electromagnetic process, each vertex contributes to its amplitude with a factor of  $i g_e \gamma^\mu$ , where:

$g_e$  : is the coupling constant,  $g_e = e \sqrt{\frac{4\pi}{hc}} = \sqrt{4\pi\alpha}$  (dimensionless).

$\alpha = \frac{1}{137}$  : the fine structure constant.

$\gamma^\mu$ : Dirac 4x4 matrices.

Photons are massless; hence the range of the electromagnetic force is infinite, and that is why we actually can see galaxies and stars billions of light-years away.

### 1.1.2.2 Quantum Flavor Dynamics (QFD)

Weak interactions are mediated either by a neutral current ( $Z^0$ ) or by charged ones ( $W^\pm$ ), and affects the particles who carry the *weak charge*, which are all the fermions<sup>22</sup> of the SM. The primitive vertices of the QFD are exactly like the one of the QED, replacing the photon with the three bosons  $Z^0$  and  $W^\pm$ . Except that, unlike photons who are electrically neutral, the  $Z^0$  and  $W^\pm$  carry the weak charge, hence, they can couple to each other (Figure 1-10).

---

<sup>22</sup> Just the left-handed particles, and right-handed antiparticles.

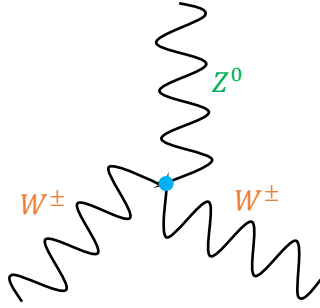


**Figure 1-10:** the direct coupling of  $W^\pm$  and  $Z^0$

The weak interaction is the only one capable of changing a quark's flavor or a muon to an electron (with some neutrinos to conserve the lepton number), and that's why it is the one responsible for the radioactivity (refueling the sun<sup>23</sup> by changing an *up* quark to a *down* quark), and the muon decay.

The QFD is a chiral theory, and this is because the weak interaction cares whether a particle is lefthanded or righthanded. In fact, only lefthanded particles, and right-handed antiparticles, carry the weak charge, which might answer the question of why there are no righthanded neutrinos, nor left-handed antineutrinos, in the SM<sup>24</sup>, hence, they (theoretically) do not have a mass, and this, as we shall see, is one of the shortcomings of the SM.

In the GWS model, each vertex contributes to the amplitude of a given weak process with a factor of:

$$\frac{-i}{2\sqrt{2}} g_W \gamma^\mu (1 - \gamma^5) : \text{for a vertex involving } W^\pm.$$

$$\frac{-i}{2} g_Z \gamma^\mu (c_V^f - c_A^f \gamma^5) : \text{for a vertex involving } Z^0.$$

Where,

$g_W = \frac{g_e}{\sin \theta_W}$  : is the coupling constant of the charged weak interactions.

$g_Z = \frac{g_e}{\sin \theta_W \cos \theta_W}$  : is the coupling constant of the charged weak interactions.

$\theta_W$  : is the weak mixing angle, also known as the Weinberg angle.

$c_V^f$ : is the correction to the *vector* weak charge.

$c_A^f$ : is the correction to the *axial-vector* weak charge.

As we can mention, the weak coupling constants  $g_W$  and  $g_Z$  are coupled to the electromagnetic coupling constant  $g_e$ , also, they are related to the weak mixing angle  $\theta_W$ .

---

<sup>23</sup> And hopefully, the ITER's tokamak in the coming future.

<sup>24</sup> Since neutrinos interact only via the weak charge (that is why they are so hard to be hunted), so righthanded neutrinos will not interact at all! and they are called *sterile neutrinos*.

Both  $c_V^f$  and  $c_A^f$  are in function of  $\theta_W$  ([Table 1-10](#)).

<b>f</b>	<b><math>c_V</math></b>	<b><math>c_A</math></b>
$\nu_e, \nu_\mu, \nu_\tau$	$\frac{1}{2}$	$\frac{1}{2}$
$e^-, \mu^-, \tau^-$	$-\frac{1}{2} + 2 \sin^2 \theta_W$	$-\frac{1}{2}$
$u, c, t$	$\frac{1}{2} - \frac{4}{3} \sin^2 \theta_W$	$\frac{1}{2}$
$d, s, b$	$-\frac{1}{2} + \frac{2}{3} \sin^2 \theta_W$	$-\frac{1}{2}$

*Table 1-10:* Neutral vector and axial-vector couplings in the GWS model. [[19](#)]

The masses of W bosons and Z boson are also related through  $\theta_W$  by Equation [\(1-6\)](#).

$$M_W = M_Z \cos \theta_W \quad (1-6)$$

$\theta_W$  can be the most important parameter in the GWS model, yet there is no way to calculate it by theory, hence, it is a free parameter of the SM. The only way to give  $\theta_W$  a value is the experience, and just after doing this, we can calculate the mediators' masses and the coupling constants.

The Z and W bosons are very massive, and that is the reason behind the short range of the weak interactions.

### 1.1.2.3 Quantum Chromodynamics (QCD)

The QCD is the theory describing the strong interaction, it is called Chromodynamics because the charges sensitive to the strong interaction are named colors, and we have already seen in section [1.1.1.5](#) how this charge has been introduced.

The strong interaction is the one confining quarks in hadrons and holding the atoms' nuclei. And as its name indicates, it is the strongest force of the four fundamental forces ([Table 1-8](#)). Quarks and gluons are the only fundamental particles carrying a color charge, so unlike the photons, the gluons can interact with each other, forming what so-called a *glueball* [[58](#)]. Gluons are vector bosons carrying a color and an anticolor,  $g_{C\bar{C}}$ , and since we have three colors, there would be nine combinations of a color and an anticolor. However, the QCD is based on the  $SU(3)_c$  symmetry, and in terms of the group theory,  $SU(3)$  has only 8 generators, and that is why we have 8 gluons instead of 9. But this, to be honest, is just a theoretical twist, we could have described the strong interaction in a  $U(3)$  symmetry group instead of  $SU(3)$ , and then we would have 9 gluons!

The coupling constant of the strong force is similar to the one of the QED, but instead of the fine structure constant  $\alpha$  we have the strong structure constant  $\alpha_s$ :

$$g_s = \sqrt{4\pi\alpha_s} \quad (1-7)$$

As in this work we are interested in a 4-top quarks decay into a fully hadronic final state, we will briefly introduce the hadronization and jet formation.

In a high energy collision, quarks and gluons can be produced, but only travel for a very short distance before they are hadronized<sup>25</sup> [48], [49], the maximum distance they can go far from each other is roughly  $10^{-15} \text{ m}$ , which is the diameter of hadrons and the range of the strong force, and this as we mentioned is due to the quarks confinement.

Before being hadronized, the quark goes through an intermediate stage, called the fragmentation, where it emits a gluon, then another and another... (Figure 1-11), emitted gluons themselves emit other gluons, giving rise to a splendid cascade called the parton shower. The fragmentation is what defines how the jets will be. [59]

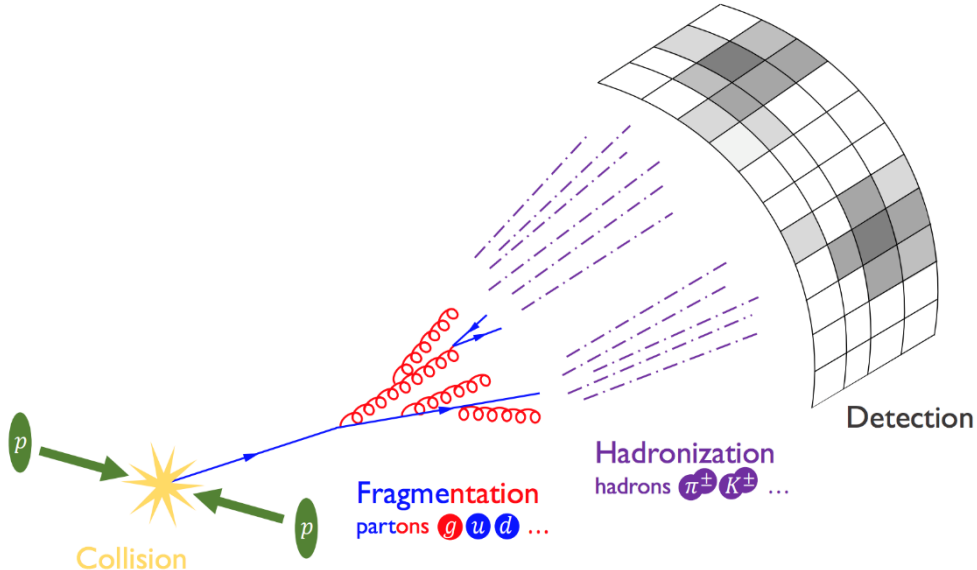


**Figure 1-11:** Cartoon of the jet formation process. This representation shows four stages, the  $p$ - $p$  collision gives rise to an energetic quark, the fragmentation of the quark making a parton shower, the hadronization of partons into two jets, and finally the detection of the final state particles (Credit to Eric M. Metodiev ©).

Now that we have introduced the matter particles and the force carriers, we have almost introduced all the particle content of the SM (except the Higgs boson), and what is left to “*claim an understanding of the physical world we see*”, as cited in the quote at the beginning of this chapter, is to have the rules to calculate the resulting world, and that’s exactly what the next section will be about. But before that, let us quickly count how many elementary particles are there in the SM, taking into consideration that particles with different colors and those with different chirality are in fact different particles.<sup>26</sup>

<sup>25</sup> Or decay, if they were top quarks, into a bottom quark and a W boson.

<sup>26</sup> At the end of the day, we only define particles by how they respond to different forces.

quark	6 flavors * 3 colors * 2 chiralities = 36	45 fermions +
Electron	3 generations * 2 chiralities = 6	45 anti-particles
Neutrino	3 left-handed neutrinos	= 90 fermions
Photon	1 photon	
Weak bosons	3 weak bosons	13 Boson <sup>27</sup>
Gluons	8 gluons	
Higgs	1 Higgs boson	
Total Number of Elementary Particles		103 particles

Table 1-11: the particle content of the Standard Model.

Having said that, the mathematical formulation of the SM does not lay on the 103 elementary point-like particles, but instead, it counts on the quantum fields, where particles are just excitations in their fields, while their antiparticles are reversed excitations of the same field.

## 1.2 The Standard Model Lagrangian

The SM Lagrangian  $\mathcal{L}_{SM}$  describes the dynamics of the quantum fields giving birth to the particles of the SM. In this section, we shall see the gauge symmetry under which the  $\mathcal{L}_{SM}$  is invariant, then, related to how different fields transform under these symmetries, we will define new labels to the quarks and leptons, in order to write our Lagrangian compactly. Next, we will expose the famous  $\mathcal{L}_{SM}$  and its different terms after the EWSB.

### 1.2.1 Gauge Symmetry Group

Symmetries had always the greatest priority in theoretical and high energy physics, I would really like to go through so many notions related to the subject, namely, the definition of the term, the classification of symmetries, the Noether theorem, the unitary  $\mathcal{U}(n)$  and special unitary  $\mathcal{SU}(n)$  groups in the frame of the groups' theory, symmetry breaking and Goldston theorem... But unfortunately, I am running out of space reserved for the first chapter. However, among other classifications, a symmetry can be either a space-time symmetry, like space translation, rotations, and Lorentz boosts, or an internal symmetry like the gauge symmetry. The SM Lagrangian  $\mathcal{L}_{SM}$  is found to be invariant under both spacetime transformations, since the theory is relativistic so it should be symmetric under Poincaré transformations, and three internal symmetries described by the Lie groups  $\mathcal{SU}(3)_c$ ,  $\mathcal{SU}(2)_L$  and  $\mathcal{U}(1)_Y$ . Hence, the total symmetry group of the SM is as shown in Equation (1-8).

$$\mathcal{P} \times \mathcal{SU}(3)_c \times \mathcal{SU}(2)_L \times \mathcal{U}(1)_Y \quad (1-8)$$

Where,

---

<sup>27</sup> Why bosons have no antiparticles? An answer would be that the notion of antiparticles came with the Dirac equation to explain the negative energy states, and Dirac equation only describes fermions. However, Klein Gordon's equation as well predicts negative energy states, also, we know that mesons have antiparticles, and they are bosons!

$\mathcal{P}$  : is the Poincaré ten-dimensional symmetry group, its generators are  $P^\mu$ , the 4 generators of translations (in space and time), and  $M^{\mu\nu}$ , the 6 generators of Lorentz transformations (3 rotations and 3 boosts). According to Noether's theorem, *to each symmetry corresponds a conserved quantity*, and thanks to Poincaré symmetry, the energy, the momentum, and the angular momentum are conserved quantities in all the SM processes.  $P^\mu$  and  $M^{\mu\nu}$  are not commutative operators, and we say that the Poincaré group  $\mathcal{P}$  is non-Abelian.

$SU(3)_C$  : is the internal symmetry of the strong interaction, as the  $SU(n)$  Lie groups have  $(n^2 - 1)$  generators, the  $SU(3)_C$  has 8, and this is because we have 8 gluons as the strong force carriers. Quarks are represented in the triplet representation of  $SU(3)_C$ , while gluons are associated with the octet representation. The other particles are simply singlets of  $SU(3)_C$ , since they do not feel the strong force ([Table 1-12](#)). The charge conserved by this symmetry is the charge of color, and that is the reason for the “*C*” subscript.

$SU(2)_L \times U(1)_Y$  : as we have mentioned in a previous footnote ([16](#)), the weak and electromagnetic interactions are only two manifestations of the same force, the electroweak force, and this is the internal symmetry of the electroweak theory. The subscripts *L* and *Y* are respectively referring to *Left-handed* and the *Hypercharge* to cite that the electroweak theory is chiral, and that is because it behaves in different ways depending on the *handedness* of particles in subject.  $SU(2)_L \times U(1)_Y$  has  $3 + 1$  generators, and the theory presents four bosons,  $W_1, W_2, W_3$ , and  $B$ . Left-handed fermions come in doublets of  $SU(2)_L$ , the  $W_i$  form a triplet, while the other particles are singlets invisible for the weak interaction. The charges conserved by  $SU(2)_L$  and  $U(1)_Y$  are respectively the *weak Isospin* and the *hypercharge*, which are related by the Gell-Mann-Nishijima relation ([1-9](#)).

$$Q = I_3 + \frac{Y}{2} \quad (1-9)$$

Where, the hypercharge of Equation ([1-1](#)) is redefined after the discovery of the other three flavors coming with the *charm*, the *top*, and the *bottom* quantum numbers,  $C$ ,  $T$  and  $B'$ .

$$Y = B + S + C + T + B' \quad (1-10)$$

Where,

$C = 1$  for a charm quark,  $-1$  for its antiquark, and zero for other particles. Hence,  $C = n_c - n_{\bar{c}}$

$T = 1$  for a top quark,  $-1$  for its antiquark, and zero for other particles. Hence,  $T = n_t - n_{\bar{t}}$

$B' = -1$  for a bottom quark,  $1$  for its antiquark, and zero for other particles. Hence,  $B' = -(n_b - n_{\bar{b}})$

### 1.2.2 Quarks and Leptons Fields' Labels

The fields are labeled in a way to minimize the writings in the SM Lagrangian, the fields' labels, and their contents are summarized in [Table 1-12](#).

field	Field label	contents	Hypercharge ( $Y$ )		representations	
			$U(1)_Y$	$SU(2)_L$	$SU(3)_C$	
Quarks	$Q_i$	$(u_L, d_L), (c_L, s_L), (t_L, b_L)$	1/3	2	3	
	$u_{R,i}$	$u_R, c_R, t_R$	4/3	1	3	
	$d_{R,i}$	$d_R, s_R, b_R$	-2/3	1	3	
leptons	$L_i$	$(\nu_{e,L}, e_L), (\nu_{\mu,L}, \mu_L), (\nu_{\tau,L}, \tau_L)$	-1	2	1	
	$e_{R,i}$	$e_R, \mu_R, \tau_R$	-2	1	1	
Gauge	$B_\mu$	$B_\mu$	0	1	1	
	$W_\mu^i$	$(W_\mu^1, W_\mu^2, W_\mu^3)$	0	3	1	
	$G_\mu^a$	$G_\mu^a, a \in [1, \dots, 8]$	0	1	8	
	Higgs	$\phi$	$(\phi^+, \phi^0)$	1	2	1

Table 1-12: the contents of SM fields, and their transformation under the three gauge symmetry groups.

### 1.2.3 The Famous Lagrangian $\mathcal{L}_{SM}$

The classic way to introduce this section is to start writing down the  $\mathcal{L}_{SM}$  in its most general, compact, and invariant form before the EWSB (Equation (1-11)), then noticing that such Lagrangian describes a world where, none of the elementary particles is massive, and has no photons, basically, a lightweight and dark world very much different from the one we observe! After this, the EWSB will be presented as a spontaneous breaking of the electroweak symmetry into the electromagnetic one, and the photon is born. Finally, the missing mass terms will appear thanks to the so-called Higgs mechanism <sup>28</sup>.

$$\mathcal{L}_{SM} = -\frac{1}{4} \sum_{gauge} F_{\mu\nu}^a F^{a\mu\nu} + \sum_{fermions} \bar{\psi} i\gamma^\mu \mathcal{D}_\mu \psi + (\mathcal{D}_\mu \phi)^\dagger (\mathcal{D}^\mu \phi) - V(\phi) \quad (1-11)$$

This chronological picture is gratefully presented in [60], [61], [62], [63]. However, for the sake of brevity, we will jump right into the famous Lagrangian describing our world as it is today [64], and explain what each term of its terms stands for.

$$\mathcal{L}_{SM} = -\frac{1}{4} F_{\mu\nu} F^{\mu\nu} \quad (1-12)$$

$$+ i \bar{\psi} \not{\partial} \psi + h.c. \quad (1-13)$$

$$+ \psi_i y^{ij} \psi_j \phi + h.c. \quad (1-14)$$

$$+ |\mathcal{D}_\mu \phi|^2 - V(\phi) \quad (1-15)$$

<sup>28</sup> In fact, it is Brout-Englert-Higgs (BEH) mechanism.

- **Gauge Sector:**  $\mathcal{L}_{gauge} = -\frac{1}{4}F_{\mu\nu}F^{\mu\nu}$

The gauge sector is nothing but a scalar product of the gauge fields strength tensors  $F_{\mu\nu}$ , it contains terms that are necessary for the 12 gauge fields (c.f. [Table 1-12](#)) to even exist (the kinetic terms), and other terms to take care of the interactions (if any) between them.

The fields strength tensors  $F_{\mu\nu}^a$  of a given field  $A_\mu^a$  is given by:

$$F_{\mu\nu}^a = \partial_\mu A_\nu^a - \partial_\nu A_\mu^a + g f^a{}_{bc} A_\mu^b A_\nu^c \quad (1-16)$$

The first two terms are the kinetic terms, while the last term is the interaction term.  $g$  is the *gauge coupling parameter*, and  $f^{abc}$  are the *structure constants* of the associated gauge group, these constants are the coefficients appearing in the commutation relations of the gauge group generators.<sup>29</sup> For example, the  $B_\mu$  field is associated with the  $\mathcal{U}(1)_Y$  gauge group, which is an abelian group (i.e. its generators are commuting between each other, which is trivial for  $\mathcal{U}(1)_Y$ , since it only has one generator), hence  $f^{abc} = 0$ , and the field strength tensor  $B_{\mu\nu}$  only contains the kinetic terms ([Equation \(1-17\)](#)).

$$B_{\mu\nu} = \partial_\mu B_\nu - \partial_\nu B_\mu \quad (1-17)$$

On the other hand,  $\mathcal{SU}(2)_L$  and  $\mathcal{SU}(3)_C$  are non-Abelian groups, since the three (eight) Pauli (Gell-Mann) matrices  $\tau^i$  ( $\lambda^i$ ), the generators of the  $\mathcal{SU}(2)_L$  ( $\mathcal{SU}(3)_C$ ) group, cannot be diagonalized simultaneously [\[60\]](#). Explicitly, the structure constants of  $\mathcal{SU}(2)_L$  are related to the totally antisymmetric tensor of Levi-Civita  $\frac{i}{2}\varepsilon_{ijk}$ , hence, the 3  $W_\mu^i$  fields strength tensors are gathered in [Equation \(1-18\)](#).

$$\mathbf{W}_{\mu\nu} = \partial_\mu \mathbf{W}_\nu - \partial_\nu \mathbf{W}_\mu + \frac{i g_2}{2} \varepsilon_{ijk} \mathbf{W}_\mu \wedge \mathbf{W}_\nu \quad (1-18)$$

Where  $W_\mu^1$ ,  $W_\mu^2$  and  $W_\mu^3$  are assembled in the vector  $\mathbf{W}_\mu = (W_\mu^1, W_\mu^2, W_\mu^3)$ , and  $g = -g_2$ .

The case of  $\mathcal{SU}(3)_C$ , and the 8  $G_\mu^a$  gauge fields, is less trivial. However, its structure constants are totally antisymmetric and are given by [\[65\]](#):

$$f^{123} = 1 \quad (1-19)$$

$$f^{147} = -f^{156} = f^{246} = f^{257} = f^{345} = -f^{367} = \frac{1}{2} \quad (1-20)$$

$$f^{458} = f^{678} = \frac{\sqrt{3}}{2} \quad (1-21)$$

---

<sup>29</sup> Hence the name *structure constants*, since the structure of a group is the commutation relations between its generators.

The  $G_\mu^a$  gauge fields strength tensors are [60], [65]:

$$G_{\mu\nu}^a = \partial_\mu G_\nu^a - \partial_\nu G_\mu^a + g_3 f_{bc}^a G_\mu^b G_\nu^c \quad (1-22)$$

And the Gauge sector Lagrangian is:

$$\mathcal{L}_{gauge} = -\frac{1}{4} G_{\mu\nu}^a G_a^{\mu\nu} - \frac{1}{4} W_{\mu\nu} W^{\mu\nu} - \frac{1}{4} B_{\mu\nu} B^{\mu\nu} \quad (1-23)$$

The weak bosons and the electromagnetic fields are given in terms of  $W_\mu^1, W_\mu^2, W_\mu^3, B_\mu$  and  $\theta_w$ , the Weinberg angle, as [60, p. 45]:

$$A_\mu^{em} = \sin\theta_w W_\mu^3 + \cos\theta_w B_\mu \quad (1-24)$$

$$Z_\mu^0 = \cos\theta_w W_\mu^3 - \sin\theta_w B_\mu \quad (1-25)$$

$$W_\mu^\pm = \frac{\sqrt{2}}{2} (W_\mu^1 \pm i W_\mu^2) \quad (1-26)$$

- **Fermionic Sector:**  $\mathcal{L}_{fermions} = i \bar{\psi} \not{D} \psi + h.c.$

This sector contains the kinetic terms of all the fermionic fields, in addition to their interactions with the gauge fields. It might seem confusing at the first glance since no gauge fields are appearing in the expression, but it is all hidden in the covariant derivative  $\not{D}$ .

First thing first,  $\psi$  is labeling the fermionic fields all mentioned in Table 1-12, and  $\bar{\psi}$  is its Hermitian conjugate.  $\mathcal{D}_\mu$  is the covariant derivative, while the slash is the *Feynman* notation of an operator multiplied by *Dirac* matrix  $\gamma^\mu$ , i.e.:

$$\not{D} = \gamma^\mu \mathcal{D}_\mu \quad (1-27)$$

The covariant derivative contains more or fewer terms depending on which field it is applied. However, its longest form (Equation (1-28)) is given for the left-handed quark fields ( $Q_i$ , c.f. Table 1-12).

$$\mathcal{D}_\mu = \partial_\mu - ig_1 \frac{Y}{2} B_\mu - ig_2 \frac{\tau_j}{2} W_\mu^j - ig_3 \frac{\lambda_a}{2} G_\mu^a \quad (1-28)$$

Where  $Y$  is the hypercharge, that equals  $\frac{1}{3}$  for  $Q_i$ . When applied on a right-handed field, the  $\mathcal{D}_\mu$  does not contain the second term anymore, as well as the 3<sup>rd</sup> term disappears for the leptonic fields.

All said, the  $\mathcal{L}_{fermions}$  is explicitly given by Equation (1-29).

$$\begin{aligned}
\mathcal{L}_{fermions} = & \bar{Q}_i i \gamma^\mu \left( \partial_\mu - \frac{i g_1}{6} B_\mu - \frac{i g_2}{2} \tau_j W_\mu^j - \frac{i g_3}{2} \lambda_a G_\mu^a \right) Q^i \\
& + \bar{u}_{R,i} i \gamma^\mu \left( \partial_\mu - \frac{2 i g_1}{3} B_\mu - \frac{i g_3}{2} \lambda_a G_\mu^a \right) u_R^i \\
& + \bar{d}_{R,i} i \gamma^\mu \left( \partial_\mu + \frac{2 i g_1}{3} B_\mu - \frac{i g_3}{2} \lambda_a G_\mu^a \right) d_R^i \\
& + \bar{L}_i i \gamma^\mu \left( \partial_\mu + i \frac{g_1}{2} B_\mu - \frac{i g_2}{2} \tau_j W_\mu^j \right) L^i \\
& + \bar{e}_{R,i} i \gamma^\mu (\partial_\mu + i g_1 B_\mu) e_R^i + h.c.
\end{aligned} \tag{1-29}$$

It worth mentioning that we have adopted the Einstein summation convention [66], where two contracted indices are summed over all their possible values. Namely here, the generation subscript  $i$  takes 3 values, 1, 2, and 3, as well does the index  $j$  of  $\mathcal{SU}(2)_L$ . The subscript  $a$  of  $\mathcal{SU}(3)_C$  is summed over a range of 1 to 8, and finally the spacetime index  $\mu$  takes four values; 0, 1, 2, and 3.

The last term, *h.c.* stands for *hermitian conjugate*, and it is there to ensure that the Lagrangian is a real scalar. Since in this sector all the terms are self-adjoint [64], this term can be omitted, and its presence is just a reminder nothing more.[64]

- **Yukawa Sector:**  $\mathcal{L}_{Yukawa} = \psi_i y^{ij} \psi_j \phi + h.c.$

This sector is the least trivial, especially when it comes to the quark fields. Be that as it may, it is the way fermions gain mass, it is called Yukawa coupling, and it couples left-handed and right-handed fields of fermions with the BEH field<sup>30</sup>. So, it is mandatory for a massive fermion in the SM to have a right-handed component, which neutrinos have not, yet they might have mass!

$y^{ij}$  are the 9 entries of the Yukawa  $3 \times 3$  matrix, which are free parameters of the SM to determine experimentally [60], [62, p. 40], [64]. 4 other parameters are introduced by the CKM (Cabibbo-Kobayashi-Maskawa) matrix, which determines the quarks flavor mixing, those parameters are three mixing angles  $\theta_{12}$ ,  $\theta_{13}$  and  $\theta_{23}$ , in addition to the phase  $\delta_{13}$ <sup>31</sup>, which sum up to 13 free parameters in the Yukawa sector only! [60]

The hermitian conjugate here is mandatory since the previous terms are not self-adjoint which threatens the reality of the Lagrangian. However, an interpretation of it would be that it describes the coupling of antimatter to the BEH field. [64]

- **Higgs Sector:**  $\mathcal{L}_{Higgs} = |\mathcal{D}_\mu \phi|^2 - V(\phi)$

The first term  $|\mathcal{D}_\mu \phi|^2$  of this sector describes the coupling between the BEH field  $\phi$  and the electroweak interaction fields, and as previously, the  $\mathcal{SU}(2)_L \times \mathcal{U}(1)_Y$  terms are hidden in  $\mathcal{D}_\mu$ . It is this term that

---

<sup>30</sup> We can see this as if the fermions are continually gaining and losing a unit of the weak hypercharge from and into the Higgs field, switching between their left-handed and right-handed components. And that might answer the question of what handedness do the electrons in my cup of coffee have!

<sup>31</sup> Which is the only CP-violating parameter in the SM.

gains the weak interaction bosons mass after the EWSB, while the photon is protected by the  $\mathcal{U}(1)_{EM}$  gauge symmetry group, so it stays massless.

The other term is the Higgs potential, given by Equation (1-12).

$$V(\phi) = \mu^2 \phi^\dagger \phi - \lambda (\phi^\dagger \phi)^2 \quad (1-30)$$

The minima of this potential differ depending on the sign of  $\mu^2$ . If  $\mu^2 > 0$ , i.e.  $\mu$  is not a purely imaginary complex number, then  $V(\phi)$  has only one minimum, located at the origin (Figure 1-12 (a)), and the  $\mathcal{SU}(2)_L \times \mathcal{U}(1)_Y$  symmetry is intact . However, if  $\mu$  is not a purely imaginary, then  $\mu^2 < 0$ , the  $V(\phi)$  has two non-zero minima (Figure 1-12 (b)), and the EW symmetry is spontaneously broken into the electromagnetic symmetry.[61, p. 11]

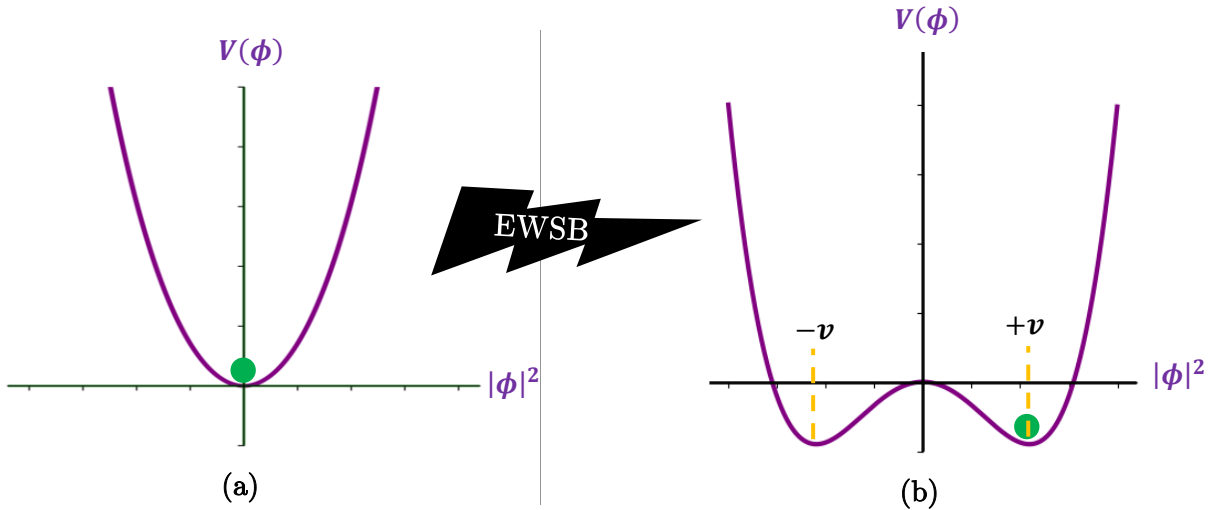
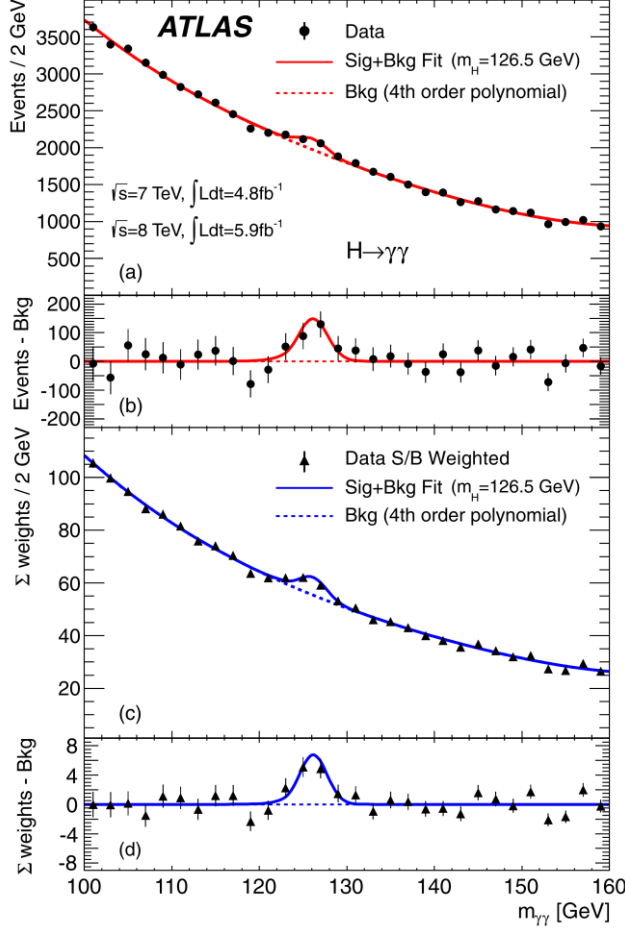


Figure 1-12: plots of the BEH potential in function of  $|\phi|^2$  in both cases, before and after the EWSB. In (a)  $\mu^2 > 0$  and the EW symmetry is intact since the vev = 0. In (b),  $\mu^2 < 0$ , the vev  $\neq 0$  and chosen to be  $+v$  breaking the EW symmetry.

## 1.3 Successes and Weaknesses of the Standard Model

### 1.3.1 The Higgs Boson Discovery

The standard model of particle physics (SM) is truly one of the most astonishing achievements that have been accomplished at all. Guided over the years by experimental evidences here, and mathematical theories there, so it can land its final form as we study it today. Besides predicting the existence of quarks, gluons, weak bosons, the precise cross-section and branching ratios calculations, and the masses of the  $W^\pm$  and  $Z^0$ , the prediction of the existence of the Higgs scalar field that has a non-zero vacuum expectation value (vev), i.e. there is Higgsiness everywhere, stays one of the biggest prediction of the SM, and the discovery of the Higgs Boson in 2012 (Figure 1-13) is the ultimate success of this Model.



**Figure 1-13:** The discovery of the Higgs boson by the ATLAS detector at an energy of 126.5 GeV, decayed into two energetic photons. (Credit to ATLAS collaboration/CERN)

However, The SM is not perfect, and some observed phenomena cannot have an explanation in its framework, and we have already mentioned some, and below we stress some others in no particular order.

### 1.3.2 No Gravity!

Gravity does not have its place in the Standard Model as a fundamental interaction, since the hypothetic graviton was never observed.

### 1.3.3 Masses of Neutrinos

As we have mentioned in section 1.2.3 while discussing the Yukawa sector, there are no right-handed neutrinos in the SM (c.f. footnote 24) which means that the neutrinos of the SM are massless. Massless particles are moving in space with the speed of light (at the vacuum), so they are frozen in time (since the faster you travel in space the slower you move in time), and this means they experience no time at all, hence they cannot evolve nor change. However, neutrinos have been observed to oscillate between the three generations, and this is considered as a direct evidence of them having mass, and a flaw in the SM. [63]

There are multiple models beyond the SM providing a mechanism to explain the observed mass of neutrinos. A remarkable one is the *One-loop Type II Seesaw Mechanism*, which provides not only an explanation of how neutrinos get massive but also a stable candidate for Dark Matter [67].

### 1.3.4 Matter Anti-matter Asymmetry

The CP violation is manifested in the matter anti-matter asymmetry observed in our universe [42], [68]. The big bang theory predicts equal amounts of matter particles and their antiparticles constituting the antimatter, which means that the world should be empty containing only the energy and some photons left from the annihilation processes. However, our universe as we observe it today is made of matter, and only a few antiparticles are observed here and there before they quickly annihilate with the corresponding particles.

One may suggest that there might be some entire galaxies far away, formed only from antimatter [69] (shall we call them anti-galaxies?) just like matter particles from our Milky Way. Nevertheless, astrophysicists think that the making of such galaxies would have left some fingerprints and disturbances in the cosmic microwave background, so maybe mapping the big bang just a few moments after it happened might answer this open question.

On the other hand, the only way the CP violation is taken into account in the SM is through the weak interactions, using the free parameter  $\delta_{13}$  introduced in the CKM matrix as we have mentioned earlier [60, p. 47]. However, the predicted difference is not enough to explain all the matter we see around us today.

### 1.3.5 Hierarchy Problem

The hierarchy problem can be seen from different angles and perspectives, it may refer to the very huge gap between the strengths of the gravity force and the other three forces (Table 1-8), as it can be related to the cosmological constant and the Planck mass [70]. However, as the previous two perspectives do involve gravity, it seems to me that those are not really the SM's problems. So, the hierarchy problem that is left to discuss is the one related to the Higgs boson's mass, where its fundamental value suggested by the SM is way different than the effective value measured by the experiment. The two are related by the renormalization process that applies corrections to the former in a way to get the latter. [61]

$$m_h^2 = m_{h,0}^2 + \Delta m_h^2 \quad (1-31)$$

Where  $\Delta m_h^2$  are the contributions of all the SM particles to the Higgs mass, one is the Top quark that is the heaviest particle of the SM, with a mass that exceeds 170 GeV.

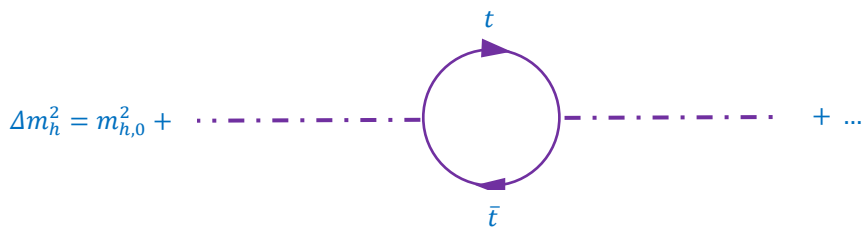


*Figure 1-14: the contribution of the Top-quark loop to the effective Higgs mass*

In absence of any internal symmetry protecting it, this process suggests a Higgs boson with a mass of  $10^{19} GeV$  (the Planck mass), which is huge compared to the measured mass ([Figure 1-13](#)) [61].

### 1.3.6 Dark Matter and Dark Energy

The term “Dark” in physics is usually used to describe things that we know nothing about. Actually, no! Dark matter is a matter that does not interact through electromagnetic force, it emits neither absorbs light, and that is why we call it *dark*, its existence is only known through their immense gravitational effects, capable of bending even light<sup>32</sup> [71]. Using the Einstein lens, astrophysicists can conclude the mass of this invisible matter, and they conclude that it makes 85% of the matter in the universe, while everything we see, using our eyes, our telescopes, or any other detector, accounts for the remaining 15% [71]. Also, to explain the accelerated expansion of the universe, astrophysicists invented an unknown form of energy that they called Dark Energy, which opposes to the attractive gravitational effect of matter [72]. Dark Energy is thought to form 68% of the universe, so that DM makes up 27%, and the remaining 5% is all that the SM can explain (not so perfectly though) [72].

### 1.3.7 So Many Free Parameters

The SM has a bunch of parameters that are not predicted by the theory, and the only way to reach their values is the experience. Such parameters are called *free parameters*, there are 18 of them in the SM, and we have already mentioned 13 in the Yukawa sector. The remaining five are,  $\alpha$  the coupling strength of the electromagnetic force,  $g_3$  the coupling constant of the strong force, Weinberg angle  $\theta_W$ ,  $\lambda$  in the Higgs potential, and at last  $v$  the vacuum expectation value of the Higgs field.

### 1.3.8 The Holy Grail of Unification

It is a common belief that at the very beginning, the three fundamental forces were all unified as a fundamental interaction with possibly many force carriers yet with one and only coupling constant [73]. However, the SM only predicts a two by two unification at high energies, but the three coupling constants are not all unified and even diverge! ([Figure 1-15](#))

Unifying the three fundamental forces of the SM in a supersymmetric Grand Unified Theory (GUT) is the first step to walk if we wish to unify all the fundamental forces in the framework of a Theory of Everything (ToF).

---

<sup>32</sup> Mass is energy at the end!

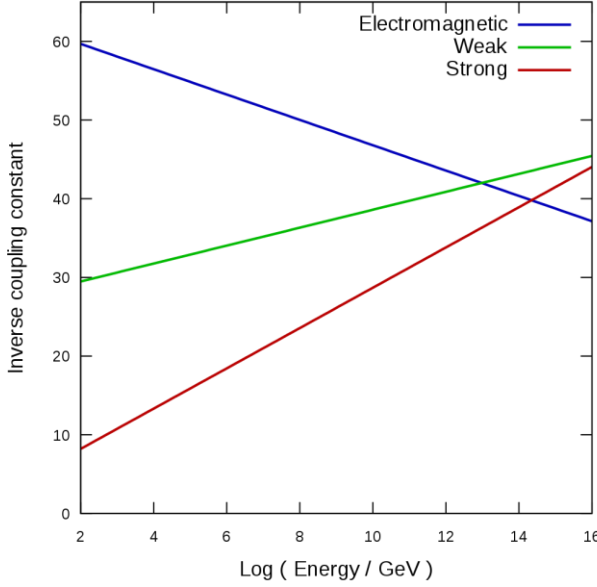


**Figure 1-15:** the evolution of the inverse of coupling constants of the three fundamental forces described by the SM in function of the energy levels. The couplings do not all meet at high energies. (credit to Victor Blacus)

## 1.4 Beyond the Standard Model (BSM)

In order to answer the previous open questions and others, many theories and models have been developed over the last decades. Namely, the supersymmetry (SuSy) that addresses the hierarchy problem and beautifully solves it by adding to each particle a superpartner (sparticle bosons) canceling its contribution to the effective Higgs mass [61]. Also, it saves the string theory from being an only-for-bosons theory (even if it contains the graviton), and it expands it to a superstring theory, generating all the fermionic and bosonic states as a candidate to a theory of everything [74, p. 141]. However, these theories and others are out of this work's scope, our main interest is the BSM theories that provide additional heavy gauge bosons, at the top of it the GUTs.

The first theoretical framework that has introduced an additional gauge boson BSM was the Sequential Standard Model (SSM) [75], where a new gauge boson called  $Z'$  has the same couplings as  $Z^0$  of the SM but much heavier, with a polar mass lying in the range of the TeV. In terms of the gauge symmetry group, an additional  $U(1)'$  symmetry group is added to the one of the SM (c.f. Eq. (1-8)) to form the SSM symmetry group (Eq. (1-32)).

$$\mathcal{P} \times \mathcal{SU}(3)_C \times \mathcal{SU}(2)_L \times \mathcal{U}(1)_Y \times \mathcal{U}(1)' \quad (1-32)$$

On the other hand, the GUTs are based on much bigger gauge groups (called the grand unification groups) like the  $SU(5)$  [76],  $SO(10)$  [77], [78], and the  $E_6$  [75], [77]. These groups give birth to additional gauge vector bosons through their decompositions to smaller gauge groups.

The decomposition of the  $E_6$  gauge group is given by:

$$E_6 \rightarrow \mathcal{SO}(10) \times \mathcal{U}(1)_\psi \rightarrow \mathcal{SU}(5) \times \mathcal{U}(1)_\psi \times \mathcal{U}(1)_\chi \quad (1-33)$$

Where our  $Z'$  new gauge boson is defined as a mixing of the two additional  $\mathcal{U}(1)$  groups (Eq. (1-34)), while the mixing angle  $\theta$  reflects how  $Z'$  is supposed to couple to different SM leptons.

$$Z'(\theta) = Z'_\psi \cos \theta + Z'_\chi \sin \theta \quad (1-34)$$

Another model involving the  $Z'$ , in addition to two other new gauge bosons  $W'^\pm$ , is the Left-Right Symmetric Model (LRM) [79]. The LRM is one of the simplest extensions of the SM, where a right-handed  $\mathcal{SU}(2)_R$  group is associated with the SM  $\mathcal{SU}(2)_L$ . In other words, to each left-handed SM lepton, there is a right-handed lepton, so in this context, the SM neutrinos family is extended to contain three right-handed neutrinos, solving the puzzle of the neutrino's oscillations and mass.

The gauge group of the LRM is as given in Eq (1-35).

$$\mathcal{SU}(3)_C \times \mathcal{SU}(2)_L \times \mathcal{SU}(2)_R \times \mathcal{U}(1)_{B-L} \quad (1-35)$$

The search of a  $Z'$  boson resonance in  $t\bar{t}t\bar{t}$  final state events, currently taking place at the ATLAS experiment, is a non-model-based study. i.e. they are first looking for deviations from the SM expectations, then if some bumps in the plots are discovered, the models fitting to the properties of the newly discovered heavy boson will be adopted, otherwise, a lower limit will be established for the mass of the  $Z'$ , eliminating some theoretical models from the list<sup>33</sup>. For these reasons, and for the sake of brevity, we stop at this level, leaving elaborated descriptions of these models for future work.

---

<sup>33</sup> Which means that in experimental physics, “no discoveries” are actually “new discoveries”.

## Chapter 2

# Top Quark (New)Physics

*We discovered the top quark, not in one lightning stroke, but over a long period of time, event by event.*

Nick Hadley, DØ physicist

*Smart lad, to slip betimes away from fields where glory does not stay, and early though the laurel grows, it withers quicker than the rose.*

AE Housman, “To an Athlete Dying Young”

The heaviest particle of the SM was theorized back in 1973 [42], named Top quark in 1975 [43], and discovered in 1995 by the two experiments along the Tevatron accelerator, DØ [49] and CDF [48] (c.f. section 1.1.1.6).

Due to its memorable mass of  $173.2 \pm 0.9 \text{ GeV}$ , the chubby top quark has a unique coupling to the Higgs boson (strong Yukawa coupling) that almost equals 1 [80, p. 20].

$$y_t = \frac{\sqrt{2}m_t}{v} \approx 1 \quad (2-1)$$

Where  $v$  is the  $v\bar{v}v$  of the Higgs field, as mentioned before.

Furthermore, the top quark stands out from the other flavors with its very short lifetime which is about  $5.0 \times 10^{-25} \text{ s}$ . Such a lifetime is significantly shorter than what we call the hadronization time that is in the range of  $10^{-23} \text{ s}$ , and this is why the Top decays before it can form a hadron.

All the above makes the top quark of high importance and gravity to researches beyond the SM (BSM). Deviations in the SM predictions on the production and/or the decay of the top quark may be strong signs for its coupling to new and undiscovered particles, a  $Z'$  gauge boson for example!

In this chapter, we will introduce some properties of the Top quark ( $t$ ), namely its production modes and its decay channels. Since this work investigates the four-top production BSM, we will introduce both  $t\bar{t}$  and  $t\bar{t}t\bar{t}$  productions in the SM and beyond. The recently announced discovery of ATLAS in the LHC P2020 of a spectacular four-top production will be visited.

## 2.1 Top Quark Production

The top quark can be produced as a single quark via electroweak processes accompanied with a b quark and a W boson. However, it is more likely to be produced as  $t\bar{t}$  pairs through the strong interactions. In both cases, the cross-section of the top quark depends essentially on the collision energy that can be reached by the accelerator. [81, p. 14]

In the QCD, the  $t\bar{t}$  pair production can be through two different kinds of processes,  $q\bar{q}$  annihilation or gluon-gluon fusion (Figure 2-1). In  $pp$  collisions, as the ones happening in the LHC, the gluon-gluon fusion processes dominants those of  $q\bar{q}$  annihilation with almost 90% at  $\sqrt{s} = 14 \text{ eV}$ .

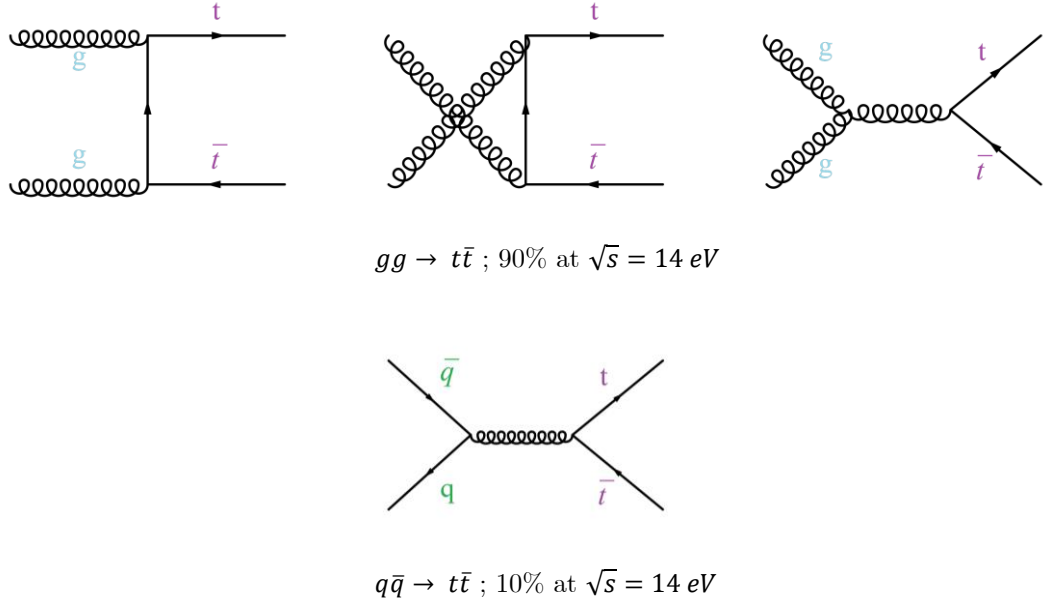


*Figure 2-1: Feynman Diagrams of the Leading-Order (LO) production mechanisms of the  $t\bar{t}$  pairs. The given proportions are for  $pp$  collisions with an energy of  $\sqrt{s} = 14 \text{ TeV}$ .*

### 2.1.1 Top Quark Pair Cross Section $\sigma_{t\bar{t}}$

The mass of the top quark can be experimentally measured in two separate ways, either directly, by measuring the decay products (kinematic mass reconstruction) or, indirectly, by using cross-section measurement. Moreover, any significant difference between the two measured values can be a strong evidence of new physics (NP) (Figure 2-2), and this motivates many searches of measuring the top quark pair cross-section to a high precision, where a complete NNLO calculation is mandatory.

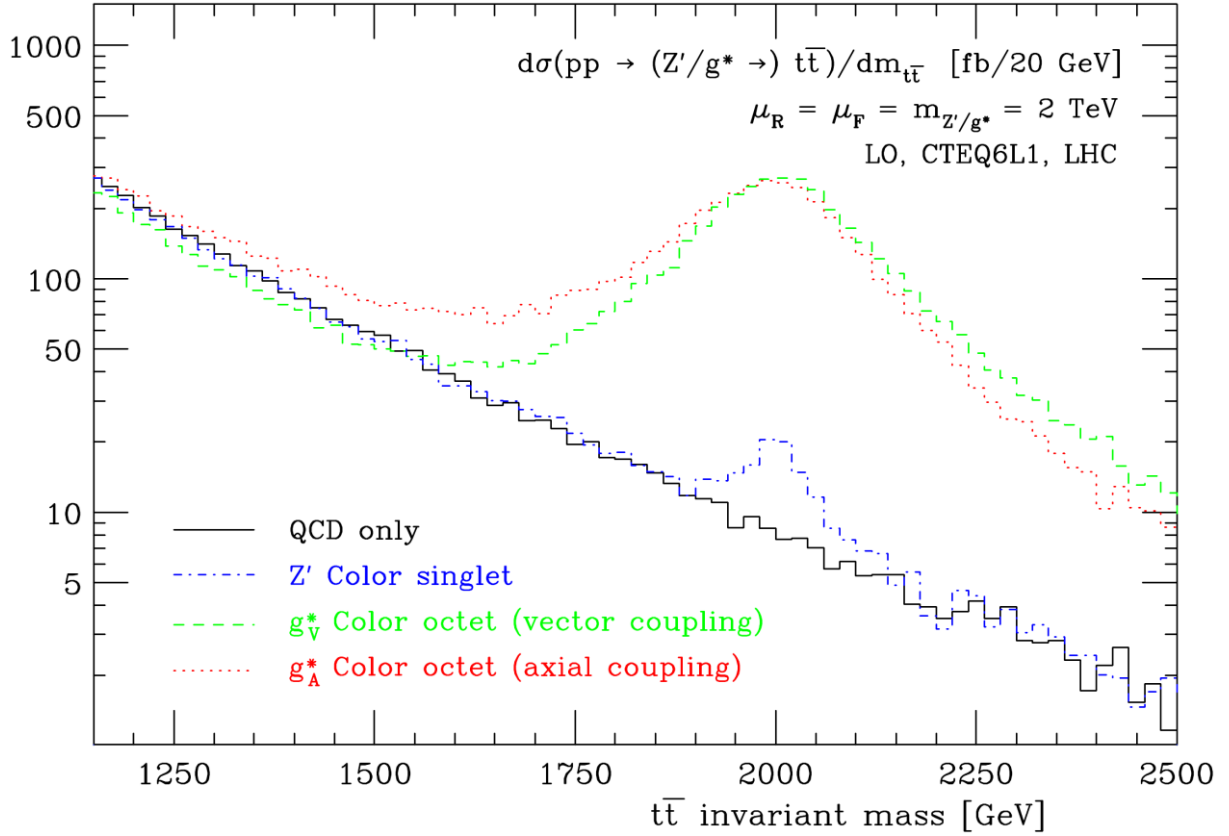


**Figure 2-2:** Theoretical spectrum of  $t\bar{t}$  pair mass in different frameworks. The “QCD only” plot refers to the SM predictions. At a mass of 2 TeV, models with additional colorless gauge boson  $Z'$  present a bump. So, if data shows such a bump it would be evidence for a new particle discovery. figure taken from [82, p. 18]

The cross-section calculations rely on the factorization theorem [82, p. 24], where the total cross-section  $\sigma(s, m_t)$  is separated into two parts (equation (4-3)); short distance part  $\hat{\sigma}_{t\bar{t}}$  and a long distance part  $\phi_{i,A}$  called the Parton Distribution Function (PDF), (the two parts are also known as hard and soft parts respectively).

$$\sigma(s, m_t) = \sum_{i,j} \int_0^1 \int_0^1 dx_1 dx_2 \phi_{i,A}(x_1, \mu_F) \phi_{j,B}(x_2, \mu_F) \hat{\sigma}_{ij \rightarrow t\bar{t}} \left( \frac{m_t^2}{\hat{s}}, \mu_R, \mu_F, \alpha_s(\mu_R) \right) \quad (2-2)$$

Where,

A and B are the hadrons in collision.

$\phi_{i,A}(x_1, \mu_F)$  : the PDF, and it refers to the probability to find a parton  $i$  (quark or gluon) within a hadron A with a longitudinal momentum portion of  $x_1$  (i.e.  $x_1 = \frac{p_i}{p_A}$ ) at a scale  $\mu_F$ . PDFs are universal and obtained experimentally.

$s$ : the accelerator energy.

$\hat{s} = s x_1 x_2$  : is the center of the mass-energy of the partons in interaction.

$\mu_F$  and  $\mu_R$  : are respectively the factorization and renormalization scales.

$\alpha_s$  : the strong coupling constant.

$m_t$ : the mass of top quark.

However, for fixed order approximations, like the leading order (LO), the next-to-leading order (NLO), and the next-to-next-to-leading order (NNLO), we use the Feynman rules and his diagrams to calculate the differential cross-section of a given process.

At LO, the Feynman diagrams of the top quark pair production are given in [Figure 2-1](#), the  $q\bar{q}$  annihilation channel corresponds to the following cross-section:

$$\frac{d\sigma_{q\bar{q} \rightarrow t\bar{t}}}{dt} = \frac{4\pi\alpha_s^2}{9s^4} [(m^2 - t)^2 + (m^2 - u)^2 + 2m^2s] \quad (2-3)$$

While the other three diagrams of the gluon-gluon fusion all contribute to the following expression of the cross-section:

$$\begin{aligned} \frac{d\sigma_{g\bar{g} \rightarrow t\bar{t}}}{dt} = & \frac{\pi\alpha_s^2}{8s^2} \left[ \frac{6(m^2 - t)(m^2 - u)}{s^2} - \frac{m^2(s - 4m^2)}{3(m^2 - t)(m^2 - u)} \right. \\ & + \frac{4}{3} \frac{(m^2 - t)(m^2 - u) - 2m^2(m^2 + t)}{(m^2 - t)^2} \\ & + \frac{4}{3} \frac{(m^2 - t)(m^2 - u) - 2m^2(m^2 + u)}{(m^2 - u)^2} \\ & - 3 \frac{(m^2 - t)(m^2 - u) - m^2(u - t)}{s(m^2 - t)^2} \\ & \left. - 3 \frac{(m^2 - t)(m^2 - u) - m^2(t - u)}{s(m^2 - u)^2} \right] \end{aligned} \quad (2-4)$$

Where,  $s$ ,  $u$ , and  $t$  are the well-known Mandelstam variables, and they are given in function of the momenta of the ingoing and the outgoing particles in the Feynman diagrams, by:

$$s = (p_1 + p_2)^2 \quad (2-5)$$

$$u = (p_1 - p_4)^2 \quad (2-6)$$

$$t = (p_1 - p_3)^2 \quad (2-7)$$

Nevertheless, in LO the scale uncertainty of the total top pair cross-section is unacceptable and exceeds 50% [[82, p. 35](#)], which requires a further correction, like the NLO.

In 1987, P. Nason, S. Dawson, and R. K. Ellis were able to perform a complete NLO calculation for the total top quark pair production cross-section, with the uncertainty being reduced from 50% to 15%. [[83](#)]

Even if 15% is still quite a large uncertainty, no *complete* calculation of the total top quark pair production cross-section in orders higher than NLO is ever done. However, different techniques can be used for higher-order approximations, such as *Langenfeld, Moch, Uwer* [84], [85], *Kidonakis* [86], *Ahrens et al.* [87], *Beneke et al.* [88], and *Cacciari et al* [89]. The results obtained by these techniques are shown in Figure 2-3.

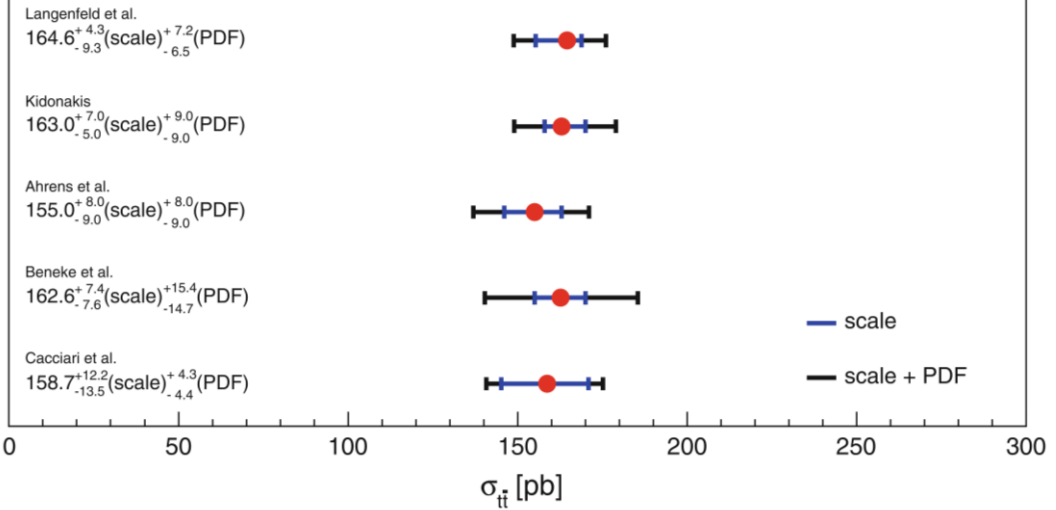


**Figure 2-3:** theoretical predictions for  $t\bar{t}$  pair production with different NNLO approximations. Predictions are done for  $pp$  collisions at  $\sqrt{s} = 7$  TeV. Figure taken from [81, p. 17]

The measurements of the  $\sigma_{t\bar{t}}$  in function of  $\sqrt{s}$  are summarized in Figure 2-4, as well as the theoretical prediction done at NNLO+NNLL for  $pp$  collisions (like in the LHC) and  $p\bar{p}$  (like the ones that were happening in the Tevatron).

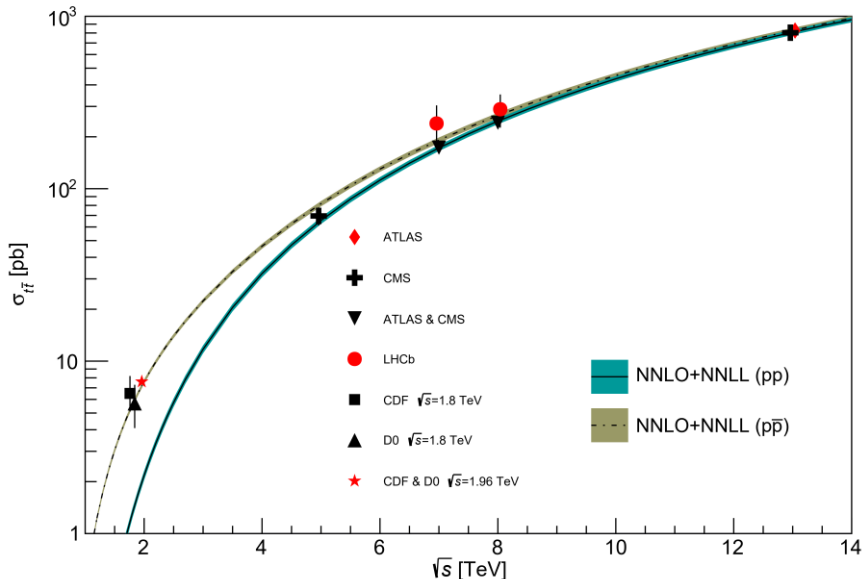


**Figure 2-4:** Measurements and predictions of  $\sigma_{t\bar{t}}$  in function of  $\sqrt{s}$  for  $m_{top} = 172.5$  GeV. CDF and D $\emptyset$  measurements are taken from [90], [91] for  $\sqrt{s} = 1.8$  TeV and from [92]–[94] for  $\sqrt{s} = 1.96$  TeV, ATLAS and CMS data points are taken from [95]–[98], while those of LHCb are extracted from [99]. Finally, the theoretical predictions are based on [100]. Figure taken from [101, p. 743]

As can be seen in the above figure, at  $\sqrt{s} = 13 \text{ TeV}$ ,  $\sigma_{t\bar{t}}$  is measured to exceed 800 pb. In this work, we are interested more in the production of four-top quarks  $t\bar{t}t\bar{t}$ , a very rare event predicted by the SM but has never been observed, until later in this year when the ATLAS Collaboration announced strong evidence for  $t\bar{t}t\bar{t}$  production in the multilepton final state [102].

## 2.1.2 Production of Four-Top Quarks $t\bar{t}t\bar{t}$ in the SM

In the SM, we use a perturbative approach at high energies to calculate the cross-section (or other quantities), and by taking higher-order effects into account, our predictions can be improved to impressive precisions. Some useful perturbative approaches we did mention before are the *fixed-order calculations*, such as LO, NLO, NNLO ... involving expansion in powers of the strong and electroweak coupling constants  $\alpha_s$  and  $\alpha$  taking the values 0.1 and 0.01, respectively, at the TeV scale.

A complete-NLO prediction for  $t\bar{t}t\bar{t}$  production in proton-proton collisions at 13 TeV (for the LHC<sup>34</sup>) has been calculated to be  $\sigma_{t\bar{t}t\bar{t}} = 12.0 \pm 2.4 \text{ fb}$  [103] in the framework of the SM (QCD+EW corrections). Comparing  $\sigma_{t\bar{t}t\bar{t}}$  to  $\sigma_{t\bar{t}}$  (in the range of 800 pb = 0.8 fb) we can see how rare is a  $t\bar{t}t\bar{t}$  production event. In fact, such event occurs only once for every 70 thousand  $t\bar{t}$  event at the LHC. [104]

While in LO calculations involve only the tree-level diagrams (Figure 2-5), NLO predictions are calculated taking also the one-loop diagrams into consideration (Figure 2-6), as well as all tree-level diagrams with an emission of one additional quark, gluon, or photon. [103, p. 4]

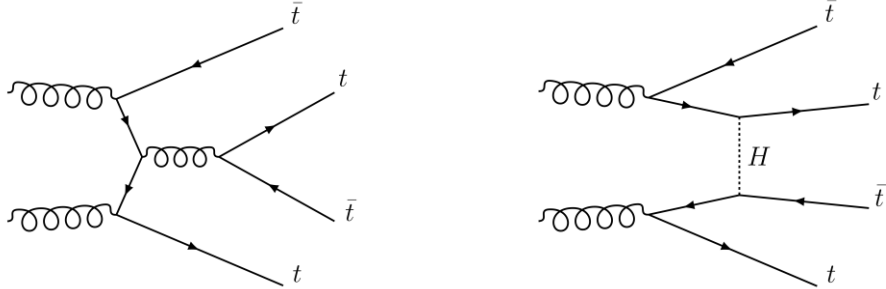


*Figure 2-5: Examples of tree-level diagrams of  $gg \rightarrow t\bar{t}t\bar{t}$  in the SM. [103, p. 7]*

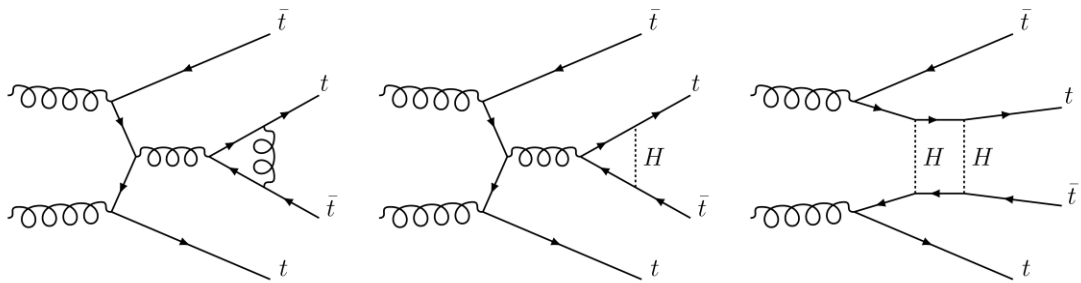


*Figure 2-6: Examples of one-loop diagrams of  $gg \rightarrow t\bar{t}t\bar{t}$  in the SM. [103, p. 7]*

---

<sup>34</sup> In the same paper, calculation have been done also for an energy of 100 TeV for future colliders.

On the morning of Sunday 29-04-2018 at 10:53 CEST, a very rare and challenging four-top quarks event might be detected by the ATLAS detector (Figure 2-7). In a paper released recently, the ATLAS Collaboration announced strong evidence for  $t\bar{t}t\bar{t}$  production in the multilepton final state using an integrated luminosity of  $139 \text{ fb}^{-1}$  of pp collisions data at  $\sqrt{s} = 13 \text{ TeV}$  [102]. The observed significance with respect to the background-only hypothesis is 4.3 standard deviation, while the expected significance is measured to be 2.4.  $\sigma_{t\bar{t}t\bar{t}}$  is measured to be  $24^{+7}_{-6} \text{ fb}$ . This experimental value is conforming with the SM prediction ( $12.0 \pm 2.4 \text{ fb}$ ) with a standard deviation of 1.7.

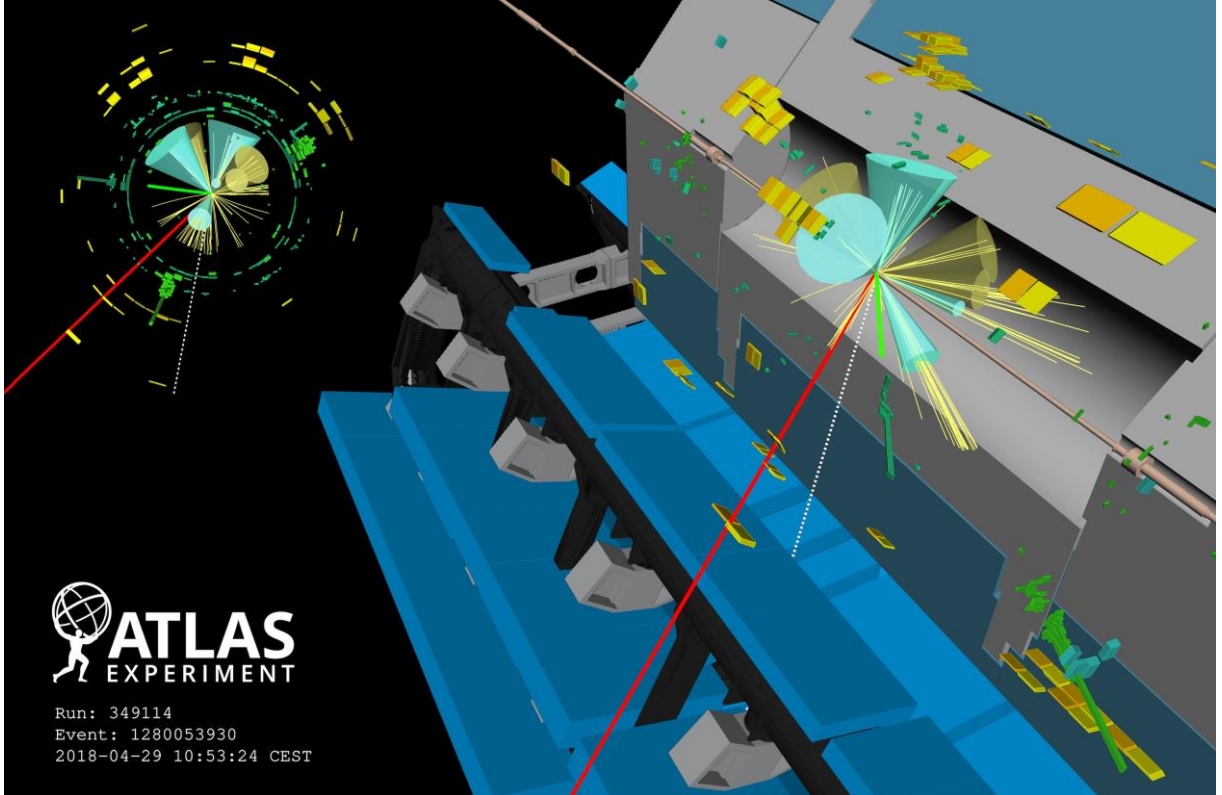


**Figure 2-7:** Event display of a candidate four-top-quark event in a semi-leptonic final state, where two of the top quarks decay leptonically (giving birth to a muon in red and one electron in green), while two others decay hadronically. This is the heaviest particle final state ever seen at the LHC, with almost 700 GeV in total. (Credit to ATLAS Experiment © CERN)

### 2.1.3 Production of Four-Top Quarks $t\bar{t}t\bar{t}$ BSM

Many models BSM involve additional gauge bosons out of the SM, that strongly interact with the heaviest particle of the SM; the top quark, opening a new gate to NP. As examples of these models, we find the simplest extension of the SM, the two Higgs Doublet Models (2HDM) [105]–[107], left-right extensions of the SM [108], and others. These models provide new particles that can couple to the top sector, and this coupling might be illustrated as heavy resonances (in the scale of TeV), and this motivates us to look after  $t\bar{t}$  resonant states as they are the heaviest  $q\bar{q}$  states of the SM.

Based on the paper in reference [109], we will focus on the tree-level production of four-top quarks  $t\bar{t}t\bar{t}$ , where a  $t\bar{t}$  pair was originated from the gluon-gluon fusion, and they are called *spectators*, while the

other  $t\bar{t}$  pair is issued from the decay of a top-philic<sup>35</sup> color singlet vector resonance, and they are named the *hardest top quarks*. Such a production process is illustrated in Figure 2-8.

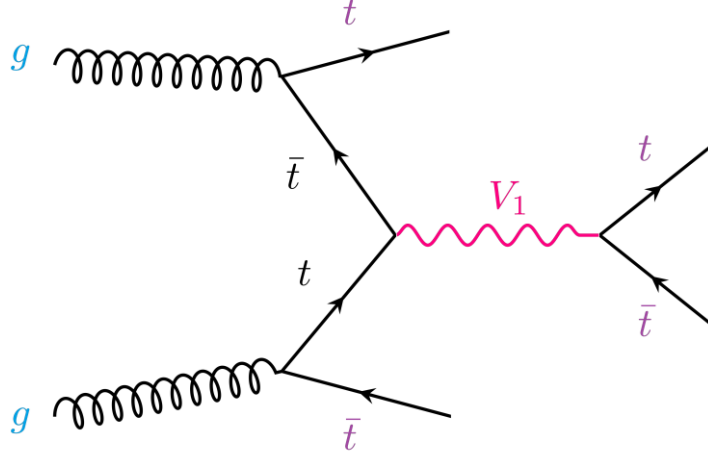


**Figure 2-8:** A four-top quark production process beyond the SM. The  $V_1$  is a color singlet (so that the color charge is conserved at the two vertices) vector boson BSM.

The coupling of  $V_1$  with the  $t\bar{t}$  pair is described with the following interaction part of the Lagrangian [109, p. 2]:

$$\mathcal{L}_{int} = \bar{t}\gamma_\mu(c_L P_L + c_R P_R)t V_1^\mu \quad (2-8)$$

Where,

$P_{R/L} = \frac{1 \pm \gamma^5}{2}$  are the projection operators used for extracting the right/left-handed components of the top field.

$c_{R/L}$ : are the coupling constants of the right/left-handed top quarks with the vector singlet  $V_1^\mu$ .

We can define the chirality angle  $\theta$  and the global coupling constant  $c_t$  of  $V_1^\mu$  with the top quark as following [109, p. 2]:

$$\tan \theta = \frac{c_R}{c_L} \quad (2-9)$$

$$c_t = \sqrt{(c_R)^2 + (c_L)^2} \quad (2-10)$$

Projecting (2-9) and (2-10) in (2-8), we obtain:

---

<sup>35</sup> A resonance that couples primarily to the top quark, and weakly to the other quarks, in a way that we can ignore any other couplings rather than those with the top quark.

$$\mathcal{L}_{int} = c_t \bar{t} \gamma_\mu (\cos \theta P_L + \sin \theta P_R) t V_1^\mu \quad (2-11)$$

The production of a  $t\bar{t}$  pair is originated from the decay of  $V_1$  color singlet vector boson, as mentioned earlier. The decay width of  $V_1$  to  $t\bar{t}$  is given by [109, p. 2]:

$$\Gamma(V_1 \rightarrow t\bar{t}) = \frac{c_t^2 M_{V_1}}{8\pi} \sqrt{1 - \frac{4m_t^2}{M_{V_1}^2}} \times \left[ 1 - \frac{m_t^2}{M_{V_1}^2} (1 - 3 \sin(2\theta)) \right] \quad (2-12)$$

Where  $M_{V_1}$  is nothing but the mass of the resonance  $V_1$ , being in the range of the TeV [109, p. 2], the heaviest particle of the SM is dwarfed by the new vector boson.  $m_t \ll M_{V_1}$ , hence,  $\frac{m_t^2}{M_{V_1}^2}$  is even smaller and can be neglected compared to one. The expression of the  $\Gamma(V_1 \rightarrow t\bar{t})$  becomes:

$$\Gamma(V_1 \rightarrow t\bar{t}) \approx \frac{c_t^2 M_{V_1}}{8\pi} \quad (2-13)$$

In particle physics, there are two key measurements that are important to understand a particle-production process; the transverse momentum  $p_T$  and the pseudo-rapidity  $\eta$  [110, p. 2].  $p_T$  spectra provide crucial information about the Quark-Gluon Plasma (QGP) created at the collision point, while  $\eta$  spoils essential clues about the geometry of the early system just after the collision [110, p. 2].

In (Figure 2-9), the theoretical predictions of  $p_T$  and  $\eta$  of the four tops, the two spectators and the two hardest top quarks, are plotted.

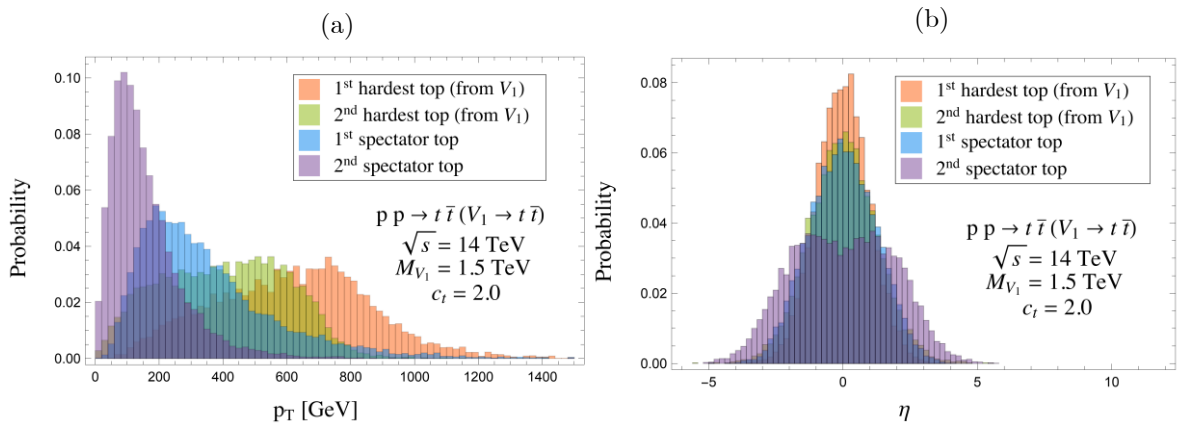


**Figure 2-9:** (a) The transverse momentum spectra of the four-top quarks for a resonance mass of 1.5 TeV and coupling constant  $c_t = 2.0$ . We notice that the first hardest top has a peak at almost  $M_{V_1}/2$ , the second hardest top peaks at a little lower value, and while the first spectator top peaks at a value slightly higher than  $m_t \approx 173$  GeV the other spectator has a peak at a value slightly lower than  $m_t$ . (b) The pseudo-rapidity presents a symmetry as supposed. Figures taken from [109, p. 3]

## 2.2 Top Quark decay

As we have discussed at the opening of section 2.1, the top quark can be produced either via electroweak interactions or via the strong ones, with the latter being more likely to occur than the former. However, the decay process of the top quark always involves the electroweak interaction, being the only force able to change the flavor of quarks. In the framework of the SM, the top quark decays into a down-type quark (d, s, or b) and a W boson, via the following processes:

$$t \rightarrow W^+ + q \quad (2-14)$$

$$\bar{t} \rightarrow W^- + \bar{q} \quad (2-15)$$

Where  $q = d, s, b$ .

The probability of each process is related to the square of the three elements of the CKM matrix (determining the quarks flavor mixing, c.f. the Yukawa sector in section 1.2.3) involving a top quark and a down-type quark, i.e.  $|V_{td}|^2$ ,  $|V_{ts}|^2$ , and  $|V_{tb}|^2$ . The latest values of the nine magnitudes of the CKM elements (March 2020) are measured in [101, Ch. 12]. Moreover, using a global fit and imposing the three generation unitarity constraint of the SM, we obtain the final form of the CKM matrix (4-3) [101, p. 266].

$$V_{CKM} = \begin{pmatrix} 0.97401 \pm 0.00011 & 0.22650 \pm 0.00048 & 0.00361^{+0.00011}_{-0.00009} \\ 0.22636 \pm 0.00048 & 0.97320 \pm 0.00011 & 0.04053^{+0.00083}_{-0.00061} \\ 0.00854^{+0.00023}_{-0.00016} & 0.03978^{+0.00082}_{-0.00060} & 0.999172^{+0.000024}_{-0.000035} \end{pmatrix} \quad (2-16)$$

The branching ratio (BR) of the  $t \rightarrow W + b$  process is:

$$\mathcal{BR}(t \rightarrow W + b) = |V_{tb}|^2 = 0.998344685584 \approx 99.83\% \quad (2-17)$$

Compared to such a branching ratio, the other branches can be neglected and the top quark decays almost always to a  $b$  quark and a  $W$  boson, with the decay of this latter determines the different channels of the top quark decay.

### 2.2.1 Single Top Decay

After  $\sim 5 \times 10^{-25} s$  of its production, the top quark decays into a  $W$  boson and a  $b$  quark. In fact, the decay width of the top quark in NLO is given by [111, p. 12]:

$$\Gamma_t = \frac{G_F}{(\hbar c)^3} \frac{m_t^3}{8\pi\sqrt{2}} |V_{tb}|^2 \left(1 - \frac{M_W^2}{m_t^2}\right)^2 \left(1 + 2\frac{M_W^2}{m_t^2}\right) \left[1 - \frac{2\alpha_s}{3\pi} \left(\frac{2\pi^2}{3} - \frac{5}{2}\right)\right] \quad (2-18)$$

Where,  $G_F(\alpha_s)$  is the Fermi (strong) coupling constant,  $m_t$  ( $M_W$ ) is the mass of the top quark (W boson).

Taking the value of  $|V_{tb}|^2$  in (2-17) in consideration, we can assume that  $|V_{tb}| \approx 1$ , and for  $m_t = 172.5 \text{ GeV}$ , the value of  $\Gamma_t$  in NLO is 1.33 GeV [111, p. 12], to which corresponds a lifetime  $\tau_t$  given by:

$$\tau_t = \frac{\hbar}{\Gamma_t} = \frac{6.5821 \times 10^{-16}}{1.33 \times 10^9} = 4.95 \times 10^{-25} \text{ s} \quad (2-19)$$

The produced W boson can decay either leptonically or hadronically, in total it has nine decay modes, three of them are leptonic while the remaining six are hadronic modes. Explicitly,  $W^+$  decays to one of the nine following products;  $(e^+ \nu_e)$ ,  $(\mu^+ \nu_\mu)$ ,  $(\tau^+ \nu_\tau)$ ,  $(u_r \bar{d}_r)$ ,  $(u_b \bar{d}_b)$ ,  $(u_g \bar{d}_g)$ ,  $(c_r \bar{s}_r)$ ,  $(c_b \bar{s}_b)$ , or  $(c_g \bar{s}_g)$ , while  $W^-$  decays to  $(e^- \bar{\nu}_e)$ ,  $(\mu^- \bar{\nu}_\mu)$ ,  $(\tau^- \bar{\nu}_\tau)$ ,  $(d_r \bar{u}_r)$ ,  $(d_b \bar{u}_b)$ ,  $(d_g \bar{u}_g)$ ,  $(s_r \bar{c}_r)$ ,  $(s_b \bar{c}_b)$ , or  $(s_g \bar{c}_g)$ , and theoretically, each of the nine decays occurs with the same frequency, so they all have the same BR 11.11 %.

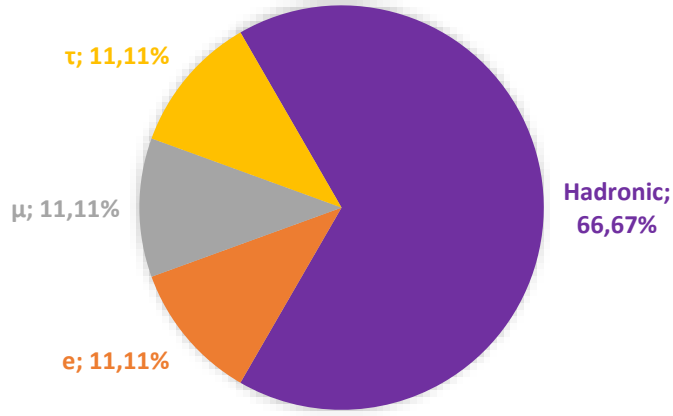


Figure 2-10: Pie chart displaying the BRs of a single top quark decay processes.

### 2.2.2 $t\bar{t}$ Quark Pair Decay

As we have discussed in section 2.1, the top quark is more likely to be produced in  $t\bar{t}$  pairs rather than a single quark. In this subsection, we give the different decay products of a  $t\bar{t}$  quark pair as well as their branching ratios.

Relying on the decay products of the W boson, the final state of  $t\bar{t}$  can be classified into three major channels; fully hadronic, dilepton, and single lepton channel.

**Fully hadronic:** both W bosons decay hadronically, and since the BR of each one is 66.67%, the BR of this channel is  $0.6667 \times 0.6667 = 0.4445$  hence,  $\mathcal{BR}_{had} = 44.45\%$ .

**Dilepton channel:** both W bosons decay leptonically. However, having three distinguishable leptons ( $e, \mu, \tau$ ) we should specify if the two W bosons decay to the same lepton ( $ee, \mu\mu$ , and  $\tau\tau$ ), and in this

case, the BR is  $0.1111 \times 0.1111 = 1.23\%$ , or if they decay into two different leptons ( $e\mu$ ,  $\tau\mu$ ,  $e\tau$ ), and in this case, we should multiply by a factor of two (since  $ll' \equiv l'l$ ) and the  $\mathcal{BR}_{ll'} = 2.46\%$ . All said, the BR of the dilepton channel is  $\mathcal{BR}_{2l} = 3 \times (1.23 + 2.46)\% = 11.07\%$ .

**Single lepton channel:** one boson decays hadronically while the other decays leptonically, so we have three outcomes;  $e + jet$ ,  $\mu + jet$ , and  $\tau + jet$ , the BR of each one is  $0.1111 \times 0.6667 \times 2 = 0.1482 = 14.82\%$  (the factor two is there since  $l + jet = jet + l$ ), so this channel has a  $\mathcal{BR}_{l+jet} = 3 \times 14.81\% = 44.46\%$ .

The above results are summarized in [Figure 2-11](#).

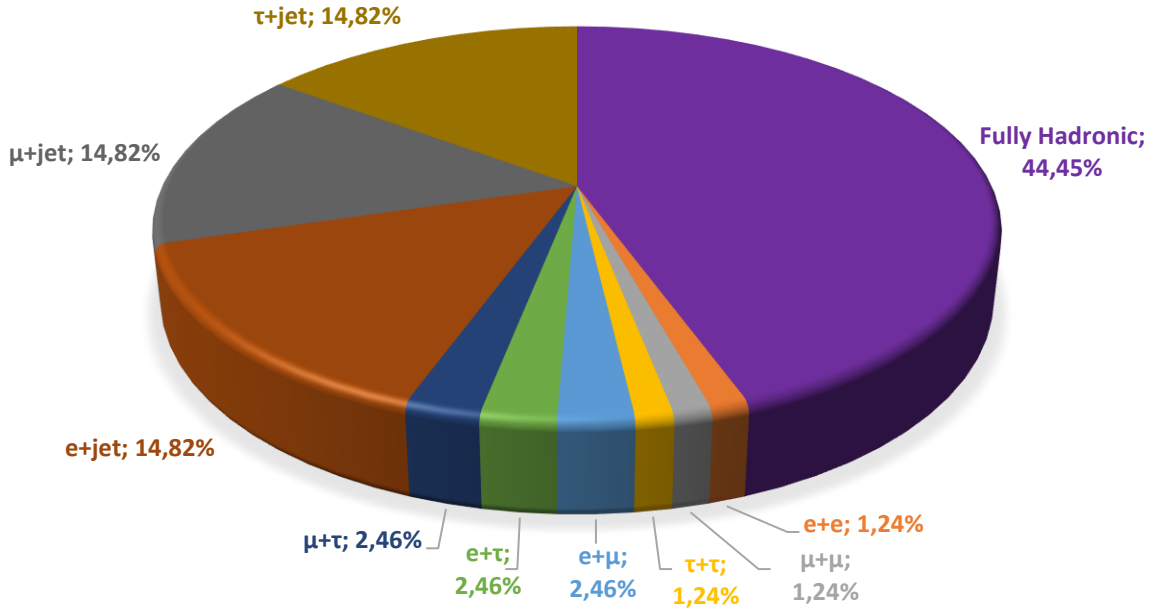


[Figure 2-11](#): Pie chart showing the different decay channels of a  $t\bar{t}$  pair, as well as their BRs.

Each of these different channels comes with its *trump card* and *bad penny*. The fully hadronic channel hit with the highest BR but suffers from a large background from QCD making the recognition of those issued from our tops a challenging job. On the other hand, the dilepton channel is well distinctive by the detector, yet it occurs with the smallest BR.

It worth mentioning that a further calculation is required, since the  $\tau$  leptons decay either leptonically or hadronically, but in this work, we will leave it at this stage since our main focus is on the  $t\bar{t}t\bar{t}$  rather than  $t\bar{t}$ .

### 2.2.3 $t\bar{t}t\bar{t}$ Four-Top Quarks Decay

The four-top quarks produced BSM as shown in [Figure 2-8](#) can decay into a variety of channels, depending on the decay products of the four W bosons (two  $W^+$  and two  $W^-$ ), three examples are illustrated in [Figure 2-12](#). While the previous dileptons, in  $t\bar{t}$  pair decay, were all opposite sign (OS),

dileptons in this case can be either OS (when one is delivered by t quark and the other by a  $\bar{t}$  antiquark) or same sign (SS) if both came from either  $t$  or  $\bar{t}$ .

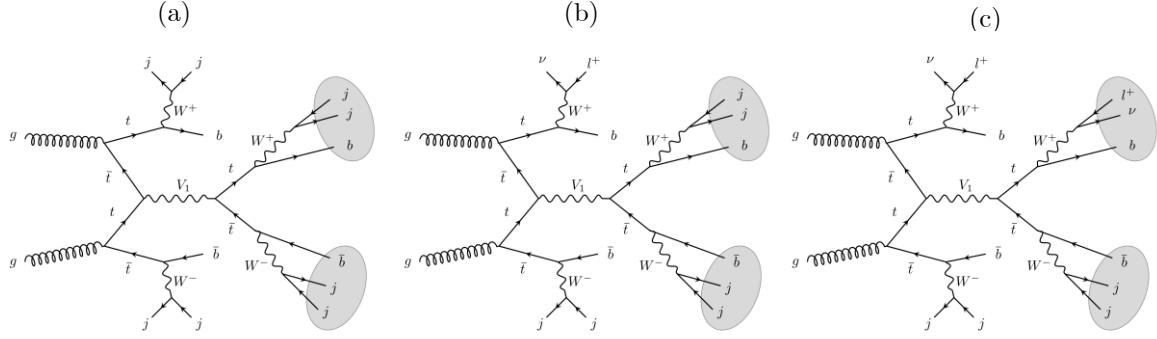


**Figure 2-12:** illustration of three examples of the decay channels of a  $t\bar{t}t\bar{t}$  four-top quarks. (a) all hadronic channel. (b) semi-leptonic channel. (c) same-sign-dilepton channel. Figures taken from [109]

In the following, we will explicitly introduce the possible decay modes of a  $t\bar{t}t\bar{t}$  four-top quarks and their branching ratios.

**Fully hadronic:** all the four W bosons decay hadronically, this is the simplest case and the BR is  $0.6667^4$

$$\mathcal{BR}_{had} = 19.76 \% \quad (2-20)$$

**1 e/ $\mu$ :** (*single-lepton*: 1 top quark decays into  $e$  or  $\mu$  while the remaining three decay into jets)

$$\mathcal{BR}_{1e/\mu} = 0.1111 \times 0.6667^3 \times 4 \times 2 \quad (2-21)$$

The 4 is there to take into consideration which top quark, of the four, decays leptonically, while the factor 2 is mandatory since the resulting lepton can be either an electron or a muon.

$$\mathcal{BR}_{1e/\mu} = 26.34 \% \quad (2-22)$$

**1  $\tau$ :** (*single-lepton*: 1 top quark decays into a tau, while the other three decay hadronically) we treat the tau lepton separately because, in opposite of the other two leptons, it decays before it can be seen by the detector.

For the same reason as above, the BR of this channel is  $0.1111 \times 0.6667^3 \times 4$ .

$$\mathcal{BR}_{1\tau} = 13.17 \% \quad (2-23)$$

**2 SS  $e/\mu$ :** (*dilepton*: 2 W bosons of the same sign decay to  $e$  or  $\mu$  while the remaining two decay hadronically)

$$\mathcal{BR}_{2ss e/\mu} = 0.1111^2 \times 0.6667^2 \times 2 \times 4 \quad (2-24)$$

We put the factor 2 because the 2 leptons can be coming from the  $W^+$  bosons or from  $W^-$ . The factor 4 is needed because the resulting two leptons can be either  $ee$ ,  $e\mu$ ,  $\mu e$ ,  $\mu\mu$ .

$$\mathcal{BR}_{2ss e/\mu} = 4.39 \% \quad (2-25)$$

**2 OS  $e/\mu$ :** (*dilepton*: 2 W bosons of different signs decay to  $e$  or  $\mu$  while the remaining two decay hadronically)

This channel differs from the previous one only in the factor 2, since the 2 produced leptons come from two W bosons with different signs, we have four ways to distribute these leptons on the W bosons. In fact, if the W bosons were organized as following  $(W^+, W^+, W^-, W^-)$  -c.f. [Figure 2-12](#)- then the 4 possible combinations are :  $(e^+/\mu^+, \text{jet}, e^-/\mu^-, \text{jet})$ ,  $(e^+/\mu^+, \text{jet}, \text{jet}, e^-/\mu^-)$ ,  $(\text{jet}, e^+/\mu^+, e^-/\mu^-, \text{jet})$  and  $(\text{jet}, e^+/\mu^+, \text{jet}, e^-/\mu^-)$ .

$$\mathcal{BR}_{2os e/\mu} = 0.1111^2 \times 0.6667^2 \times 4 \times 4 = 8.78 \% \quad (2-26)$$

**1  $e/\mu + 1 \tau$ :** (*dilepton*: 1 W boson decays to  $e$  or  $\mu$ , another to  $\tau$ , while the remaining two decay hadronically)

This again looks like the previous two cases (they are all dileptonic channels), but the possible combinations you can make this time (since we do not care about the signs) is 12, because we have four objects, this is  $4 \times 3 \times 2 \times 1 = 24$  but since one is repeated (the jet) we devise by 2.

$$\mathcal{BR}_{1e/\mu+1\tau} = 0.1111^2 \times 0.6667^2 \times 12 \times 2 = 13.17 \% \quad (2-27)$$

**2 $\tau$ :** (*dilepton*: two W bosons decay to  $\tau$ , two others decay to jets)

As we discussed above, we have 24 possible combinations of four objects, but now that we have two repeated elements, we devise by four, and this leaves us with 6 ways to distribute the outcomes on the four W bosons.

$$\mathcal{BR}_{2\tau} = 0.1111^2 \times 0.6667^2 \times 6 = 3.29 \% \quad (2-28)$$

**3  $e/\mu$ :** (*trilepton*: 1 W boson decays hadronically, while each of the others decays either to  $e$  or  $\mu$ )

$$\mathcal{BR}_{3e/\mu} = 0.1111^3 \times 0.6667 \times 4 \times 8 \quad (2-29)$$

Factor 4 is for distinguishing which of the four tops decays hadronically, while the  $8 = 2^3$  refers to the number of combinations you can make from 3  $e/\mu$ ,

$$\mathcal{BR}_{3e/\mu} = 2.93 \% \quad (2-30)$$

**2 e/ $\mu$  + 1  $\tau$ :** (*trilepton*: 1 W boson decays hadronically, one other decays to  $\tau$ , while the others decay either to  $e$  or  $\mu$ )

Four objects with one repeated, we have seen that this gives space only to 12 combinations, while we can make  $2^2 = 4$  from 2  $e/\mu$ .

$$\mathcal{BR}_{2e/\mu+1\tau} = 0.1111^3 \times 0.6667 \times 12 \times 4 = 4.39 \% \quad (2-31)$$

**1 e/ $\mu$  + 2  $\tau$ :** (*trilepton*: 1 W boson decays hadronically, two others decay to  $\tau$ , while one decays either to  $e$  or  $\mu$ ).

The only thing that will be changed from the previous case is 2 combinations of  $e/\mu$  instead of 4.

$$\mathcal{BR}_{1e/\mu+2\tau} = 0.1111^3 \times 0.6667 \times 12 \times 2 = 2.19 \% \quad (2-32)$$

$3\tau$ : (*trilepton*: 1 W boson decays hadronically, the remaining three decay to  $\tau$ )

$$\mathcal{BR}_{3\tau} = 0.1111^3 \times 0.6667 \times 4 \quad (2-33)$$

Where 4 is for distinguishing which top quark decays hadronically.

$$\mathcal{BR}_{3\tau} = 0.37 \% \quad (2-34)$$

**4 e/ $\mu$ /tau:** (*tetra-leptonic*: none of the W bosons decay hadronically)

$$\mathcal{BR}_{4e/\mu/\tau} = 0.1111^4 \times 81 \quad (2-35)$$

Where  $81 = 3^4$  is the number of combinations someone can make from the three leptons.

$$\mathcal{BR}_{4e/\mu/\tau} = 1.23 \% \quad (2-36)$$

Now all that remains to check, is if the sum of all the previous BRs equals 1.

$$\begin{aligned} \sum_i \mathcal{BR}_i &= 0.1976 + 0.2634 + 0.1317 + 0.0439 + 0.0878 + 0.1317 + 0.0329 + 0.0293 \\ &\quad + 0.0439 + 0.0219 + 0.0037 + 0.0123 = 1.0001 \approx 1 \end{aligned} \quad (2-37)$$

In [Figure 2-13](#), we gather all the above results in a pie chart.

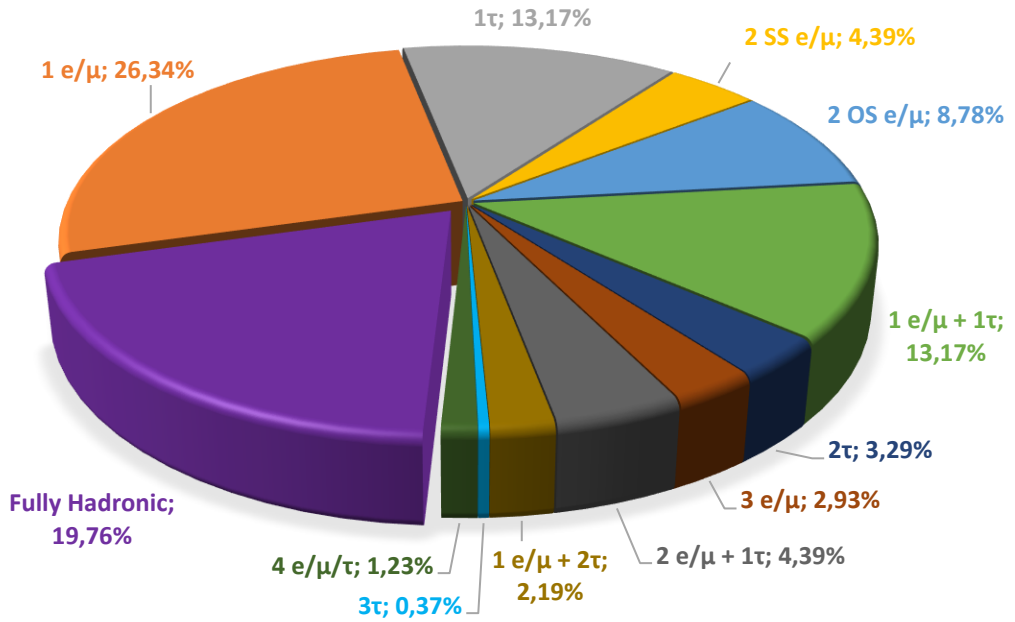


**Figure 2-13:** Pie chart of the different decay channels of  $t\bar{t}t\bar{t}$  along with their branching ratios. We notice that the single lepton channel has the largest BR, but in fact, if we take the decay of  $\tau$  in considerations, the full hadronic channel will take the lead.

From the beginning of this section, we have been working with the theoretical values of the BRs of W boson. However, the experimental values are slightly different, hence more complete BR calculations should take them into account.

As we have mentioned for the  $t\bar{t}$  pair, the fully hadronic channel has the advantage of enjoying a great BR, yet the QCD background makes the biggest obstruction for clean particle identification.

## Chapter 3

# LHC and the ATLAS Detector

*There are still many open questions that need to be answered. We have every possible idea - but the final answer can only come from experimentation. And the only experiments that can provide answers are those taking place at the Large Hadron Collider. Which makes this an exciting moment - we may get new clues from outside the Standard Model to answer the questions we still have.*

— Hubert Kroha, Max Planck Institute  
for Physics

*If you saw Atlas, the giant who holds the world on his shoulders, if you saw that he stood, blood running down his chest, his knees buckling, his arms trembling but still trying to hold the world aloft with the last of his strength, and the greater his effort the heavier the world bore down upon his shoulders - What would you tell him?*

— Ayn Rand, *Atlas Shrugged*

The LHC (Large Hadron Collider) accelerator and the ATLAS (A Toroidal LHC ApparatuS) detector are the biggest and the most important parts of *CERN's accelerator complex* (Figure 3-1). CERN stands for the “European Organization for Nuclear Research”<sup>36</sup>, it is a particle physics research laboratory founded in 1954 and it sits on the Franco-Swiss border outside of Geneva.

There are many experiments at CERN, some are using detectors along and next to the LHC beam pipe, with ATLAS experiment being the biggest [112], in addition to three other large experiments, CMS [113], ALICE [114] and LHCb [115], and three smaller ones, LHCf [116], TOTEM [117], and MoEDAL [118], using detectors sitting on the sides of ATLAS, CMS, and LHCb respectively. While others do not count on the LHC, like COMPASS [119] and NA62 [120] that use beams from the Super Proton Synchrotron (SPS) (Figure 3-1), SHINE [121] and CLOUD involving cosmic rays, DIRAC experiment

---

<sup>36</sup> Originally, it is a French acronym derived from “Conseil Européen de la Recherche Nucléaire” before it was changed to an organization.

studying the strong interaction between quarks along the Proton Synchrotron (PS) [122], ACE, AEGIS, ALPHA, ASACUSA, ATRAP, GBAR, and BASE are all “fixed-target” experiments using antiprotons from the Antiproton Decelerator (AD) [123], CAST that keeps an eye on the sun to detect new particles, in addition to ISOLDE [124] and nTOF [125] facilities, and AMS experiment controlled from CERN while it is located at the International Space Station (ISS) [126].

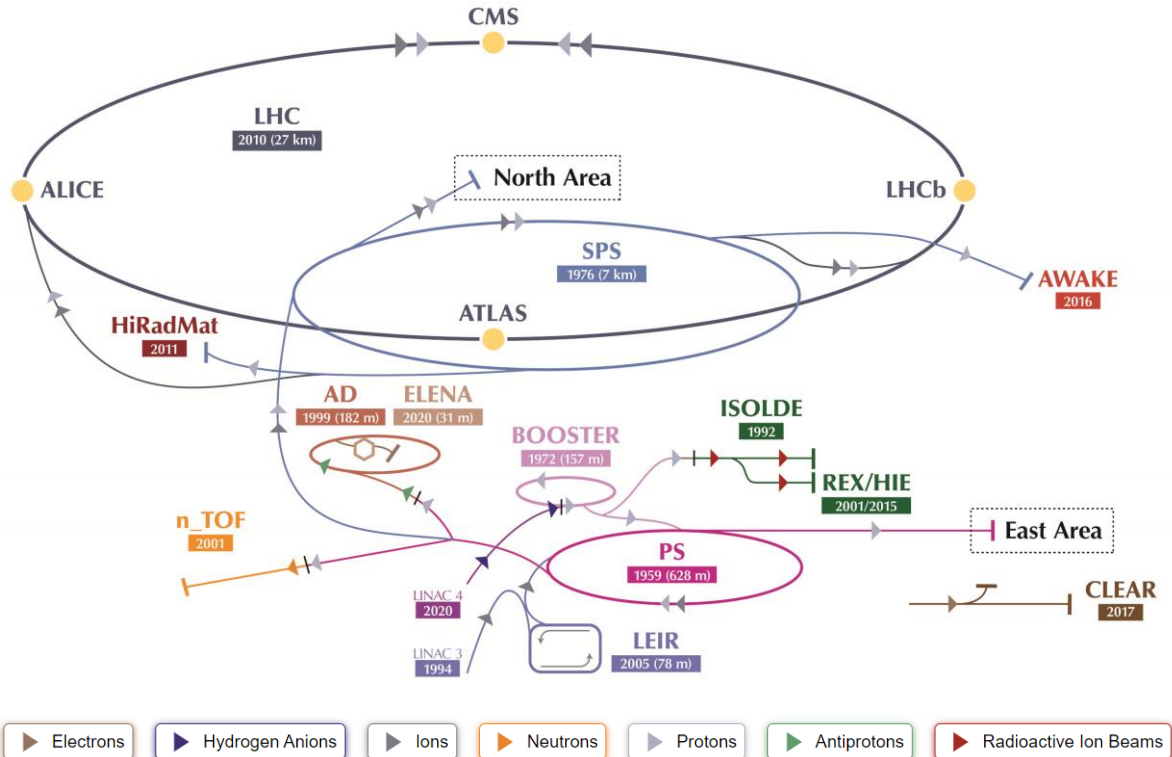


**Figure 3-1:** Sketch of the CERN Accelerator Complex. In the next run, Hydrogen anions will be accelerated to 160 MeV by the linear accelerator 4 (LINAC 4), replacing the LINAC 2 after the current Long Shutdown (LS) 2019/2020, and then after extracting the two electrons, the protons are injected into the LHC injection chain, following this path: BOOSTER  $\leftrightarrow$  PS  $\leftrightarrow$  SPS  $\leftrightarrow$  LHC, before they collide at the heart of ATLAS. (credit to CERN).

In this chapter, we are going to briefly introduce the LHC, its structure, and its operation, as well as the ATLAS detector since it is the most important of all the previously mentioned experiments<sup>37</sup>.

### 3.1 The Large Hadron Collider (LHC)

The Large Hadron Collider (LHC) [127], is a two-rings circular particle accelerator that primarily accelerates protons in two different directions, but also the lead (Pb) heavy ions<sup>38</sup>, so we have three possible configurations,  $p$ - $p$ ,  $p$ - $Pb$ , and  $Pb$ - $Pb$  collisions. The LHC two-rings took the place of the Large Electron-Positron collider (LEP) in the 27 Km long tunnel that lies 100 meters underneath the Franco-Swiss borders right outside of Geneva, Switzerland.

<sup>37</sup> Actually, it is because this work is gratefully done under the supervision of an ATLAS team leader, it will not harm to be a bit biased.

<sup>38</sup> But only for a few weeks [61, p. 31]

At the first run (2011-2012), the LHC started to collide the first proton beams with a center-of-mass energy ( $\sqrt{s}$ ) of 7 to 8 TeV, and almost doubled this energy at the run 2 (2015-2018) to reach  $\sqrt{s} = 13 \text{ TeV}$ . The LHC is designed to accelerate each proton beam to an energy of  $\frac{\sqrt{s}}{2} = 7 \text{ TeV}$ , and it is prospective that this energy will be reached in the next run (2021-2023)<sup>39</sup>. This energy is limited by the bending power of the main dipole magnets (Figure 3-2), which are 1232 dipoles made of superconducting

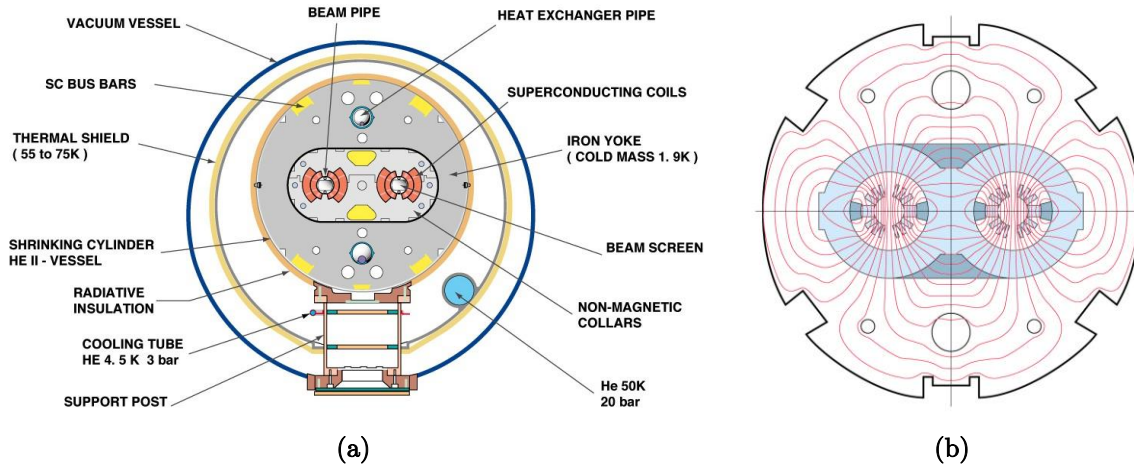


**Figure 3-2:** The main LHC dipole bending magnet. (a) A two-dimensional cut showing the main parts of an LHC dipole, the protons are accelerated inside the Beam Pipes. (b) Map of the magnetic flux bending the proton beams inside the pipes. (Credit to CERN)

coils of NbTi alloy, operating at a temperature of 1.4 K they can generate an 8.3 T magnetic field, nominal for a 7 TeV beam, taking the curvature of the LHC tunnel in consideration.

### 3.1.1 From Hydrogen Bottle to Interaction Point

Given that this work is done using data from the  $pp$  collisions of the run 2, we will only describe the protons' acceleration chain. Low energy protons cannot be injected directly into the LHC, they first go through multiple stages and pre-accelerators, constructing what is called the *LHC injection chain*, gaining energy after each stage. This chain begins with the 86 meters long linear accelerator (LINAC 4), boosting the Hydrogen anions to an energy of 160 MeV, which is more than 3 times higher than the energy delivered by its ancestor LINAC 2 (50 MeV). After extracting the two electrons, the protons are injected in the BOOSTER (PSB), a 157 meters long circular accelerator constructed of four overlayed rings, taking the protons to an energy of 1.4 GeV. From there, they are transmitted to a bigger circular accelerator, the 628 meters long Proton Synchrotron (PS) that delivers proton bunches of 25 GeV energy separated by 25 ns to the last stage of the LHC injection chain, the Super Proton Synchrotron (SPS). The SPS is also a circular accelerator, with a length of 7 Km making it second only to the LHC itself, it can reach an energy of 450 GeV.

In all the previous steps, protons were accelerated in only one direction, and each of the previous accelerators has one injection point, while the LHC has two. The ultra-relativistic proton bunches are piped into the LHC ultrahigh vacuum pipes, through two injection points, so that a beam is circulating clockwise, while another is accelerated counter-clockwise. For four minutes, the protons circulate the 27 Km long LHC with the same 450 GeV energy until the filling is complete, then, they can be accelerated

<sup>39</sup> The start is extended by one year, i.e. to the end of 2021, due to the Covid-19 pandemic. [128]

to the final energy  $\frac{\sqrt{s}}{2} = 7 \text{ TeV}$ , using radiofrequency cavities (RF) with an oscillating frequency of 400 MHz.

In addition to the 1232 dipoles each is 15 meters long used for bending the two beams, the LHC uses 392 quadrupole magnets, with lengths from 5 to 7 meters, to focus the beams. And just before the Interaction Points (IP), other magnets are used to pinch the two beams to enhance the collision probabilities. For ATLAS, focusing is done by a triplet of quadrupole magnets, starting almost 60 meters before the IP.

### 3.1.2 Notion of Luminosity

The luminosity is one of the most important parameters in accelerator physics, it is a property of the accelerator and it can be seen as its ability to produce collisions. The luminosity is related to the proton's cross-section  $\sigma_p$  and the number of events per second  $\frac{dR}{dt}$  by:

$$\mathcal{L}_p = \frac{1}{\sigma_p} \frac{dR}{dt} \quad (3-1)$$

Where,  $\sigma_p$  : can be seen as the apparent surface of a proton, so it is measured in  $\text{cm}^2$ , but we use *femtobarns* (fb) instead, with one barn is  $10^{-24} \text{ cm}^2$ . The Luminosity is hence measured in  $\text{fb}^{-1} \text{ s}^{-1}$ .

In terms of the beam properties, we can define the instantaneous luminosity as following [129, p. 364]:

$$\mathcal{L} = \frac{N^2 n_b f}{4\pi \sigma_x \sigma_y} F \quad (3-2)$$

Where,

$N$ : is the number of particles in each bunch.

$n_b$ : the number of bunches.

$f$ : the revolution frequency. For the LHC,  $f = 11.245 \text{ KHz}$ .

$\sigma_x, \sigma_y$ : are the sizes of the beams at IP ( $10\text{-}20 \mu\text{m}$ )

$F$ : geometric reduction factor (0.3-1)

The previous formula (3-2) is for the ideal head-on collisions. For real accelerators, other effects should be taken into consideration, e.g. the crossing angles [129, p. 365], but this is out of this work' scoop. By integrating Equation (3-2) over time, we get the *integrated luminosity*  $L$  in  $\text{fb}^{-1}$ .

The downside of higher luminosity is what we call the *pile-up*, which is caused by multiple collisions happening at the same time, either in the same bunch-crossing (in-time) or within the following or previous ones (out-of-time). The pile-up is a serious issue since we cannot identify the resulting physics objects and track them back to their primary vertices. The only thing we can do is the *Luminosity Leveling*, by separating beams and reducing the luminosity, otherwise, the Inner Detector sensitivity should be upgraded (namely, the vertexing capabilities) and maybe also develop the software part.

## 3.2 The Giant ATLAS Detector

Along the LHC, there are two general-purpose experiments, ATLAS and CMS, with ATLAS being the biggest. ATLAS, or **A** **T**oroidal **L**H<sub>C</sub> **A**pparatu**S**, is a multilayer cylindrical detector surrounding the LHC beam pipes at a cavern at *point 1*. The giant is 46 meters long with a diameter of 25 meters ([Figure 3-2](#)) and weighs about 7000 tonnes [112], that is more than the weight of 17 entities of the Moroccan high-speed train *Al-Boraq*, and this makes ATLAS the biggest detector of its kind, not only in CERN but in the whole world.

ATLAS covers almost the full solid angle around the IP, with multiple subdetectors encompassing each other like an onion<sup>40</sup> ([Figure 3-2](#)). In this section, we are briefly introducing these multilayered subdetectors, just after exposing the coordinate system used in ATLAS. This part of this work is written relaying on the official article describing the ATLAS experiment [112], all the figures are taken from that reference and credited to CERN. This paper is recommended for a complete study on the subject.

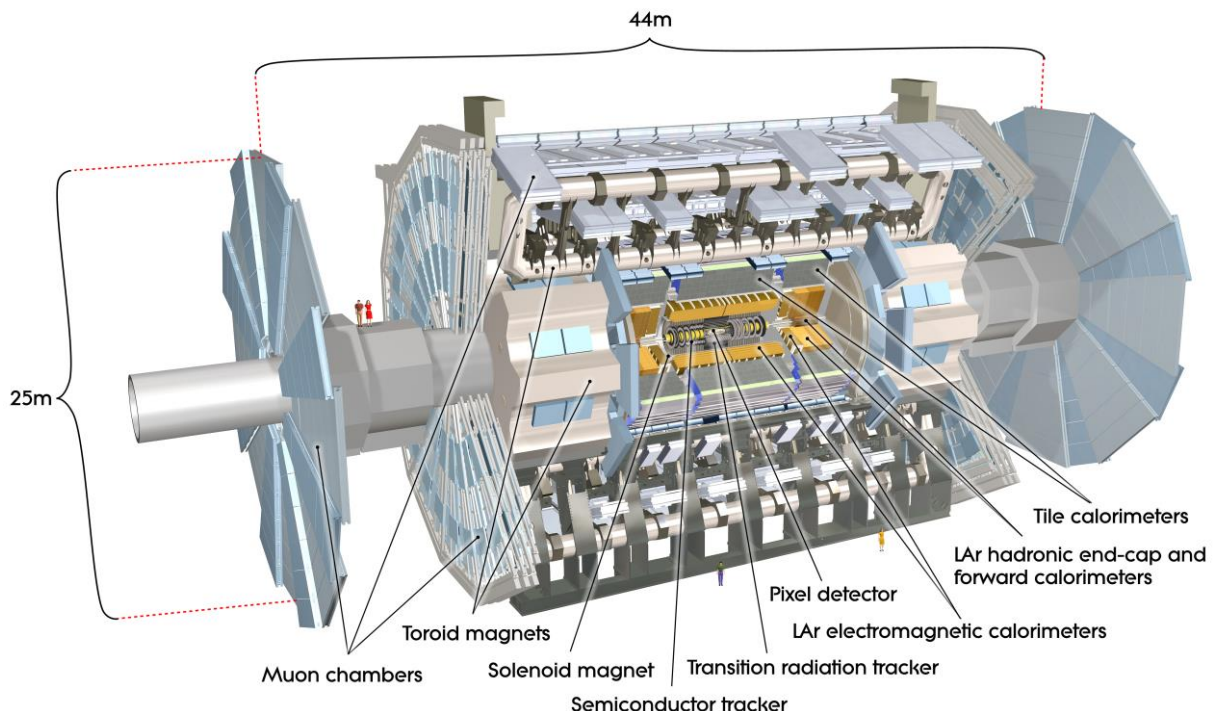


*Figure 3-3: General cut-away view of the ATLAS detector, indicating its dimensions as well as its multiple subdetectors. (Credit to ATLAS Experiment © CERN)*

### 3.2.1 ATLAS Coordinate System

Keeping its geometrical form in mind, the ATLAS uses a cylindrical coordinate system  $(r, \phi, z)$  with the IP defining its origin. But first, we need to stress the Cartesian coordinate system  $(x, y, z)$ .

<sup>40</sup> Just cylindrical

The  $z$  axis is defined by the beam axis, while its positive direction is related to those of  $x$  and  $y$  axes. The  $(x, y)$  plane is perpendicular to the beamline, with the  $x$  axis starting from the IP and pointing towards the center of the LHC tunnel, while the  $y$  axis is pointing upwards to the ground (Figure 3-4).

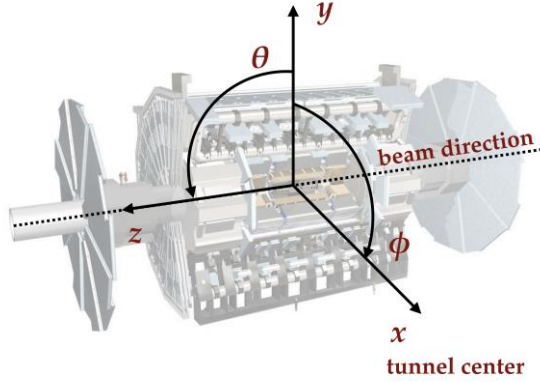


**Figure 3-4:** Representation of the Cartesian and the cylindrical coordinate systems. The half side of ATLAS where  $z > 0$  is called ‘A’ side, while the other half is referred to as the ‘C’ side. Figure taken from [130, p. 72]

$\phi$  : is the azimuthal angle

$\theta$  : is the spherical polar angle, it is useful to define the pseudo-rapidity later.

To locate a particle within the detector, we usually use the azimuthal angle  $\phi$  and the pseudo-rapidity  $\eta$ , defined in function of  $\theta$  by the following:

$$\eta = -\ln \tan\left(\frac{\theta}{2}\right) \quad (3-3)$$

For  $\theta = \frac{\pi}{2}$  (forward region of the detector) corresponds the smallest value of the pseudo-rapidity  $\eta = 0$ , while  $\theta = 0$  (the center region of the detector) corresponds to infinite pseudo-rapidity  $\eta = +\infty$ . And this makes  $\eta$  a good indicator to recognize forward particles. To describe the distance between two particles located by  $(\eta, \phi)$  we use  $\Delta R$  defined by:

$$\Delta R = \sqrt{(\Delta\phi)^2 + (\Delta\eta)^2} \quad (3-4)$$

### 3.2.2 Inner Detector

The Inner Detector (ID) [112, p. 53], is the closest subdetector to the IP. It covers a range of pseudo-rapidity  $|\eta| < 2.5$  where it can identify electrons over  $|\eta| < 2.0$ . the ID is composed of three independent subdetectors, going away from the IP, we find the silicon pixel detector, the silicon-strip semiconductor tracker (SCT), and the transition radiation tracker (TRT) (Figure 3-5).

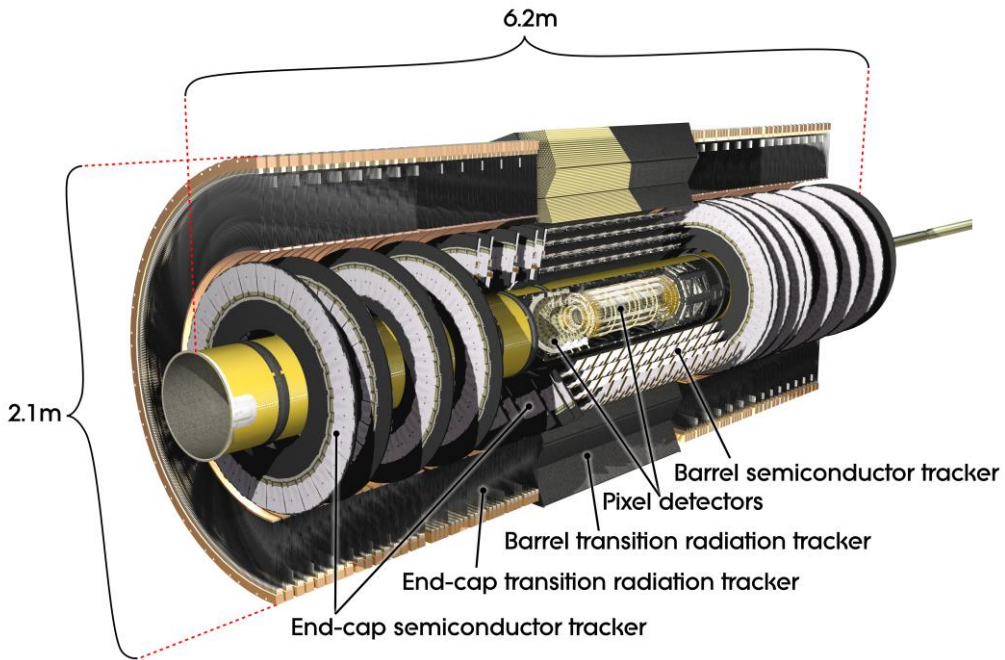


**Figure 3-5:** cut-away view of the Inner Detector. The dimensions of the detector in addition to its subdetectors either barrel or end-cap modules are shown. (Credit to ATLAS Experiment © CERN)

### 3.2.2.1 Pixel and SCT Detectors

As shown in the figure above, the pixel detector is the innermost subdetector of the ID. It is constituted of a barrel section that is of a cylindrical form, and two end-cap sections taking the shape of parallel disks centered on the z-axis (beamline). At the center, we find the four layers of the barrel section, the *Insertable B-Layer* (IBL)<sup>41</sup>, which is only 33.25 mm away from the beam pipe (Figure 3-8), followed by three layers of pixels (Figure 3-8). At each end-cap, there are three disks (Figure 3-6).

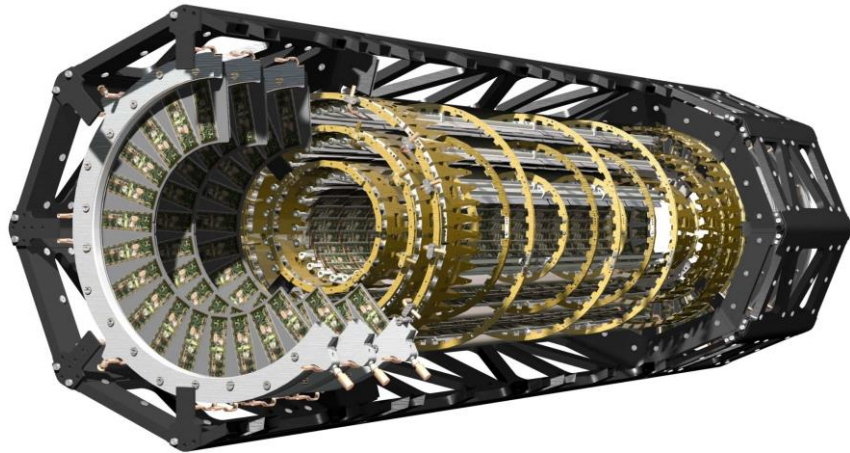


**Figure 3-6:** A perspective cut-away view of the pixel detector laying at the heart of the ID. The four layers of barrel modules and the three disks of one end-cap are shown. (Credit to ATLAS Experiment © CERN)

---

<sup>41</sup> “Insertable” because it was inserted inside the pixel detector, and it was not there before the second run of the LHC

Thanks to 80 million readout channels it has, the pixel detector has a resolution of  $10 \mu\text{m}$  in  $(r - \phi)$  and  $115 \mu\text{m}$  along the z-axis, while the IBL is even more precise, with a hit resolution of  $8 \mu\text{m}$  in  $(r - \phi)$  and  $40 \mu\text{m}$  along the z-axis.

The Semiconductor Tracker (SCT) is a four layers subdetector of the ID, it covers the pixel detector, and it is composed of four layers of barrel modules ([Figure 3-8](#)) and 18 disks, 9 at each end-cap, all based on silicon semiconductor sensors.

The SCT has a spatial hit resolution of  $17 \mu\text{m}$  in  $(r - \phi)$  and  $580 \mu\text{m}$  along the z-axis.

### 3.2.2.2 Transition Radiation Tracker

The Transition Radiation Tracker (TRT) is the latest layer of the ID, and in opposition to the pixel and the SCT subdetectors, it is not based on semiconductors, but gas-filled tubes (straws). The gas is a mixture of  $Xe$  (70%),  $CO_2$  (27%), and  $O_2$  (3%) and when ionized, the resulting electrons or ions are attracted and conducted by a gold-tungsten anode wire at the center of the straw ([Figure 3-7](#)), and this should happen in a blink of an eye thanks to a 15.3 KV potential applied between the wire and the outer casing of the straw.

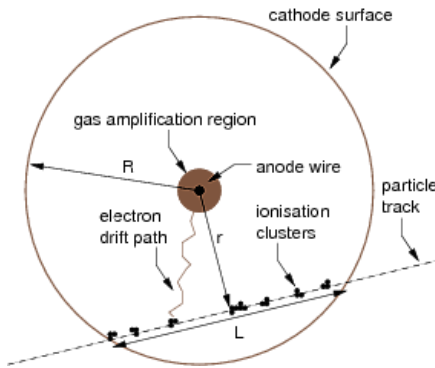


*Figure 3-7: visualization of a particle detection using a straw tube (Credit to LHCb at CERN)*

Each tube of the TRT has 4 mm in diameter, the straw wall is of  $35 \mu\text{m}$ , and the anode wire has a diameter of  $30 \mu\text{m}$ . The barrel section of the TRT is made up of 52,544 straws that are 144 cm in length, organized in 73 layers and oriented parallel to the beam-pipe<sup>42</sup> ([Figure 3-8](#)) while the endcap section is constructed of 122,880 straws contained in 160 overlayed planes, each straw is 37 cm length and aligned radially to the axis.

The spatial hit resolution of the TRT in  $(r - \phi)$  is  $130 \mu\text{m}$ , which is less than what semiconductor modules can provide. However, this is can be compensated by the huge number of straws giving a significant number of hits of a particle with the whole TRT detector.

The ID as we have mentioned is the closest detector to the IP, hence, it should have a high granularity to precisely detect and reconstruct the particle trajectories, and this is achieved thanks to its three subdetectors, pixel, SCT, and TRT detectors. In order to determine the momenta of the tracked particles, the ID is placed inside a solenoid of 5.3 m in length and 2.5 m in diameter, generating a 2T

---

<sup>42</sup> For this reason, the TRT does not provide any information along z-axis, but only  $(r - \phi)$  information.

magnetic field that bends the charged particles in the  $(r - \phi)$  plan, allowing us to deduce the momenta measuring the curvature.

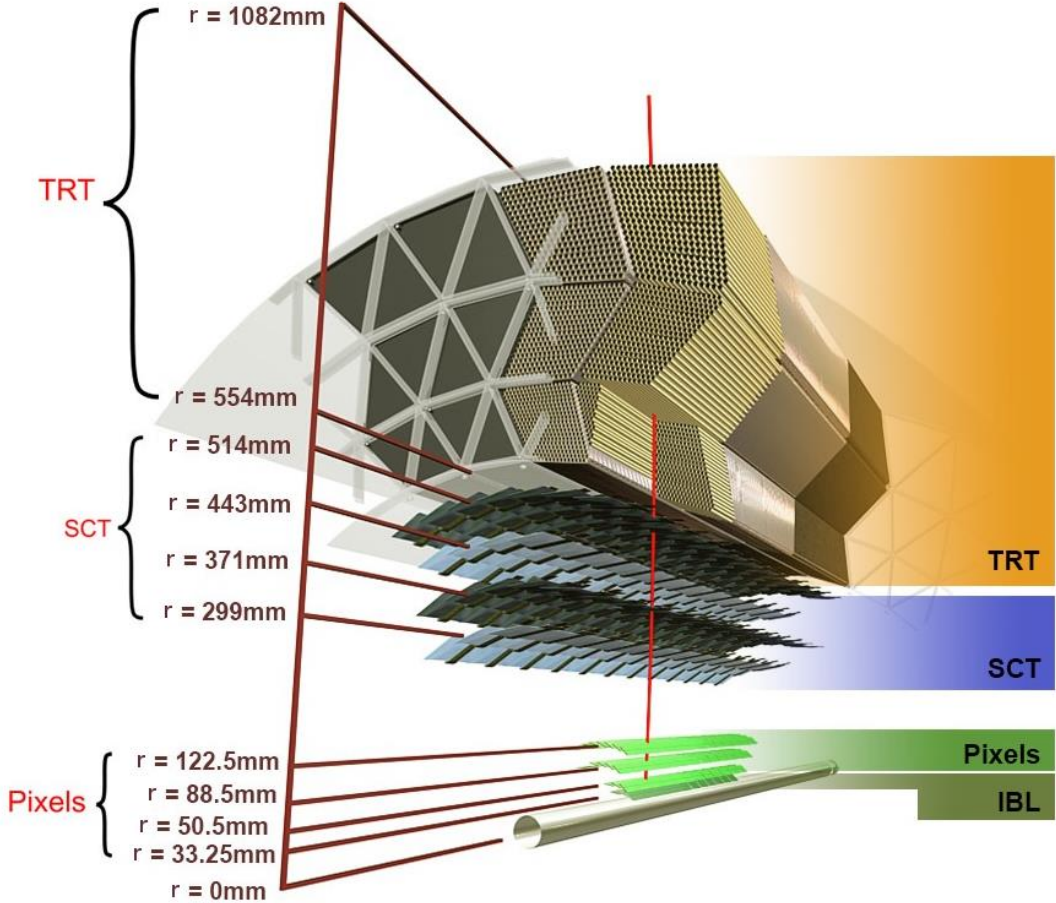


*Figure 3-8:* a sketch of the barrel section of the ID. The three subdetectors are shown, with  $r$  reflecting the distance of each layer from the beam-pipe. The orientation of the TRT straws is well presented. The figure is taken from [131]

### 3.2.3 The ATLAS Calorimeters

The calorimeters form the next subdetector of ATLAS and cover the ID. The calorimeters are meant to absorb almost all the produced particles and measure their energies. Depending on their energy and type, particles initiate a specific showering the moment they enter to the calorimeters. ATLAS has two types of calorimeters with two different purposes, the electromagnetic calorimeter, and the hadronic calorimeter. And they are based on two different technologies, either use gaps of cooled liquid-argon or scintillating tiles, with those relying on the latter covering those relying on the former (Figure 3-9).

Electromagnetic calorimeters consist of the barrel and end-cap sections covering anything within  $|\eta| < 3.2$ . Electrons and photons are stopped by passive high-density lead material, and then their energy is measured using the liquid argon cooled at a temperature of -183 as an active material.

The hadronic calorimeter consists also of the barrel and end-cap sections. The barrel is based on lead/scintillating-tile technology whereas the end-cap section of the hadronic calorimeter is of copper/LAr-based type.

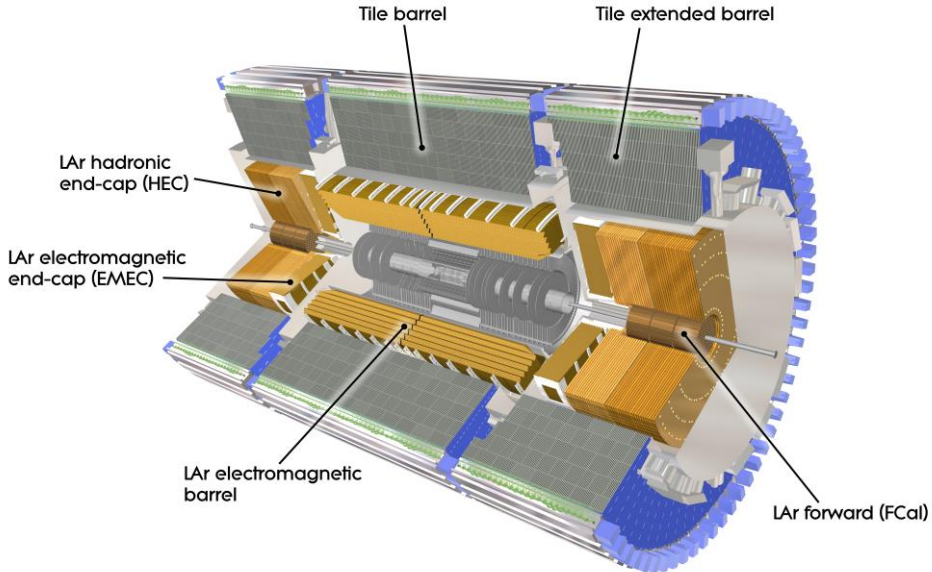


**Figure 3-9:** A skeleton of ATLAS calorimeters. The LAr calorimeter consists of a barrel, forward calorimeter (*FCal*), EM, and hadronic end caps. The tile calorimeter has a central barrel weighing 20,000 kg and two extended others, each weighs 9,600 kg. The ID is shown covered by the calorimeters. (Credit to ATLAS Experiment © CERN)

The calorimeters when combined they cover a range of a huge region of  $|\eta| < 4.9$ , and anything getting out of its trap, is either a muon or a neutrino.

### 3.2.4 The Muon Spectrometer

The outermost subdetector of ATLAS is the Muon Spectrometer (MS), it is designed to track charged particles that escape the calorimeters, which are usually muons hence the name muon spectrometer. Muons' momenta are concluded from their deflection and bending that are ensured using a magnetic system of three air-core superconducting toroidal magnets (Figure 3-10). The first one is in barrel section and it consists of 8 separate coils, each is of 25.3 m length, and together they are 830 tonnes weight, using 100 Km of superconducting wire to generate a magnetic field of 4T covering anything within  $|\eta| < 1.4$ . The two others are in end cups sections, each is consisting of 8 coils gathered in one cryostat weighing 250 tonnes, and working in a temperature of 4.7 K they can generate a magnetic field of 4T in the range of  $1.6 < |\eta| < 2.7$ .

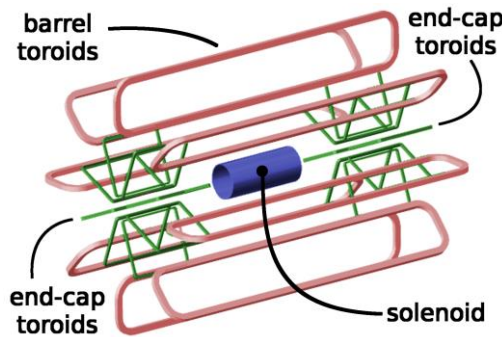


**Figure 3-10:** the magnetic system of the ATLAS detector. The figure is taken from [132]

The MS has four subsections following the structure of the previously described toroid magnets, and they are all gaseous radiation detectors that use chambers with gas-filled tubes. Namely, the four subsections of the MS are the Thin Gap Chambers (TGC), Resistive Plate Chambers (RPC), Monitored Drift Tubes (MDT), and Cathode Strip Chambers (CSC) (Figure 3-11).

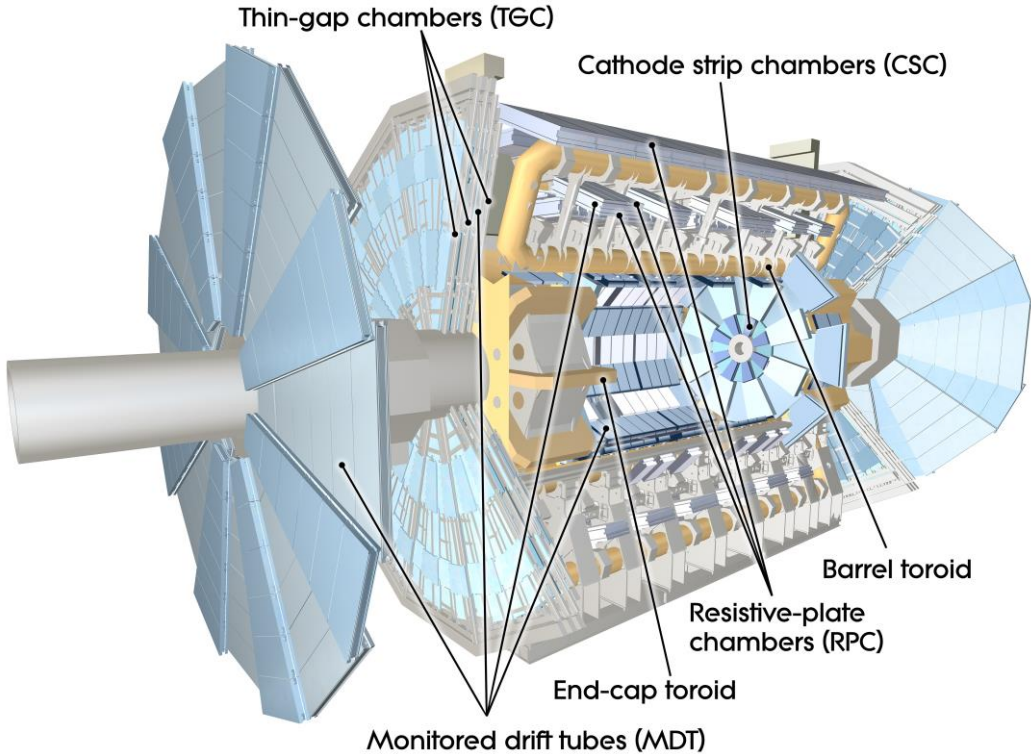


**Figure 3-11:** A perspective cut-away view of the Muon Spectrometer chambers. Both Barrel and end-cap toroid magnets are shown. The MS makes the major part of ATLAS and the MDT forward wheels are placed at the extreme end of the UX15 cavern. (Credit to ATLAS Experiment © CERN)

The four subdetectors fall into two distinct classes, *tracking chambers* that offer high precision tracking, and *trigger chambers* that are less precise but have a fast response for triggering. MDT and CSC belong to the former class, with a resolution of  $80\ \mu m$  and  $60\ \mu m$  respectively, while the PRC and TGC fit the latter class.

### 3.2.5 Trigger System and Data Acquisition

The LHC delivers more than 1.7 billion collisions to ATLAS each second, and since each event corresponds to an amount of data of  $1.5\ MB$ , this requires a bandwidth of  $64\ TB/s$  to store all the events. This is neither feasible nor necessary, that is why ATLAS uses an online event selection system called the *Trigger System* to reduce the number of events to be saved, by the Data Acquisition system, from a rate of  $40\ MHz$  to only  $1\ KHz$  (1 thousand events each second).

The trigger system includes two levels, *level-1 (L1) trigger*, which is a hardware-based trigger composed of custom-made electronics and physically exists within the ATLAS detector. The initial  $40\ MHz$  event rate is reduced down to  $100\ KHz$  thanks to L1. The second level of triggering is a bit different; it adopts CPU-based software to shorten the event rate from  $100\ KHz$  to only  $1\ KHz$ , and it is referred to as

*High-Level Trigger (HLT)*<sup>43</sup>. The Data Acquisition system then transports these data from the detector to storage for offline analysis.

In this chapter, we have briefly introduced the biggest and the most expensive research machine on the planet<sup>44</sup>, the Large Hadron Collider (LHC), the journey from Hydrogen anions to the Interaction Point (IP) was stated. Then, the giant ATLAS detector was presented along with all its three overlayed subdetectors, the Inner Detector (ID), the Calorimeter system, and the Muon Spectrometer (MS). The ATLAS magnetic system was also stressed.

In the next chapter, we will expose how does ATLAS identify the produced particles, and track them back to the primary vertices, reconstructing their trajectories.

---

<sup>43</sup> Earlier in run 1, ATLAS had two software-based triggers; the Level 2 trigger (L2) and Event Filter (EF), but since the run 2, L2 and EF were merged together in the same software, and the HLT was born!

<sup>44</sup> My way to exclude the International Space Station (ISS) since it is more expensive with a cost of 150 billion USD.

## Chapter 4

# ATLAS Physics Objects: Reconstruction & Identification

*There is only a handful of people at these companies who understand how these [algorithm] systems work, and even they do not necessarily fully understand what is going to happen with a particular piece of content. So as humans we have almost lost control over these systems. Because they are controlling the information that we see, they are controlling us more than we are controlling them.*

— Sandy Parakilas, from Netflix documentary  
“The Social Dilemma”

After we have introduced the ATLAS detector and its different subdetectors in the previous chapter, we shall now investigate how does ATLAS actually identify the products of the  $pp$  collisions that interact with the detector modules and sensors, and how different algorithms are used to reconstruct the physics objects (e.g. photons, electrons, hadrons, ...) from the electric signals retrieved from the detector cells.

In this chapter, we start by introducing the *tracking* and *vertexing* processes in section 4.1, then the reconstruction and identification of the electron are exposed in section 4.2, as well as the muons in section 4.3. Moreover, in section 4.4, the most important physics objects in this manuscript, the jets, are discussed, and the b-tagging is briefly visited taking into consideration its crucial importance in Top physics.

### 4.1 Tracking and Vertexing

While traversing the three subdetectors of the ID, charged particles leave *hits* on their modules, which are electrical signals that should be translated later into three-dimensional *space-points*. Basing on the information (signals) provided by the ID, especially from the innermost subdetectors, the Pixel Detector and the SCT, trajectories of the charged particles can be reconstructed, and from there, both the primary

and secondary vertices can be deduced. The former process is what we refer to as *tracking* [133]–[135] while we call the latter the *vertexing* [136], and both operations are crucial for any physics analysis.

### 4.1.1 Tracking

Propagating in the magnetic field generated by the solenoid magnet surrounding the ID (c.f. section 3.2.4), the charged particles produced from the  $pp$  collisions follow helical trajectories in the  $x - y$  plane. Within the ATLAS coordinate system (c.f. section 3.2.1), these trajectories can be fully described by five parameters [61, p. 70], [80, p. 59]:

$$(d_0, z_0, \phi, \theta, q/p) \quad (4-1)$$

Where,

$d_0$ : is the track impact parameter in the transverse plane.

$z_0$ : is the track impact parameter in the longitudinal plane.

$\phi$ : represents the azimuthal angle.

$\theta$ : is the polar angle as defined earlier.

$q, p$ : are respectively the electric charge and the momentum of the particle.

The five parameters are illustrated in the following sketch (Figure 4-1).

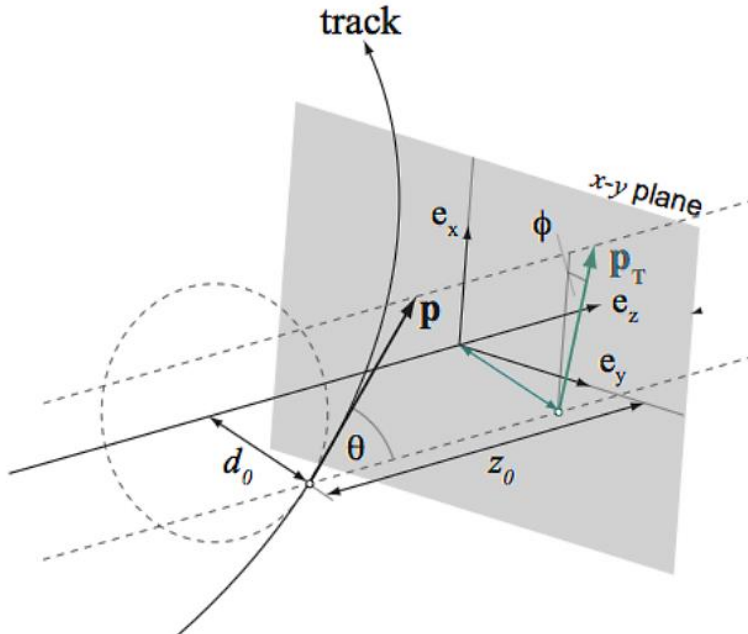


**Figure 4-1:** Sketch illustrating the five parameters characterizing a track.  $d_0$  and  $z_0$  are defined with respect to the primary vertex, which is  $(0,0,0)$  in this case.  $\phi$  et  $\theta$  are respectively the azimuthal and polar angles of the track at the point defined by  $d_0$  and  $z_0$ .  $q/p$  is deduced from the curvature of the track, while the side to which it is bent reflects the sign of the electrical charge. [61, p. 71], [80, p. 60]

To construct a *track* of a charged particle, the number of its hits with the silicone layers of the ID (the pixel and SCT) should exceed a given minimum (at least 7 hits) required by reconstruction algorithms, only then, the track can be extended by adding additional points. Generally, ATLAS tracking algorithms follow two pattern-recognition procedures with two different directions, the first is an *inside-out* approach, and it is how the majority of the tracks are constructed, while the second is an *outside-in* approach, and it complements the first one [61, p. 70].

The inside-out procedure starts by building track *seeds* from a triplet of space-points formed from hits within the pixel layers and the first innermost layer of the SCT (c.f. 3.2.2.1), but no far further. To include the other three layers of the SCT, these seeds are taken as inputs by algorithms based on the *Kalman-Filter* technique which we call *track finding algorithms*. After this stage, we have a set of track candidates, some of those candidates can be *fake* or *duplicated*, and they should be rejected. This is achieved by the *ambiguity solving algorithm* that lay essentially on information provided by the *IBL*, and only tracks passing this step can be extended to contain fitting hits from the outermost subdetector of the ID, the TRT. This approach is practical to reconstruct the trajectories of long-living particles originated from the primary  $pp$  collision and that can reach the TRT, such particles are called *prompt particles*. However, some particles do not leave hits within the two innermost subdetectors, but only on the TRT. Some examples of these particles are the so-called *conversion photons*, which are photons that skip the pixel and the SCT without being tracked (being electrically neutral) and then split into an  $e^-e^+$  pair hitting the TRT. As a result, not all hits at the TRT are assigned to a track by the inside-out procedure, and those are what we use as seeds for the *outside-in* algorithms.

The outside-in approach complements the inside-out results by building seeds from space-points formed of the remaining hits in the TRT, and then extend them inwards using specific algorithms.

After the two previous procedures, we get out with many tracks that should pass some selection requirements, and we have two kinds of selection, it is either a *loose* selection or a *tight* one.

The **loose** selection requirements are [137, p. 61]:

- $p_T \geq 400 \text{ MeV}$
- $|\eta| < 2.5$
- The number of hits in the silicon layers (IBL + Pixel + SCT) is at least 7 or more.
- The number of holes<sup>45</sup> in silicon layers is 2 or less.
- The number of holes in the pixel detector is no more than 1.

While the **tight** selection has in addition to the previous requirements, three others [137, p. 62]:

- Silicon hits should be more than 9 for  $|\eta| \leq 1.65$ , and more than 11 if  $|\eta| > 1.65$ .
- One hit should be either in the IBL or the innermost layer of the Pixel Detector.
- No Pixel holes

For  $p_T < 5 \text{ GeV}$ , the track reconstruction efficiency is between 85% and 90% [133].

---

<sup>45</sup> Missing expected hits.

## 4.1.2 Vertexing

After the tracking, the reconstructed tracks are fed to the *vertex finding algorithm* [138] in order to reconstruct the vertices of a given event. A vertex is defined by two charged particle tracks, at least, associated with the same space-point, and to establish all the vertex candidates of an event, multiple steps of the vertex finding algorithm are iterated several times. However, this algorithm should be sophisticated enough to overcome the pile-up problem, where the products of multiple  $pp$  collisions that happened at the same time are thought to be from the same event.

The Primary Vertex (PV) is deduced after calculating the square of the transverse momenta of all the tracks, for each vertex we calculate the sum of the squared transverse momenta of its associated tracks, and the one with the greatest  $\sum p_T^2$  is the PV, and it is named the *hard-scatter vertex*. The PVs are required to be positioned within the beam spot, which is the area of the bunch-crossing, and vertices that are not consistent with this condition are deemed to be secondary, tertiary..., vertices. After well spotting the primary hard-scatter vertex, only tracks originated from it are considered as significant for object reconstruction, while other objects are considered issued from another event by cause of pile-up (Figure 4-2).

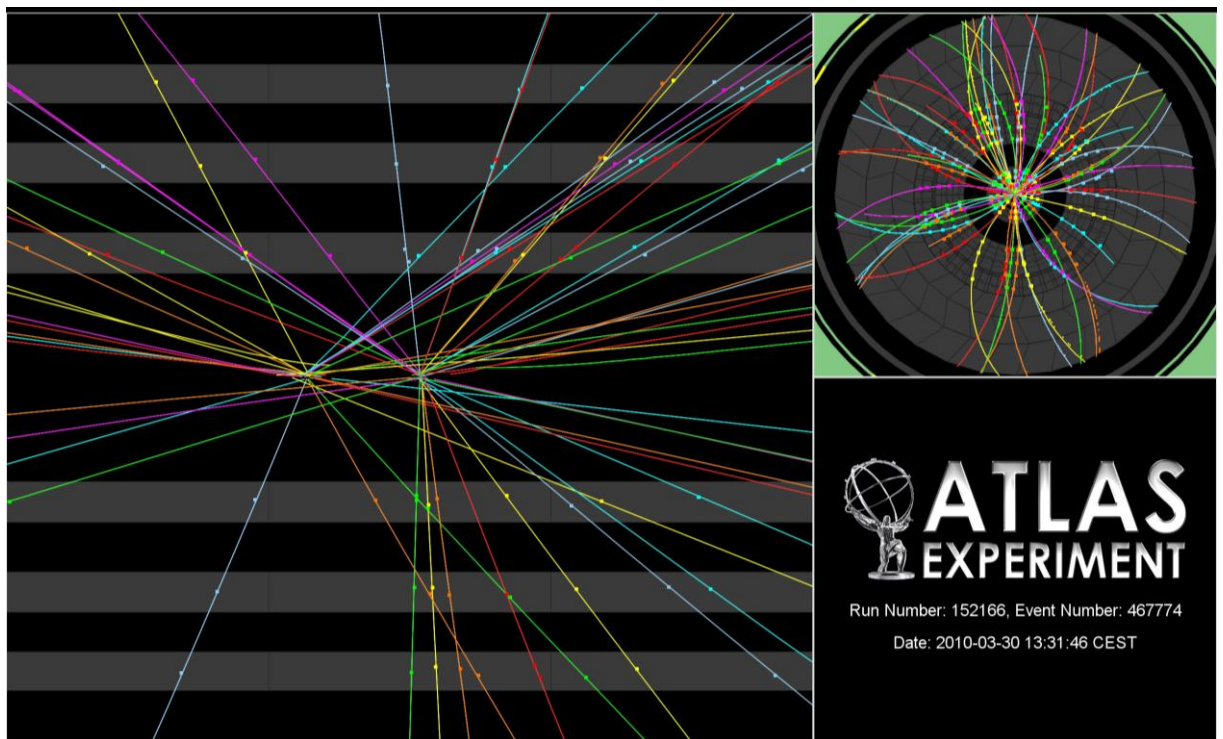


**Figure 4-2:** Collision event at 7 TeV with 2 pile up vertices. The event display at the top right corner shows the curvature of tracks in the  $xy$ -plane [139].

Vertexing efficiency is inversely proportional to the pile-up, but for vertices associated with two or more tracks, the efficiency is approximately 90% [140].

## 4.2 Electrons

Electrons are visible objects to the ID since they leave recognizable traces on its multilayers, and this is thanks to their electric charge. For this reason, their tracks as we have seen are constructed at the level of the ID, and from there, they are used as seeds for further and complete reconstruction.

### 4.2.1 Electron Reconstruction

Interring into the EM calorimeter (c.f. section 3.2.3), electrons are expected to be absorbed depositing all their energy in the LAr EM calorimeter, leaving a splendid cluster behind. The reconstruction of electrons is achieved by combining the reconstructed tracks with the EM calorimeter information.

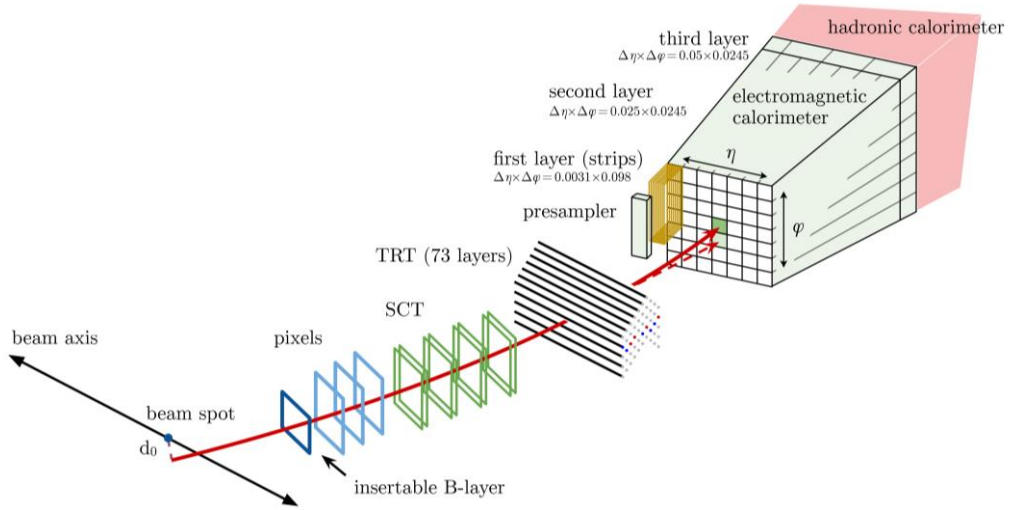


**Figure 4-3:** Sketch illustrating the reconstruction of an electron trajectory. From its creation to its absorption, the electron (red line) has 12 silicon hits, 1 with IBL, 3 with the 3 pixel-layers, and 8 with the SCT (2 with each side of the four layers), and 73 hits with the 73 layers of the TRT. The electron ends up depositing the totality of its energy along the four layers of the EM calorimeter. (Credit to ATLAS Experiment © CERN)

Before 2016, the search for localized energy in the EM calorimeter is achieved using the *sliding window algorithm*, but after 2016, it has been replaced by the *dynamic EM topo-clustering algorithm* which has become the major ATLAS electron reconstruction algorithm [61, p. 73].

As we have seen in section 3.2.3, an object stopped by the EM calorimeter is either a photon or an electron, so a localized cluster in the EM calorimeter can be originated from a prompt electron, a photon conversion, or a prompt photon. A prompt electron would be tracked by the ID, so a close-matching between an EM calorimeter cluster and a hard-scatter track must refer to a prompt electron, while a match with an ID track that has no hits in the pixel subdetector is a sign for a photon conversion, finally, a cluster that does not match to any of the constructed tracks of the ID must be a photon fingerprint.

### 4.2.2 Electron Identification

After the reconstruction of electron candidates, they are selected only if they are consistent with some requirements based on what we call the *electron likelihood identification*. And like before, there are levels to this identification, namely, it is either Very Loose, Loose, Medium, or Tight.

The inputs of the electron likelihood (LH) identification are listed in table 5.1 in ref. [80, p. 64].

For an electron candidate of  $p_T > 40 \text{ GeV}$ , loose identification has an efficiency of 93% [141].

## 4.3 Muons

Just like the electrons, the muons are recognizable by the ID, and their tracks can be constructed and be taken as seeds for further reconstruction of their trajectories. However, contrary to the electron, muons cannot be stopped by the calorimeter system (being minimum ionizing particles), and they reach the MS (c.f. 3.2.4) where they leave hits that can be tracked.

The reconstruction of muons is done by matching the built tracks in the ID and the calorimeters (even if the latter are less significant) with those independently built-in the MS [142]. The ID tracks are just like discussed in 4.1.1, while the muon reconstruction in the MS is yet to be discussed in the next section.

### 4.3.1 Muon Reconstruction in the MS

The MS has four subdetectors; the TGC, RPC, MDT, and the CSC (c.f. section 3.2.4), passing through the chambers of the different multilayered subdetectors, muons leave hits, and searching for patterns of these hits forming segments of muons candidates is the first step of the reconstruction process. From these segments, track candidates can be formed by fitting results from different MS detector layers. The algorithms used for this reason are called segment-seeded since they use the muons segments in the middle of the MS as seeds for track candidates, then they extend the reconstruction to the innermost and outermost layers [142, p. 3].

Based on the signals provided by different ATLAS subdetectors; the ID, the calorimeters, and the MS, different algorithms are used to reconstruct the trajectories of different muon *types*. Namely, we have four types [142]:

- **Combined (CB) muons:** a CB muon is reconstructed laying on the independent information from both the ID and the MS (no calorimeters involved), combining both tracks with a global fit. As we have seen in tracking, there are two recognition patterns that we can use, inside-out and outside-in, depending on if the seeding was within an inner or outer layer of the ID respectively, the same logic holds for the reconstruction of a CB muon. However, the major reconstruction pattern for muons is the outside-in pattern (unlike the tracking), where the MS tracks are extrapolated to match the ID tracks, while an inside-out reconstruction is used as a complementary path.
- **Segment-tagged (ST) muons:** a muon is said an ST muon if it hits only one layer of MS chambers, so an ID muon is classified as an ST one if its ID track is associated with one track segment either on the MDT or CSC subdetector layer. ST muons are known to have a low  $p_T$  or to pass through MS regions of reduced acceptance.
- **Calorimeters-tagged (CT) muons:** they are the muons with the lowest purity of all the four types, since they are reconstructed matching tracks of the ID to an energy leaving in the calorimeter, and as we know, muons are minimum ionizing particles.

- **Extrapolated muons (ME):** they are standalone muons that are identified by the MS but do not match with any ID track.

### 4.3.2 Muon Identification

To reduce background, we tail a muon identification to its reconstruction, by applying some quality requirements that we shall see next. Three parameters are used to identify muons:

- **$q/p$  significance:** the  $q/p$  ratio is calculated for measured  $q$  and  $p$  in the ID and MS as well as the uncertainties, where the  $q/p$  *significance* is defined as the absolute value of the difference between the two calculated ratios deviced by the sum in quadrature of the corresponding uncertainties.
- $\rho'$ : defined as the absolute value of the difference between the transverse momentum measurements in the ID and MS divided by the one of the combined tracks.
- Normalized  $\chi^2$  of the combined track fit.

We define four muon identification selections; Loose, Medium, Tight, and High- $p_T$ , with the Medium identification being the default muons selection in ATLAS.

A full description of the four muon identification selections for ATLAS is given in [142, pp. 6–7]. Nevertheless, I would like to stress that the High- $p_T$  selection is optimized for searches for high mass resonances like the one we are interested in,  $Z'$  [143], and others like  $W'$  [144]. However, since we are interested in the channel where the hardest tops (c.f. 2.1.3) we will use the Medium selection.

In (Figure 4-4), the reconstruction efficiency of muons as a function of the pseudo-rapidity  $\eta$  for a Medium selection is measured lying on  $Z \rightarrow \mu\mu$  event.

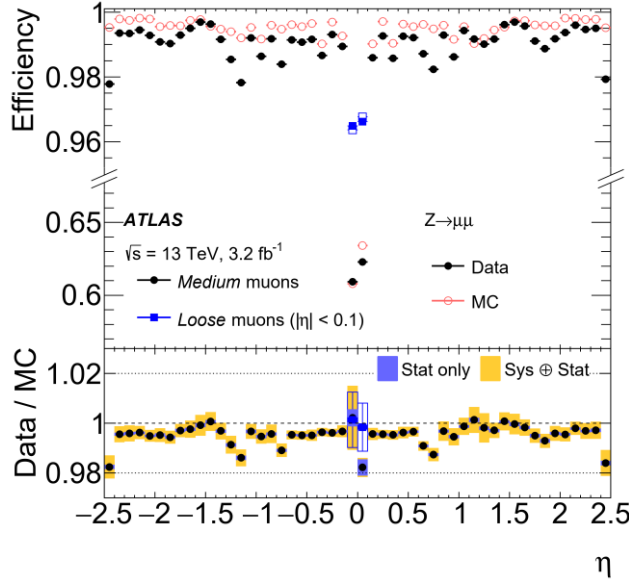


**Figure 4-4:** the reconstruction efficiency of muons as a function of the pseudo-rapidity  $\eta$  for a Medium selection as well as the loose one for  $|\eta| < 0.1$ , measured lying on  $Z \rightarrow \mu\mu$  event. We see from this results that Muons are reconstructed in ATLAS with an efficiency of nearly 100%. Figure taken from [142, p. 13].

## 4.4 Jets

As we have introduced in section 1.1.2.3, quarks and gluons produced in a high energy  $pp$  collision can only travel for a very short distance before they are hadronized (c.f. Figure 1-11), the maximum distance they can go far from each other is roughly  $1\text{ fm}$ , which is the diameter of hadrons and the range of the strong force, and this as we have mentioned is due to the quarks confinement.

The sprays of the colorless particles produced within the hadronization process are what we call jets, and they can be tracked by the ID and mainly interact with the calorimeters of ATLAS.

Jets are the most important and central physics objects for this work, precisely, we are interested in *hadronic jets* produced in the hadronic  $pp$  collisions. In the following, we shall discuss the jets reconstruction, then, we will introduce the *b-tagging* used to identify jets with bare-bottomness since our top quarks decay essentially to a b-quark and a W boson.

### 4.4.1 Jets Reconstruction

Traveling through the ATLAS detector, the jets deposit their energy, where the majority of this energy is dropped in the *Hadronic Calorimeter*, forming fabulous clusters. These clusters are reconstructed from the topological deposits in the most fundamental elements of the calorimeter, the *calorimeter cells*, and the reconstructed clusters are referred to as *topo-clusters*, where the algorithm used for this purpose is called the *topological clustering algorithm* [145]. Another algorithm, named the *Jet Vertex Fraction* (JVF) algorithm, uses the information from the ID to associate topo-clusters to ID tracks, and depending on the likelihood of a jet being originated from the PV it assigns weights to the track candidates. Using the JVF,  $\eta$ , and a minimum jet  $p_T$ , the jets that possibly can be from the pile-up are rejected [146]. Finally, a jet finding algorithm is fed with these energy clusters to form the final physics object representing the jets.

ATLAS uses the *anti- $k_T$*  jet clustering as the default jet finding algorithm, that aims to construct objects representing the jets from the topo-clusters<sup>46</sup>. The *anti- $k_T$*  fits in the class of *sequential recombination algorithms*, hence, it tries to minimize the distance  $\Delta R$  between two jets (defined as we have seen in equation (3-4)). However, instead of using  $\Delta R$ , the *anti- $k_T$*  algorithm uses a  $k_T$ -weighted distance labeled  $d_{ij}$  (equation (4-3)), to locate the closest-to-each-other pair of clusters after iterating over all the topo-clusters, then it combines them in a single cluster. This iteration is of course limited by a distance  $R$  that defines the jet radius (otherwise it will gather all the clusters in one and only jet).

In addition to the distance between the  $i^{th}$  and  $j^{th}$  clusters,  $d_{ij}$ , the *anti- $k_T$*  algorithm takes another distance as input,  $d_{iB}$ , which is the distance between the  $i^{th}$  cluster and the beam-line.

$$d_{ij} = \min\left(\frac{1}{k_{T,i}^2}, \frac{1}{k_{T,j}^2}\right) \frac{\Delta R_{ij}^2}{R^2} \quad (4-2)$$

---

<sup>46</sup> In general, it can be any other jet constituents rather than the topo-clusters, like the truth-level particles from MC [147, p. 31].

$$d_{iB} = \frac{1}{k_{T,i}^2} \quad (4-3)$$

Where,

$k_{T,i} = \frac{p_{T,i}}{\hbar} = p_{T,i}$  : the transverse momentum of the  $i^{th}$  cluster.

$\Delta R_{ij}^2 = (\eta_i - \eta_j)^2 + (\phi_i - \phi_j)^2$  : the unweighted distance between the  $i^{th}$  and  $j^{th}$  clusters.

Iterating over all the clusters, calculating the previous parameters, the *anti- $k_T$*  algorithm proceeds as follows:

1. Calculate  $d_{ij}$  and  $d_{iB}$ .
2. If  $d_{ij} < d_{iB}$ , then the  $i^{th}$  and  $j^{th}$  clusters are combined.
3. If  $d_{ij} > d_{iB} \forall j$ , then the  $i^{th}$  cluster is removed and considered as a jet.
4. While a cluster is still remaining, repeat the process.

The radius parameter  $R$  used by ATLAS varies depending on the physics in question. Typically,  $R = 0.5$  is used for small jets like the single quarks and gluons jets, while  $R = 1$  for large jets like the energetic  $Z \rightarrow q\bar{q}$ ,  $W \rightarrow q\bar{q}$  and  $t \rightarrow bW \rightarrow q\bar{q}b$  decays, where the last one is the decay process we are interested in for this work. In (Figure 4-5) the results of the *anti- $k_T$*  algorithm for  $R = 1$  are illustrated.

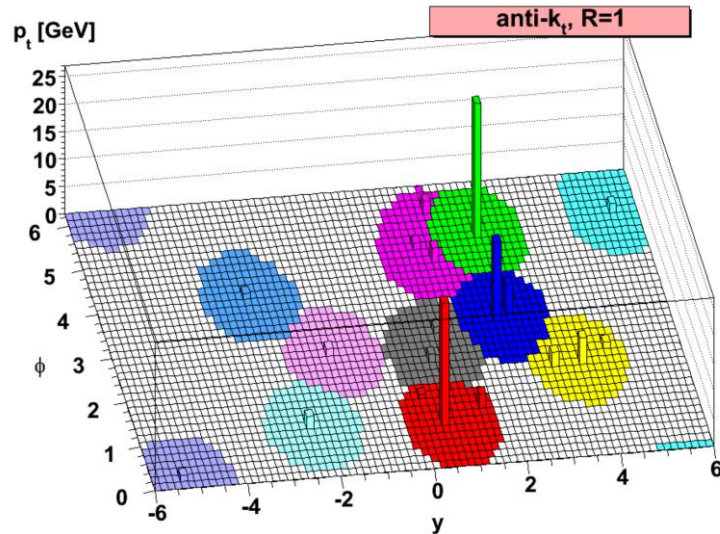


Figure 4-5: Illustration of the results of the *anti- $k_T$*  algorithm for  $R = 1$ . The colored circles in the  $(y - \phi)$  plane are related to the  $R$  parameter. Figure taken from [148, p. 4]

#### 4.4.2 b-jets

b-tagging refers to the identification of jets formed of b-hadrons originating from a b-quark fragmentation, and separate them from other flavor-jets like c-jets and light-jets. It is of high importance for many physics analyses that include high- $p_T$  b-jets in their final states, e.g.  $H \rightarrow b\bar{b}$  in Higgs physics,

and  $t \rightarrow bW$  in top physics which is the main physic in this work, supersymmetry, and many other BSM physics searches.

Due to the huge background from the light-jets, b-tagging is actually a challenging task. However, it is doable by laying on the properties of the b quarks, such as its relatively long life-time that allows it to go up to 3 mm away from the IP before it decays and forms a secondary vertex (Figure 4-6).

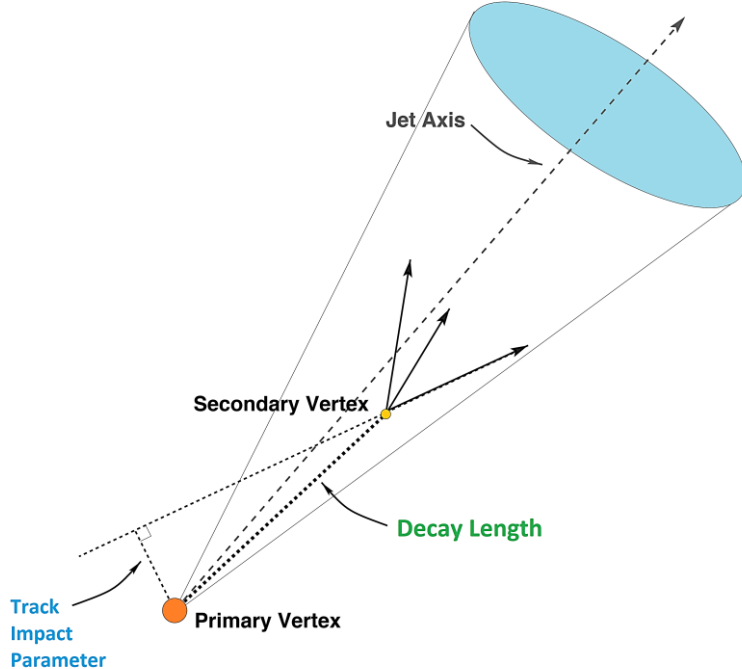


**Figure 4-6:** cartoon displaying the decay of a b quark to b-hadrons forming a secondary vertex (SV). The distance from the PV to the SV is the decay length (in the range of few millimeters). The dashed lines between the PV and SV represent the transverse and longitudinal components of the momentum vector (c.f. eq. (4-1)), and they determine the Track Impact Parameter used to distinguish different flavor-jets. Figure taken from [149, p. 2].

To perform the b-tagging, ATLAS has developed various algorithms during the different LHC runs, the most relevant algorithms are the *IP3D* algorithm [150], the *SV1* algorithm [150], the *JetFitter* algorithm [151], and the *MV2c10* algorithm [152] in use since the run II. It worth mentioning that in ATLAS there is a whole group taking care of this stuff called the *ATLAS Flavor Tagging Group*.

Now that we have all the arsenal needed to understand how a produced particle would interact with the ATLAS detector, we will close this chapter with a masterpiece of art (Figure 4-7), showing particle interactions with different ATLAS subdetectors.

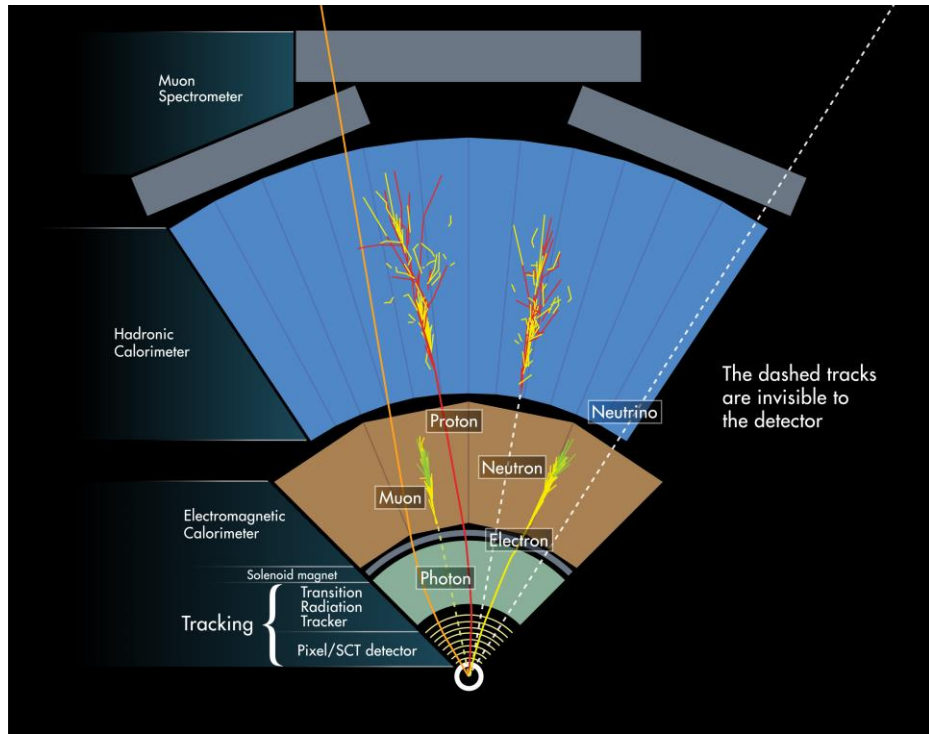


**Figure 4-7:** Sketch showing interactions of different particles with the barrel section of the detector, the cut is taken in the  $(r - \phi)$  plane. In the ID, we can see that negatively charged particles ( $\mu^-$  and  $e^-$ ) are bent to the right with different angles (so they have different momenta), the positively charged proton is deviated to the left, while the electrically neutral particles are not affected by the central solenoid magnet, hence cannot be tracked by the ID. The electron and photon are absorbed within the EMC while the hadrons ( $p^+$  and  $n^0$ ) are not stopped until the Hadronic Calorimeter, giving birth to a spectacular showering. The muon and the neutrino are the only particles capable to reach the outermost subdetector, the MS, with the former can be tracked while the latter is completely invisible to ATLAS. (Credit to ATLAS Experiment © CERN)

## Chapter 5

# Search for a Top-Philic Resonance BSM: A First Step

*What we do see depends mainly on what we look for. [...] In the same field the farmer will notice the crop, the geologists the fossils, botanists the flowers, artists the coloring, sportsmen the cover for the game. Though we may all look at the same things, it does not all follow that we should see them.*

— John Lubbock, *The Beauties of Nature and the Wonders of the World We Live in*

*A journey of a thousand miles begins with a single step.*

— Lao Tzu, ancient Chinese philosopher

The top quark is indeed one of the most important particles of the SM, in fact, there is a whole physics area related to it, called *top physics*, that aims to study and exploit its unique properties for a deeper understanding of the world we live in. Being the heaviest particle of the SM due to its biggest Yukawa coupling constant to the Higgs field, the top quark is a key opening a wide gate to physics BSM.

In *ATLAS experiment*, an analysis team is taking the challenge of investigating the existence of a top-philic resonance BSM, e.g. the BSM vector boson  $Z'$ , in an extremely rare event of the SM presenting four top-quarks in its final state. The *BSM4Tops* analysis team is currently working on tasks related to the single-lepton decay channel, the next step is to perform analysis in a more challenging channel, the fully-hadronic decay channel, in order to combine the multiple channels as discussed in Ref. [109, p. 15].

In this work, we focus on the fully-hadronic channel, by trying to adapt the configuration file used in the top analysis to an all-jets selection, and this is discussed in detail in Sect. 5.2.1. But before this, we start this chapter by presenting the SM backgrounds of our  $t\bar{t}t\bar{t}$  event in Sect. 5.1, then, the main

program of the top analysis (`top-xaod`) is discussed at the opening of Sect. 5.2. Finally, we locally run our program using an MC sample, this sample is identified in Sect. 5.2.2.1 just before closing this chapter with Sect. 5.2.2.2, where some results are plotted from the output file, for different cuts in our selection.

## 5.1 BSM- $t\bar{t}t\bar{t}$ Backgrounds in the SM

As we have calculated earlier, the fully-hadronic decay channel of the four-top quarks has a large BR ( $\sim 20\%$ ) (c.f. 2.2.3) at the cost of an enormous multi-jet background. In this section, we are presenting the dominant and subdominant SM backgrounds, basing on the work done in ref. [109].

In our case, the QCD background is larger in orders of magnitude than the signal [109, p. 7]. However, it can be reduced to a manageable level using a conjunction of boosted hadronic top-taggers and multiple b-tagging [109, p. 7]. Nevertheless, some background events are irreducible, namely the SM  $t\bar{t}t\bar{t}$ , and  $t\bar{t} + jets$ , which are the dominant backgrounds, in addition to subdominant backgrounds that include multi-jet events with up to four light-flavor jets,  $b\bar{b} + jets$ ,  $b\bar{b}b\bar{b}$ ,  $Z_{b\bar{b}} + jets$  (where  $Z_{b\bar{b}}$  is the SM Z boson decaying into a  $b\bar{b}$  pair), and the single top events  $t\bar{b} + jets$  [109].

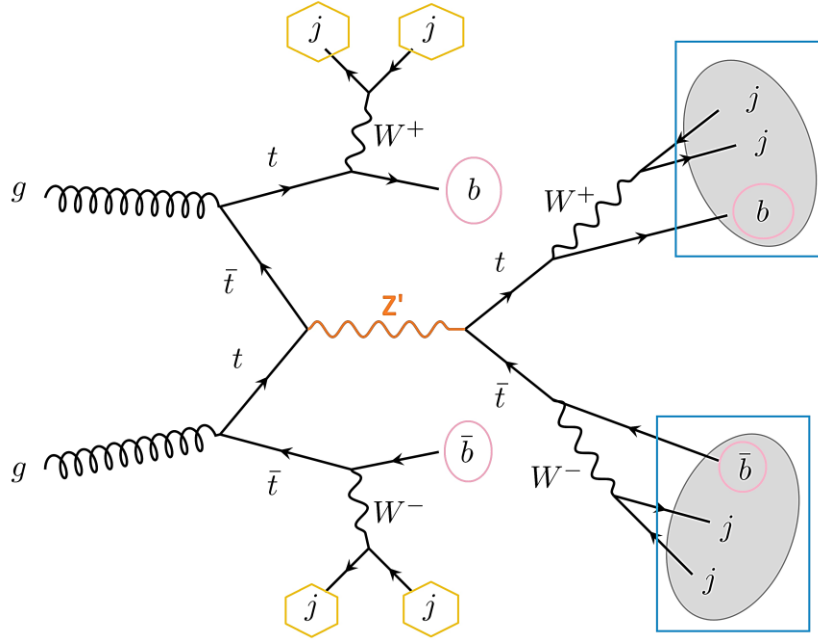


**Figure 5-1:** fully-hadronic decay products of the  $t\bar{t}t\bar{t}$ . Represented in, four b-jets (pink circles) two from the spectator tops, and two others from the hardest tops within the two re-cluster jets (RCJs, blue rectangles), and four jets outside of the RC (called additional jets, yellow hexagons).

Basing on the simplified interaction Lagrangian of equation (2-11) (c.f. section 2.1.3), the signal and background events are simulated using MADGRAPH5+PYTHIA, then, a high- $H_T$  cut is demanded as a preselection to eliminate the SM multi-jet backgrounds, where  $H_T$  is defines as the sum of transvers momenta of all final state partons. e.g. for  $H_T > 800 \text{ GeV}$  the simulated cross sections of different backgrounds are summarized in (Table 5-1).

Backgrounds	$\sigma$ [fb]
$t\bar{t}\bar{t}$	3.1
$t\bar{t} + jets$	$2.6 \times 10^4$
$t\bar{b} + jets$	$2.8 \times 10^3$
QCD	$4.2 \times 10^6$
$Z_{bb} + jets$	$3.4 \times 10^3$

Table 5-1: simulated cross sections for different backgrounds. Values are taken from [109, p. 8]

Next, two different cuts (Table 5-2) are applied before reconstructing the 1.5 TeV  $Z'$  resonance (Figure 5-2).

Cuts	definition
	$N_{fj} \geq 2 ; R = 0.7$
Basic Cuts	
	$P_T^{fj} > 500 \text{ GeV} ;  n_{fj}  < 2.5$
Ditop Selection	$N_t \geq 2$

Table 5-2: Basic and Ditop selections for the fully hadronic channel.  $N_{fj}$  and  $P_T^{fj}$  are respectively the number and transvers momentum of “fat jets”, which are jet with a radius parameter of 0.7 and they can be any flavor-tagged.  $N_t$  is the number of top-tagged jets. [109]

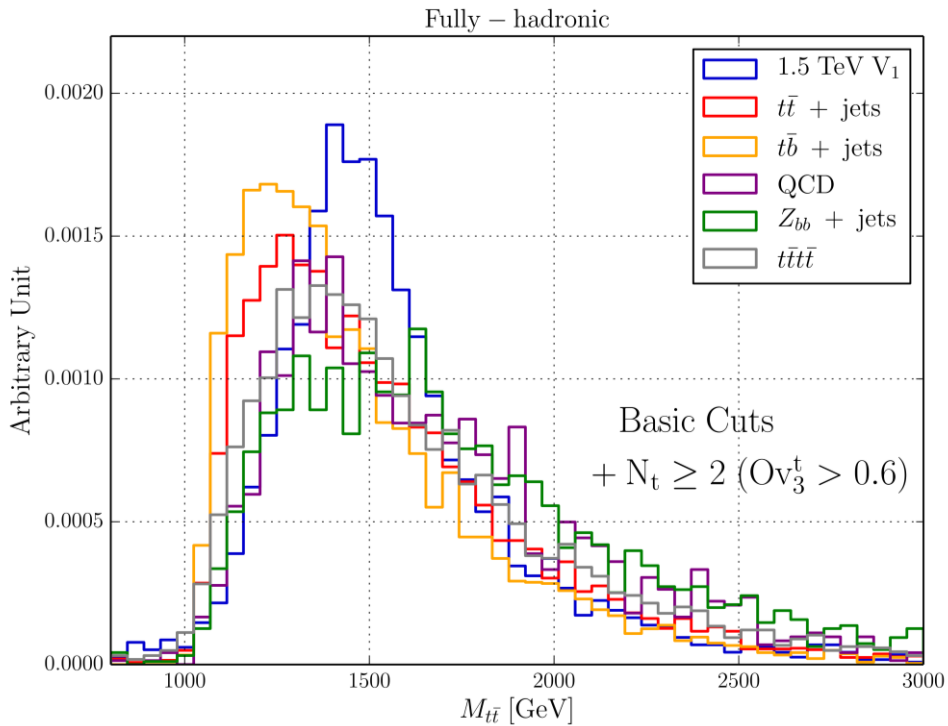


Figure 5-2: the reconstructed mass of the  $Z'$  prime resonance from those of the hardest top jets. As we can notice, the backgrounds are significantly huge. The reconstructed resonance peaks at 1.5 TeV. Figure from [109].

## 5.2 Top Analysis

The work done in this manuscript is implemented within the framework of the so-called *AnalysisTop*.

*AnalysisTop* is an ATLAS xAOD analysis framework, that calibrates all physics objects related to the top quark (c.f. [Chapter 4](#)), applies physics objects cuts defined by the user, applies overlap removal, as well as event level cuts customized by the user too. It is well supported by the top reconstruction group and highly configurable. The *AnalysisTop* framework can be used with no need to edit the central *Athena*<sup>47</sup> package, and it gives the possibility to save the output defined by the user in flat n-tuples root files [153].

A few months ago, *AnalysisTop* is no longer a standalone release, and it became part of the *AnalysisBase* which is basically a collection of software and tools developed in ATLAS and that are necessary for any analysis.

In this section, we are going to introduce the main code for the n-tuples production, we will stress what every line in the configuration file is there for, and then we can show the results of applying different cuts using a Monte Carlo (MC) sample.

`top-xaod` is the main program for the production of the n-tuples, it takes two text files as inputs, one is the configuration file that contains all the customized event cuts and event selections (writing down that configuration file was supposed to be half of the current work), while the other holds the path to the sample(s) to which the `top-xaod` applies CP corrections and object selection (hardcoded), it proceeds the configurations we define in the configuration file, and it saves the events that pass the selection in a root file we call n-tuple. The main command to locally run the program is:

```
top-xaod      configuration-file.txt      sample-path.txt
```

a standard output (output of the command shown in the terminal) will show the different steps of the validation cuts, as well as some warning messages, and then it will start processing the events of the sample. The used sample in this work contained 40K events, hence the standard output contained the following:

```
Processing event 100 / 40000 (current file: 100 / 40000)
Processing event 200 / 40000 (current file: 200 / 40000)
Processing event 300 / 40000 (current file: 300 / 40000)
Processing event 400 / 40000 (current file: 400 / 40000)
Processing event 500 / 40000 (current file: 500 / 40000)
...
Processing event 39700 / 40000 (current file: 39700 / 40000)
Processing event 39800 / 40000 (current file: 39800 / 40000)
Processing event 39900 / 40000 (current file: 39900 / 40000)
```

---

<sup>47</sup> Athena is based on Gaudi project providing the necessary interfaces for building high energy physics experiment frameworks.

After processing all the events in the sample (or the number of events specified in the configuration file), the events passing the selection process are saved in an output root file, and the final yields are printed out in the standard outputs.

### 5.2.1 Configuration File Options

The configuration file can be seen as the instruction book that guides the `top-xaod` program while doing its job, hence, our analysis is configured in many different ways (single-lepton analysis, SS dilepton, hadronic...) through a simple text file. However, changing it to suit certain analysis is not a straightforward process, it takes quite a long time and effort.

The configuration file has so many options, and they keep growing and each time new features are added. Nevertheless, not all options are mandatory to be included in the configuration files, and those are assigned with default values. The complete list of options can be found in the ATLAS GitLab [154]. However, we only present the meaning and purpose of the options used in our configuration file.

```
1. LibraryNames libTopEventSelectionTools libTopEventReconstructionTools libBSM4tops
```

Those are the libraries that should be loaded, the last one is added for a BSM extended analysis.

```
2. #NEvents 1000
```

This option determines the number of events to be processed, the hash sign means that the `top-xaod` will escape this line, and all the events will be processed. This option is very useful while still adapting the configuration file, since the purpose is to check if it runs properly first, then we can iterate over all the events.

```
3. ObjectSelectionName top::ObjectLoaderStandardCuts
4. ElectronCollectionName Electrons
5. MuonCollectionName Muons
6. TauCollectionName None
7. PhotonCollectionName None
8. METCollectionName MET_Reference_AntiKt4EMPFflow
9. LooseMETCollectionName MET_Reference_AntiKt4EMPFflow
10. LargeJetCollectionName AntiKt10LCTopoTrimmedPtFrac5SmallR20Jets
11. LargeJetSubstructure None
12. LargeRJESJMSConfig CombMass
13. JetCollectionName AntiKt4EMPFflowJets_BTagging201903
14. UseRCJets True
```

These are the used object collections, there might be several choices for each option, and those assigned to `None` are ignored. Seeking a full hadronic selection, photons and leptons are ignored, however, electrons and muons cannot be ignored at this stage, otherwise, the code will not run, and we will take care of them later. We can notice the `AntiKt` in jet collection names, which is the main finding algorithm of jets as we have mentioned earlier in Sec. 4.4.1.

```
15. ElectronID TightLH
16. ElectronIDLoose MediumLH
```

```

17. MuonQuality Medium
18. MuonQualityLoose Medium
19. ElectronIsolation FCTight
20. ElectronIsolationLoose None
21. MuonIsolation FCTightTrackOnly
22. MuonIsolationLoose None
23. UseElectronChargeIDSelection False
24. ElectronPt 15000
25. MuonPt 15000
26. JetPt 25000
27. BoostedJetTagging JSSWTopTaggerDNN:DNNTaggerTopQuarkInclusive80
   JSSWTopTaggerDNN:DNNTaggerTopQuarkContained80
28. BTaggingWP DL1:FixedCutBEff_77 DL1r:FixedCutBEff_77 DL1:FixedCutBEff_70
   DL1r:FixedCutBEff_70 DL1:FixedCutBEff_60 DL1r:FixedCutBEff_60
   DL1:FixedCutBEff_85 DL1r:FixedCutBEff_85 DL1r:Continuous DL1: Continuous

```

Tight, medium, and tight are different identification selections, and the transverse momenta of our three objects (electrons, muons, and jets) are defined. `BoostedJetTagging` is for the hardest jets identification, and `BTaggingWP` is where we define the b-tagging and the b-tagging working points (WP). `DL1` and `DL1r` are the taggers, while the `FixedCutBEff_*` are the WPs.

```

29. OutputFormat top::CustomEventSaver
30. OutputFilename output.root
31. OutputEvents SelectedEvents

```

The above three lines tell the program to save only selected events in a root file named `output.root`. The name of the file is something we should keep in mind to avoid overwriting previous outputs.

```

32. PRWConfigFiles_FS
  dev/AnalysisTop/PileupReweighting/user.iconnell.Top.PRW.MC16e.FS.v2/prw.merged.root
33. PRWConfigFiles_AF
  dev/AnalysisTop/PileupReweighting/user.iconnell.Top.PRW.MC16e.AF.v2/prw.merged.root
34. PRWActualMu_FS
  GoodRunsLists/data18_13TeV/20190318/physics_25ns_Triggerno17e33prim.actualMu.OflLumi-13TeV-010.root
35. PRWActualMu_AF
  GoodRunsLists/data18_13TeV/20190318/physics_25ns_Triggerno17e33prim.actualMu.OflLumi-13TeV-010.root
36. PRWLumiCalcFiles
  GoodRunsLists/data18_13TeV/20190318/ilumicalc_histograms_None_348885-364292_OflLumi-13TeV-010.root

```

This is the pile-up configuration, the `PRWConfigFiles` are for MC (precisely the `MC16e`), `PRWActualMu`, and `PRWLumiCalcFiles` are for data, and `FS` (`AF`) refers to a full (fast) simulation sample.

```

37. GRLDir GoodRunsLists
38. GRLFile data15_13TeV/20170619/physics_25ns_21.0.19.xml
    data16_13TeV/20180129/physics_25ns_21.0.19.xml
    data17_13TeV/20180619/physics_25ns_Triggerno17e33prim.xml
    data18_13TeV/20190219/physics_25ns_Triggerno17e33prim.xml

```

The above two options are related to the Good Run Lists (GRL). As we shall see later, the GRL is one of the mandatory cuts (called *veto cuts*) that only keeps events that are declared in the `GRLFile` option (the four `.xml` data files).

```

39. UseAodMetaData True
40. IsAFII True
41. TopParticleLevel False

```

The option in line 39 is used to extract the type of the sample (FS or AFII) from the sample itself reading its metadata, and when set to be `True`, the option `IsAFII` is not necessary anymore and will be ignored, except if the `UseAodMetaData` could not figure out the type of the sample. Our MC16e sample is generated for a fast simulation, hence the `IsAFII` is set to be true. The `TopParticleLevel` ensures that a particle-level tree<sup>48</sup> will be created in the output, in our case we are only interested in the nominal tree.

The last part of the configuration file takes care of the selections. Our fully-hadronic selection is labeled `BSM_alljets_DL1_RCJ`, but first, we define some sub-selections, that will be included later within the main selection.

**Veto cuts: BASIC**

```

42. SUB BASIC
43.      INITIAL
44.      GRL
45.      GOODCALO
46.      PRIVTX
47.      RECO_LEVEL

```

The `SUB` option in line 42 is how we inform `top-xaod` that `BASIC` is a sub-selection that applies five cuts (lines 43-47). These cuts are special being *mandatory* cuts in a reconstruction-level analysis, and for this reason that we call them *veto cuts*. The start of the cutflow is set by `INITIAL`, `GRL` excludes events that are not listed in our `GRLFile`, to filter the noise bursts in the LAr and Tiles of the calorimeters (c.f. 3.2.3) we use the `GOODCALO` cut, `PRIVTX` ensures that our event contains at least one PV, and `RECO_LEVEL` reflects the fact that our selection (or any other selection containing the `BASIC` sub-selection) is a reconstructed-level selection.

**b-tagging pre-selections**

```

48. SUB Nbttag_DL1
49.      JET_N_BTAG_DL1:FixedCutBEff_77 >= 2
50. SUB Nbttag_DL1r
51.      JET_N_BTAG_DL1r:FixedCutBEff_77 >= 2

```

<sup>48</sup> A tree is data container provided by ROOT to store objects of the same class.

Two sub-selection are defined for b-tagging purposes, they are named `Nbtag_DL1` and `Nbtag_DL1r`, since they use `DL1` and `DL1r` taggers respectively, and both are requiring at least two b-tagged jets with an efficiency of 77%.

#### *Trigger decision*

```
52. SUB ALLHAD
53.   . BASIC
54.   TRIGDEC HLT_j460_a10t_lcw_jes_L1J100
```

`ALLHAD` sub-selection uses the `BASIC` sub-selection in addition to a trigger decision cut `HLT_j460_a10t_lcw_jes_L1J100`. So next time we include the `ALLHAD` sub-selection, the `BASIC` one is included as well.

#### *RC jet sub-selection*

```
55. SUB RCJ
56.   RCJET_N 350000 >= 2
57.   RCJET_N 500000 >= 1
58.   RCJETMASS_N 50000 >= 2
```

The RC jets are those issued from the hardest tops (c.f. [Figure 5-1](#)). Here we only allow events at least including either 2 RCJs with a transverse momentum cut of 350 GeV each, or one RCJ of 500 GeV. `RCJETMASS_N` is used to distinguish between hadronic jets from top decay and jets from other sources.

#### *final selection*

```
59. SELECTION BSM_alljets_DL1_RCJ
60.   . ALLHAD
61.   . Nbtag_DL1
62.   . RCJ
63.   EL_N 15000 == 0
64.   MU_N 15000 == 0
65. SAVE
```

Now we assemble all the previous sub-selections (with `BASIC` being included in `ALLHAD`) and we exclude all events presenting an electron or a muon. The `SAVE` option in line 65 is crucial since without it the cuts in our `SELECTION` will be applied but the events passing those requirements will not be saved in the output file.

### 5.2.2 Local Running

In this section we present the results of running the `top-xaod` program locally, using as inputs the previously explained configuration file, and an `MC16e` sample. The MC sample properties are exposed as well as the contents of the output root file. Finally, for different validation cuts, we plot the histograms of some parameters of interest, namely  $p_T$ ,  $\eta$ , and  $\phi$ , being the parameters used to reconstruct a given particle trajectory.

### 5.2.2.1 MC16e Sample

The used sample is an MC16e sample (i.e. matches the 2018 data). As we know, the ATLAS samples use a standard nomenclature, so that many metadata information can be deduced only from the sample name. In our case, the sample is dubbed the following name:

```
mc16_13TeV.700047.Sh_228_ttbar_AllHadronic_EnhMaxHTavrgTopPT.deriv.DAOD_TOPQ1.e7947  
_s3126_r10724_p4031
```

where:

`mc16_13TeV` : is the project name.

`700047` : is the dataset number.

`Sh_228_ttbar_AllHadronic_EnhMaxHTavrgTopPT` : is physics short.

`Deriv` : is the production step.

`DAOD_TOPQ1` : is the data type.

`e7947_s3126_r10724_p4031` : is the AMI Tag (also known as *the version*).

Other information can be retrieved using the ATLAS Metadata Interface (AMI), using either the AMI website [155] or through the following command in an `lxplus` session:

```
ami show dataset info mc16_13TeV.700047.Sh_228_ttbar_AllHadronic...
```

Some properties shown at the output are: the generator is `Sherpa(v.2.2.8p3)`<sup>49</sup>, the geometry version is `ATLAS-R2-2016-01-00-01`, and the beam energy is `6.5 TeV`.

### 5.2.2.2 Results

Now that we have discussed both inputs fed to the `top-xaod` program, we can run our code (after well setting the environment). In order to observe the effect of each level of the eight applied cuts, we apply them successively generating eight n-tuples as outputs. In the beginning, we only apply the veto cuts, then the trigger decision cut, followed by the b-tagging cut, then the three RCJ cuts, and finally the two leptons elimination cuts. The number of events surviving the cut is saved in the cutflow leaf<sup>50</sup>, and in (Figure 5-3) we overlayed the results in a single plot. And of course, one might check that lepton leaves, such as the electrons and muons energies, have no entries.

---

<sup>49</sup> And that is meaning of the ‘sh’ in the physics short.

<sup>50</sup> Element of a ROOT tree.

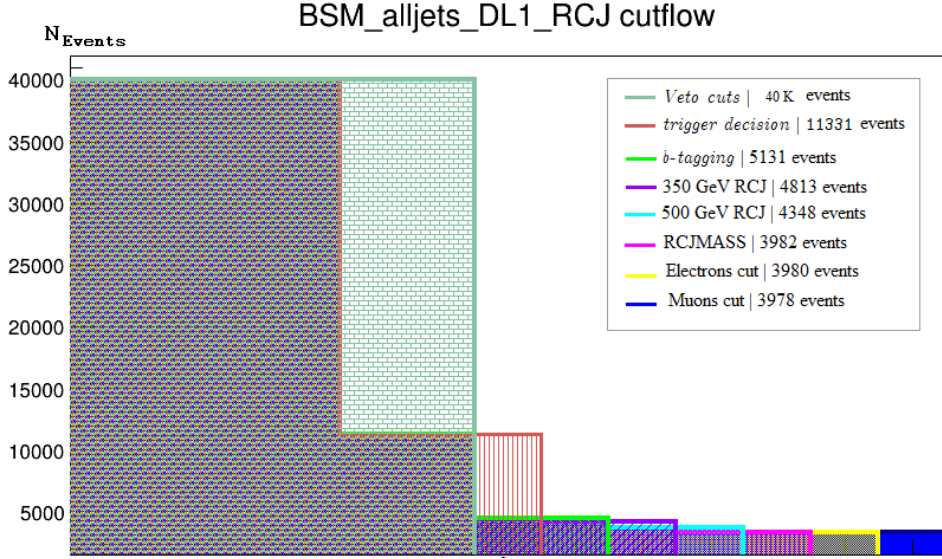


**Figure 5-3:** The cutflow of our `BSM_alljets_DL1_RCJ` selection. Veto cuts did not reduce the size of the sample, i.e. all the events pass the veto cuts, trigger decision cut takes away most of the events, only 11331 events did survive this cut, 6200 events did not respect the requirements of the  $b$ -tagging cuts, so they were rejected and only 5131 events are remaining, the three RCJ cuts leave us with 3982 events, and after excluding four events presenting electrons or muons, the final number of events passing our selection is 3978 events.

We do the same for four other jet parameters, namely,  $\eta_{jet}$ ,  $\phi_{jet}$ ,  $p_T^{jet}$ , and  $M_{jet}$ . In principle, we can do the same for any object in our outputs, since the eight n-tuples contain the same trees and branches, only with a different number of entries, since for each cut level added, the number of entries gets reduced.

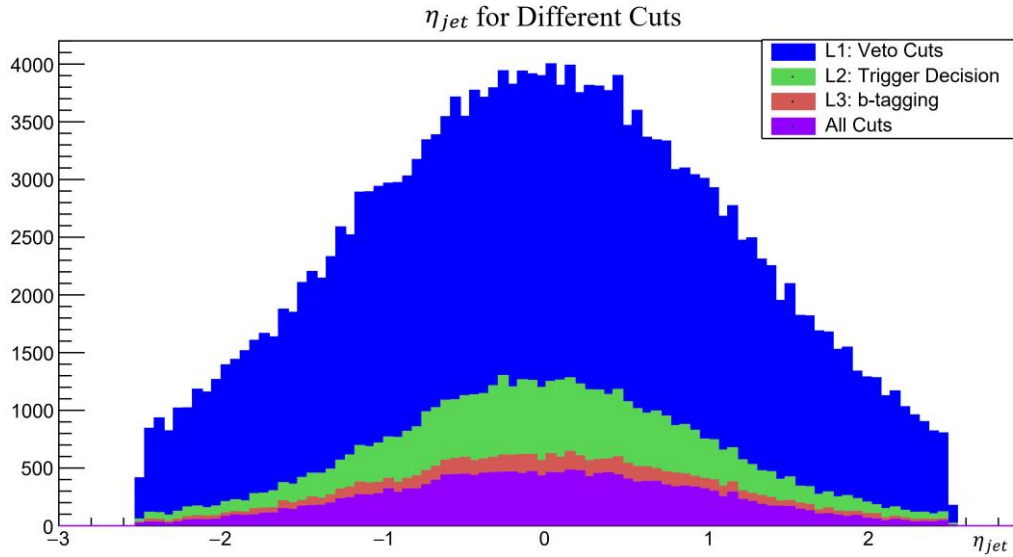


**Figure 5-4:** The pseudo-rapidity of jets after applying different cuts.  $L_i$  refers to different levels of our `BSM_alljets_DL1_RCJ` selection (c.f. Sect. 5.2.1). We notice that  $\eta$  has a normal distribution (as it should be) with  $|\eta_{jet}| < 2.5$ , and the only difference between the different cut levels is the number of entries getting smaller and smaller for each cut added.

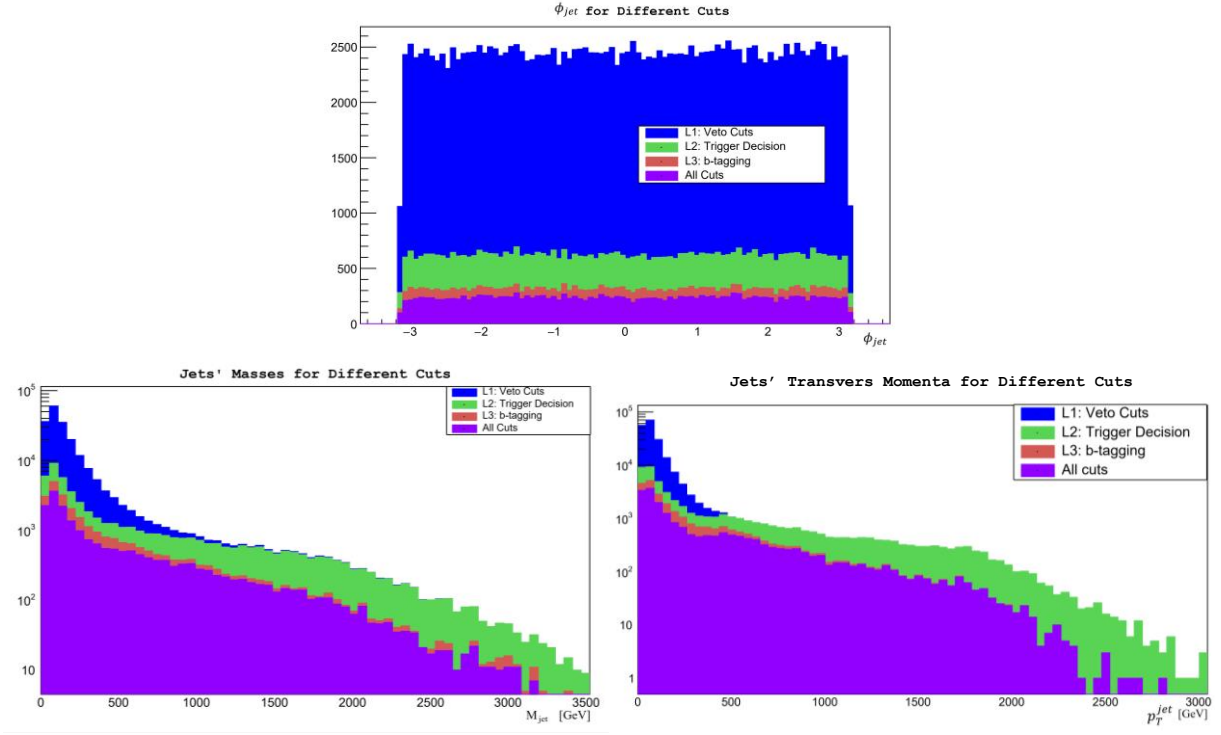


**Figure 5-5:** Jets' parameters of interest for different cuts. (Top) the azimuthal angle  $\phi$ , (down right) the transvers momenta  $p_T$ , (down left) the masses  $M_{jet}$  that shows hundreds of energetic jets with masses in the range of TeV. The two latter are plotted on a logarithmic scale.

The previous diagrams are related to jets in a global manner, i.e. without a flavor-tagging. However, the output file contains branches for the RC jets that can be issued from the hardest tops (Figure 5-1), the products of the  $Z'$  decay. In the following diagrams we present the evolution of some parameters of interest; e.g.  $\eta_{RCJ}$ ,  $p_T^{RCJ}$ , and  $M_{RCJ}$ .

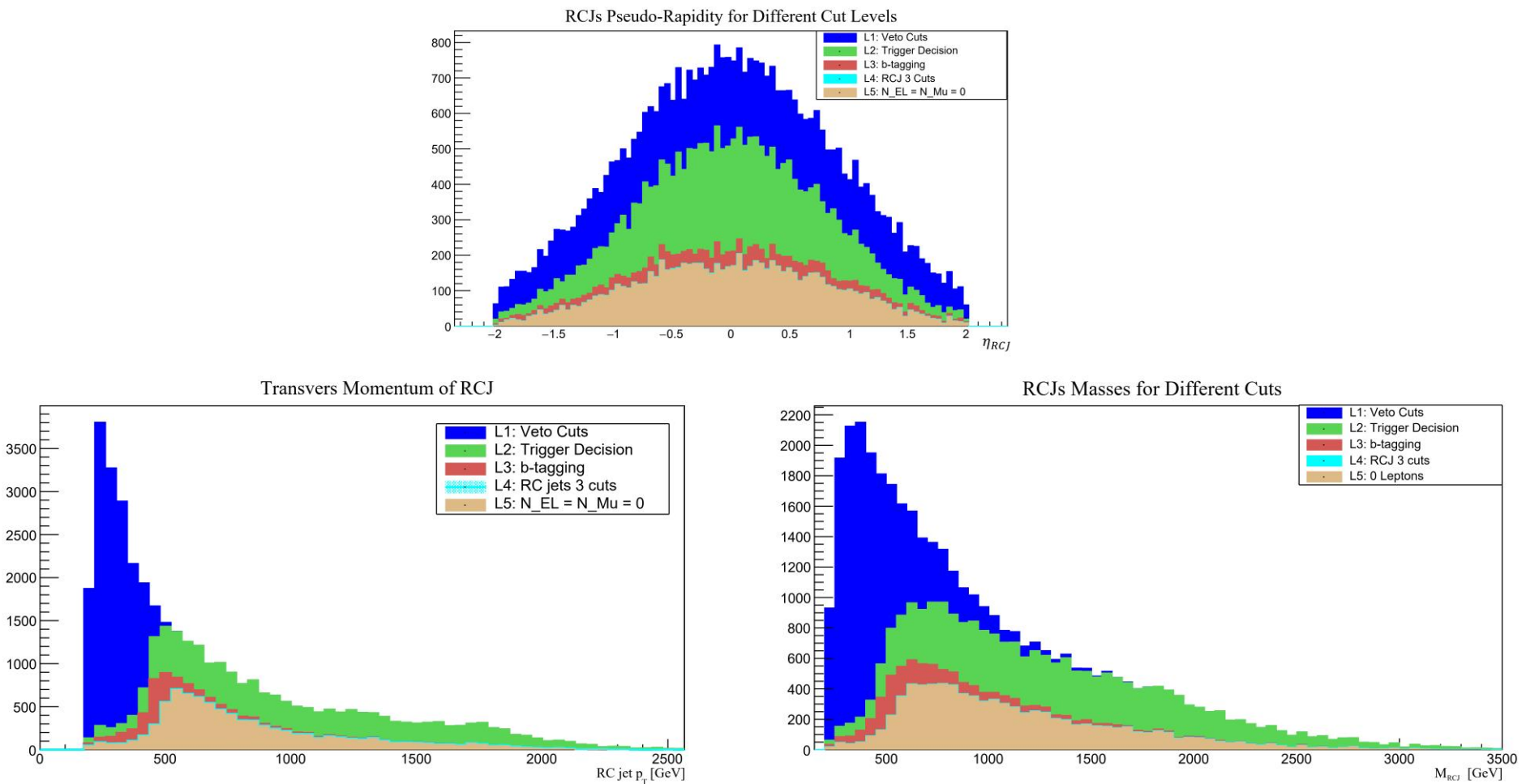


**Figure 5-6:** Parameters of interest for RCJs. (Top)  $\eta_{RCJ}$ , it keeps the previous shape, except that it peaks with 800 RC jets instead of 4000 jets, which gives an insight about how few RCJs are. (Down Left)  $p_T^{RCJ}$ , we notice that after applying the RCJ cuts, the histograms peak at a  $p_T^{RCJ} > 500$  GeV. (Down Right) range of the RCJs masses, after applying all cuts in our selection, the  $M_{RCJ}$  peaks at  $0.5 \text{ TeV} < M_{RCJ} < 1 \text{ TeV}$ , which makes the mass of a  $Z'$  candidate in the range of  $[1 \text{ TeV}, 2 \text{ TeV}]$ .

RCJs are basically meant to select top-tagged jets. Moreover, the outputs contain branches for the truth tops, and we finish this chapter by plotting two histograms from some leaves of the `truth_top` branches.

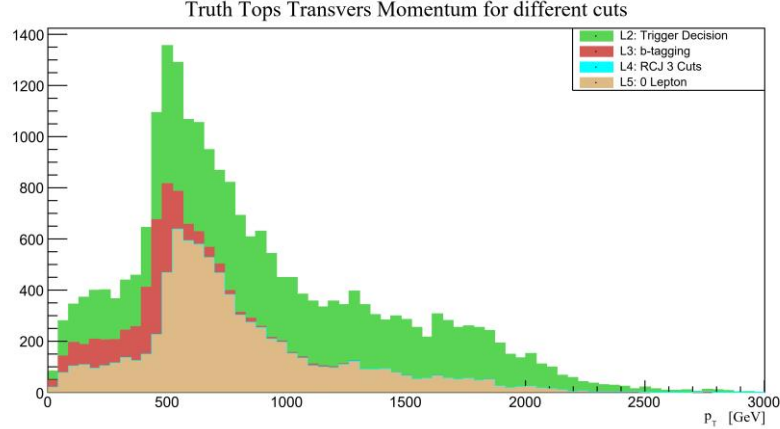


**Figure 5-7:** Transverse momenta of truth tops. This histogram is similar to the previous one ( $p_T^{RCJ}$ ), where after all cuts are applied, the histogram peaks a bit above 500 GeV with almost 600 jets, which confirms that RCJ cuts are distinguishing the top-tagged jets from other flavor-tagged jets.

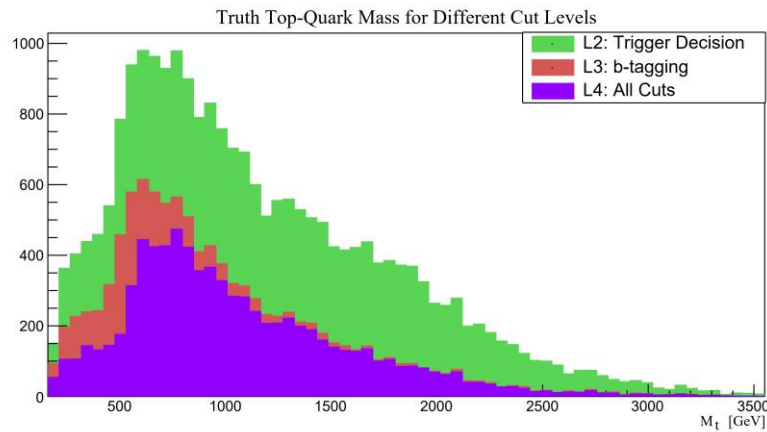


**Figure 5-8:** Truth top-quarks masses. After all cuts are applied, the  $M_T$  peaks at a value around 0.75 TeV, so if two of such massive tops were originated from the same vertex, it might suggest a 1.5 TeV  $Z'$  resonance.

# Concluding Remarks

In this Master thesis, we were interested in probing the observation of a new heavy gauge boson outside of the SM framework, as a resonance state within a very rare event predicted by the SM, the four top-quarks  $t\bar{t}t\bar{t}$ , using the ATLAS detector. This work was not aiming to accomplish a complete analysis, this is as everyone knows requires a full team, a considerable amount of time, and absolutely beyond a Master's student's abilities and/or timeframe. Nevertheless, in addition to a (hopefully) obliging bibliography about the SM and beyond, the top physics, the LHC, and the ATLAS detector, the main tasks addressed in this manuscript were, on the theoretical side, to re-calculate the BRs of the 12 deferent decay channels of a  $t\bar{t}t\bar{t}$  event, and on the analysis side, to adapt the configuration file used as input for the main program in `AnalysisTop`, the `top-xaod`, to suit a fully-hadronic decay channel. The former task revealed results tunning to the ones we received, moreover, the sum of BRs we have calculated was 1.0001, while it was 0.996 in the given document, and this is due to us considering two digits after decimal instead of just one taken in the same document. As for the latter task, the configuration file was tested for different MC samples; MC16a, MC16d, MC16f, and MC16e, as well as data samples, and it did run with only some warnings but without any errors. However, we only presented in the last section some results from the output file we have obtained using the MC16e sample, and this is because it was the one with the greatest number of entries, so the plots are quite satisfying.

The first chapter of this document engaged in its first part the SM, being the main theoretical framework in particle and high energy physics, the structure we have presented this chapter was pretty different to the usual morphology. Being proudly raised in a theoretical lab, I was fortunate to take an introductory course of the SM in a theoretical manner, starting from the Fermi Theory of Weak Interactions, to the EWSB. Though, questions like how did we get to this current picture of elementary particles from the *atomos* philosophy? Was it by experiments or by theories these particles were introduced? if all fermions are described with Dirac's equation, why there are no right-handed neutrinos? If bosons are described by the Klein-Gordon equation that also suggests negative energy states, why there are no anti-bosons? Are my hands made of left-handed or right-handed electrons? All these questions and others, drove us to allocate a considerable space for the history of the SM, and since we know that doing this in a Ph.D. thesis will (probably) not be possible, so if not now, then when? Limitations and shortcomings of the SM were discussed, and some BSM approaches suggesting new heavy gauge bosons, such as the SSM, LRM, and the GUTs were briefly presented, taking into consideration that the current  $Z'$  search taking place in ATLAS experiment by the BSM4Tops analysis team is a non-model-based study.

Being the most important particle for this manuscript, we have assigned the second chapter for the top quark. Firstly, we have discussed its production modes in the SM and BSM, where we concluded that the top quarks are mainly produced in  $t\bar{t}$  pairs with a cross-section  $\sigma_{t\bar{t}}$  measured to exceed 800 pb at

$\sqrt{s} = 13 \text{ TeV}$ . Nevertheless, they can also be produced in a very rare event, the  $t\bar{t}t\bar{t}$  four-tops, where a complete-NLO prediction for  $t\bar{t}t\bar{t}$  production in proton-proton collisions at 13 TeV has been calculated to be  $\sigma_{t\bar{t}t\bar{t}} = 12.0 \pm 2.4 \text{ fb}$  in the framework of the SM. With such a tiny cross-section, a  $t\bar{t}t\bar{t}$  event has never been observed until lately, where the ATLAS Collaboration announced strong evidence for  $t\bar{t}t\bar{t}$  production in the multilepton final state using an integrated luminosity of  $139 \text{ fb}^{-1}$  of pp collisions data at  $\sqrt{s} = 13 \text{ TeV}$ , and  $\sigma_{t\bar{t}t\bar{t}}$  is measured to be  $24^{+7}_{-6} \text{ fb}$ . The deviation between the calculated and measured  $\sigma_{t\bar{t}t\bar{t}}$  is a strong motivation for BSM searches, such as the search for a  $t\bar{t}t\bar{t}$  events with a heavy  $Z'$  gauge boson, that are not taken into consideration for the calculated  $\sigma_{t\bar{t}t\bar{t}}$  but can contribute to the measured one. The production of  $t\bar{t}t\bar{t}$  BSM is presented using a general Lagrangian without lying on any of the BSM approaches. Finally, the decay of the single top, as well as the  $t\bar{t}$  pairs have been presented just before the closure of the chapter with elaborating the possible decay modes of  $t\bar{t}t\bar{t}$  four-tops, and calculating their BRs. The outcomes of these calculations were that the single-lepton decay channel enjoys the biggest BR, with a proportion of 26.34 %, which supports the decision of the BSM4Tops analysis team, currently working on tasks related to the single-lepton decay channel. The fully-hadronic channel comes second with a BR of 19.76 %, hence, the next step is to perform analysis in this more challenging channel, in order to combine the multiple channels.

The third chapter is meant to introduce the LHC accelerator, as well as the ATLAS detector, where we have presented the CERN Accelerator Complex, mentioning that LINAC4 has been lately connected to the injection point of the PSB, replacing its ancestor LINAC2 in the LHC acceleration chain in the next run. The ATLAS subdetectors, the ID, the Calorimeters, and the MS, have all been exposed without so many details about the electronics of the modules, keeping in mind the limited space and length a master thesis cannot exceed. Lastly, the two levels of the trigger system, L1 trigger and HLT, have been mentioned, as well as the data acquisition system, explaining their crucial role in reducing the number of events to be saved, by the Data Acquisition system, from a rate of  $40 \text{ MHz}$  to only  $1 \text{ KHz}$ .

After introducing the ATLAS detector, we have investigated in chapter 4 how does it actually identify the different products of the  $pp$  collisions that interact with the detector modules and sensors, and how different algorithms are used to reconstruct the physics objects from the electric signals retrieved from the detector cells, where we have stressed the tracking and vertexing, while we focused on the reconstruction and identification of electrons, muons, and jets, being the physics objects declared in our configuration file (though the first two will be completely rejected at the selection process).

In the last chapter, we have cited the SM backgrounds of the BSM- $t\bar{t}t\bar{t}$  process, including the SM- $t\bar{t}t\bar{t}$ . Later, we have declared the elements of the configuration file and explained the different cut-levels of the fully-hadronic selection, labeled `BSM_alljets_DL1_RCJ`. Next, we run the code locally, using our configuration file in addition to an MC16e sample, the metadata of this sample is retrieved using AMI, and we have cited some. In order to see the effect of each cut-level, we applied them successively, generating 8 outputs, with the same trees and branches, but with different numbers of entries, and we have noticed that after each cut-level, the number of events passing the selection is reduced, this decrease is relative to the used sample, for example, we note the last two cuts eliminating the electrons and muons are only excluding two events each, and this is due to the fact that the used sample is prepared for a full hadronic analysis. Applying all the cuts on the 40 thousand events sample, we end up with 3978 events successfully passing the events selection and being saved in the output file. From the nominal

trees of the 8 output files, we overlay histograms for different parameters of interest, from the three different branches, namely, the jet, the RCJ, and the truth top branches.

During this research journey, we have learned many know-hows, acquired expertness, and developed several skills, especially on the software and experiment sides, that helped us supply the current work. Namely, we became competent in using the Linux Command Line Interface (CLI) through the extensive use of the `lxplus` (LinuX Public Login User Service) accounts, in addition to the basics of `ROOT`, `python`, and `C++` programming languages in one hand, and on the other hand, using the Grid, getting datasets with `rucio`, and submitting jobs with `Panda`. Also, due to the COVID-19 pandemic, we have been able to remotely attend multiple events related to the field, explicitly, the ATLAS Induction Day, the 8<sup>th</sup> annual conference on Large Hadron Collider Physics (LHCP2020), and the 40<sup>th</sup> International Conference on High Energy Physics (ICHEP2020).

In closing, we would like to mention that the current document follows in its structure the UCI template, and it has roughly 32,344 words, respecting the [30K, 40K] range adapted worldwide. And as a final point, this numeric version of this work is a `Foxit ConnectedPDF` document, so comments and remarks can be applied by the reader and received directly by the author.



# Bibliography

- [1] A. Salam and J. C. Ward, "Weak and electromagnetic interactions", *Il Nuovo Cimento*, vol. 11, no. 4, pp. 568–577, Feb. 1959, DOI: [10.1007/BF02726525](https://doi.org/10.1007/BF02726525).
- [2] P. W. Higgs, "Broken Symmetries and the Masses of Gauge Bosons", *Phys. Rev. Lett.*, vol. 13, no. 16, pp. 508–509, Oct. 1964, DOI: [10.1103/PhysRevLett.13.508](https://doi.org/10.1103/PhysRevLett.13.508).
- [3] P. C. W. Davies, "The forces of nature", Cambridge; New York: Cambridge University Press, 1979.
- [4] G. Aad et al., "Observation of a new particle in the search for the Standard Model Higgs boson with the ATLAS detector at the LHC", *Phys. Lett. B*, vol. 716, no. 1, pp. 1–29, Sep. 2012, DOI: [10.1016/j.physletb.2012.08.020](https://doi.org/10.1016/j.physletb.2012.08.020).
- [5] A. G. M. van Melsen, "From atomos to atom: the history of the concept atom", Mineola, N.Y: Dover Publications, 2004.
- [6] A. W. Thackray, "The Origin of Dalton's Chemical Atomic Theory: Daltonian Doubts Resolved", *Isis*, vol. 57, no. 1, pp. 35–55, Apr. 1966, DOI: [10.1086/350077](https://doi.org/10.1086/350077).
- [7] J. Dalton, "A New System of Chemical Philosophy", S. Russell, 1808.
- [8] Wendell. Taylor, "J. A. R. Newlands: A pioneer in atomic numbers.", *J. Chem. Educ.*, vol. 26, no. 9, p. 491, Sep. 1949, DOI: [10.1021/ed026p491](https://doi.org/10.1021/ed026p491).
- [9] E. R. Scerri, "The periodic table: its story and its significance", Second edition. New York, NY: Oxford University Press, 2020.
- [10] R. F. Mould, "A century of x-rays and radioactivity in medicine: with emphasis on photographic records of the early years", Bristol; Philadelphia: Institute of Physics Pub, 1993.
- [11] T. J. Trenn, "Rutherford on the Alpha-Beta-Gamma Classification of Radioactive Rays", *Isis*, vol. 67, no. 1, pp. 61–75, 1976, Accessed: Oct. 13, 2020. [Online]. Available: <https://www.jstor.org/stable/231134>.
- [12] "Marie Curie and the radioactivity, The 1903 Nobel Prize in Physics", Nobelprize.org. Nobel Media AB 2014. Web. 30 Jul 2018. <https://www.nobelprize.org/prizes/physics/1903/marie-curie/facts/> (accessed Oct. 13, 2020).
- [13] J. J. Thomson, "Cathode Rays", *Lond. Edinb. Dublin Philos. Mag. J. Sci.*, vol. 44, no. 269, pp. 293–316, Oct. 1897, DOI: [10.1080/14786449708621070](https://doi.org/10.1080/14786449708621070).
- [14] M. Williams, "What Is the Plum Pudding Atomic Model?", *Universe Today*, Jan. 19, 2016. <https://www.universetoday.com/38326/plum-pudding-model/> (accessed Oct. 13, 2020).
- [15] E. Rutherford, "The scattering of  $\alpha$  and  $\beta$  particles by matter and the structure of the atom", *Lond. Edinb. Dublin Philos. Mag. J. Sci.*, vol. 21, no. 125, pp. 669–688, May 1911, DOI: [10.1080/14786440508637080](https://doi.org/10.1080/14786440508637080).

- [16] M. S. Longair, “Theoretical concepts in physics: an alternative view of theoretical reasoning in physics”, 2nd ed. Cambridge, U.K.; New York: Cambridge University Press, 2003.
- [17] N. Bohr, “On the constitution of atoms and molecules”, *Lond. Edinb. Dublin Philos. Mag. J. Sci.*, vol. 26, no. 151, pp. 1–25, Jul. 1913, DOI: [10.1080/14786441308634955](https://doi.org/10.1080/14786441308634955).
- [18] “The Nobel Prize in Physics 1935,” *NobelPrize.org*. <https://www.nobelprize.org/prizes/physics/1935/summary/> (accessed Oct. 13, 2020).
- [19] D. Griffiths, “Introduction to Elementary Particles”, 2nd Edition. Weinheim: Wiley-VCH, 2008.
- [20] C. L. Cowan, F. Reines, F. B. Harrison, H. W. Kruse, and A. D. McGuire, “Detection of the Free Neutrino: A Confirmation” *Science*, vol. 124, no. 3212, pp. 103–104, Jul. 1956, DOI: [10.1126/science.124.3212.103](https://doi.org/10.1126/science.124.3212.103).
- [21] K. Winter, Ed., “Neutrino physics”, 2nd ed. Cambridge, UK; New York: Cambridge University Press, 2000.
- [22] H. Yukawa, “On the Interaction of Elementary Particles I”, *Proc.Phys.Math.Soc.Jap.*, vol. 17, pp. 48–57, Feb. 1935, DOI: [10.1143/PTPS.1.1](https://doi.org/10.1143/PTPS.1.1).
- [23] O. Piccioni, “The Discovery of the Muon”, in *History of Original Ideas and Basic Discoveries in Particle Physics*, H. B. Newman and T. Ypsilantis, Eds. Boston, MA: Springer US, 1996, pp. 143–162.
- [24] G. Danby *et al.*, “Observation of High-Energy Neutrino Reactions and the Existence of Two Kinds of Neutrinos”, *Phys. Rev. Lett.*, vol. 9, no. 1, pp. 36–44, Jul. 1962, DOI: [10.1103/PhysRevLett.9.36](https://doi.org/10.1103/PhysRevLett.9.36).
- [25] M. L. Perl *et al.*, “Evidence for Anomalous Lepton Production in  $e^+ - e^-$ -Annihilation”, *Phys. Rev. Lett.*, vol. 35, no. 22, pp. 1489–1492, Dec. 1975, DOI: [10.1103/PhysRevLett.35.1489](https://doi.org/10.1103/PhysRevLett.35.1489).
- [26] K. Kodama *et al.*, “Observation of tau neutrino interactions”, *Phys. Lett. B*, vol. 504, no. 3, pp. 218–224, Apr. 2001, DOI: [10.1016/S0370-2693\(01\)00307-0](https://doi.org/10.1016/S0370-2693(01)00307-0).
- [27] M. Gell-Mann, “STRANGENESS”, *J. Phys. Colloq.*, vol. 43, no. C8, pp. C8-395-C8-408, Dec. 1982, doi: [10.1051/jphyscol:1982825](https://doi.org/10.1051/jphyscol:1982825).
- [28] M. Gell-Mann, “The Eightfold Way: A Theory of Strong Interaction Symmetry,” TID-12608, CTSL-20, 4008239, Mar. 1961. DOI: [10.2172/4008239](https://doi.org/10.2172/4008239).
- [29] V. E. Barnes *et al.*, “Observation of a Hyperon with Strangeness Minus Three”, *Phys. Rev. Lett.*, vol. 12, no. 8, pp. 204–206, Feb. 1964, DOI: [10.1103/PhysRevLett.12.204](https://doi.org/10.1103/PhysRevLett.12.204).
- [30] M. Gell-Mann, “A schematic model of baryons and mesons”, *Phys. Lett.*, vol. 8, no. 3, pp. 214–215, Feb. 1964, DOI: [10.1016/S0031-9163\(64\)92001-3](https://doi.org/10.1016/S0031-9163(64)92001-3).
- [31] G. Zweig, “An  $SU(3)$  model for strong interaction symmetry and its breaking. Version 2”, pp. 22–101, Feb. 1964, Accessed: Oct. 13, 2020. [Online]. Available: <https://inspirehep.net/literature/4674>.
- [32] O. W. Greenberg, “Color Charge Degree of Freedom in Particle Physics”, in *Compendium of Quantum Physics*, D. Greenberger, K. Hentschel, and F. Weinert, Eds. Berlin, Heidelberg: Springer, 2009, pp. 109–111.
- [33] Belle Collaboration *et al.*, “Observation of a Narrow Charmoniumlike State in Exclusive  $B^\pm \rightarrow K^\pm \pi^\pm \pi^- J/\psi$  Decays”, *Phys. Rev. Lett.*, vol. 91, no. 26, p. 262001, Dec. 2003, DOI: [10.1103/PhysRevLett.91.262001](https://doi.org/10.1103/PhysRevLett.91.262001).

- [34] LHCb collaboration et al., “A model-independent study of resonant structure in  $B^+ \rightarrow D^+ D^- K^+$  decays”, ArXiv200900025 Hep-Ex, Sep. 2020, Accessed: Oct. 13, 2020. [Online]. Available: <http://arxiv.org/abs/2009.00025>.
- [35] LHCb collaboration et al., “Amplitude analysis of the  $B^+ \rightarrow D^+ D^- K^+$  decay”, ArXiv200900026 Hep-Ex, Sep. 2020, Accessed: Oct. 13, 2020. [Online]. Available: <http://arxiv.org/abs/2009.00026>.
- [36] J. D. Bjørken and E. A. Paschos, “Inelastic Electron-Proton and  $\gamma$ -Proton Scattering and the Structure of the Nucleon”, Phys. Rev., vol. 185, no. 5, pp. 1975–1982, Sep. 1969, DOI: [10.1103/PhysRev.185.1975](https://doi.org/10.1103/PhysRev.185.1975).
- [37] B. J. Bjørken and S. L. Glashow, “Elementary particles and  $SU(4)$ ”, Phys. Lett., vol. 11, no. 3, pp. 255–257, Aug. 1964, DOI: [10.1016/0031-9163\(64\)90433-0](https://doi.org/10.1016/0031-9163(64)90433-0).
- [38] S. L. Glashow, J. Iliopoulos, and L. Maiani, “Weak Interactions with Lepton-Hadron Symmetry”, Phys. Rev. D, vol. 2, no. 7, pp. 1285–1292, Oct. 1970, DOI: [10.1103/PhysRevD.2.1285](https://doi.org/10.1103/PhysRevD.2.1285).
- [39] J.-E. Augustin et al., “Discovery of a Narrow Resonance in  $e^+e^-$  Annihilation”, Phys. Rev. Lett., vol. 33, no. 23, pp. 1406–1408, Dec. 1974, DOI: [10.1103/PhysRevLett.33.1406](https://doi.org/10.1103/PhysRevLett.33.1406).
- [40] J. J. Aubert et al., “Experimental Observation of a Heavy Particle J”, Phys. Rev. Lett., vol. 33, no. 23, pp. 1404–1406, Dec. 1974, DOI: [10.1103/PhysRevLett.33.1404](https://doi.org/10.1103/PhysRevLett.33.1404).
- [41] Harrie Stewart Wilson Massey and D. H. Davis, “Eric Henry Stoneley Burhop, 31 January 1911 - 22 January 1980,” Biogr. Mem. Fellows R. Soc., vol. 27, pp. 131–152, Nov. 1981, DOI: [10.1098/rsbm.1981.0006](https://doi.org/10.1098/rsbm.1981.0006).
- [42] Kyoto U. Kyoto U. “CP Violation in the Renormalizable Theory of Weak Interaction”, INSPIRE. <https://inspirehep.net/literature/81350> (accessed Oct. 13, 2020).
- [43] H. Harari, “Theoretical Interpretation of  $e^+e^-$  Results”, Dec. 1979, Accessed: Oct. 13, 2020. [Online]. Available: <https://inspirehep.net/literature/143505>.
- [44] T. Y. Cao, “Conceptual developments of 20th-century field theories”, Second edition. Cambridge, United Kingdom; New York, NY: Cambridge University Press, 2019.
- [45] S. W. Herb et al., “Observation of a Dimuon Resonance at 9.5 GeV in 400-GeV Proton-Nucleus Collisions”, Phys. Rev. Lett., vol. 39, no. 5, pp. 252–255, Aug. 1977, DOI: [10.1103/PhysRevLett.39.252](https://doi.org/10.1103/PhysRevLett.39.252).
- [46] J. Yoh, “The discovery of the b quark at Fermilab in 1977: The experiment coordinator’s story”, Chicago, IL (USA), 1998, pp. 29–42, DOI: [10.1063/1.55114](https://doi.org/10.1063/1.55114).
- [47] V. M. Abazov et al., “Evidence for production of single top quarks”, Phys. Rev. D, vol. 78, no. 1, p. 012005, Jul. 2008, DOI: [10.1103/PhysRevD.78.012005](https://doi.org/10.1103/PhysRevD.78.012005).
- [48] F. Abe et al., “Observation of Top Quark Production in  $p\bar{p}$  Collisions with the Collider Detector at Fermilab”, Phys. Rev. Lett., vol. 74, no. 14, pp. 2626–2631, Apr. 1995, DOI: [10.1103/PhysRevLett.74.2626](https://doi.org/10.1103/PhysRevLett.74.2626).
- [49] S. Abachi et al., “Observation of the Top Quark”, Phys. Rev. Lett., vol. 74, no. 14, pp. 2632–2637, Apr. 1995, DOI: [10.1103/PhysRevLett.74.2632](https://doi.org/10.1103/PhysRevLett.74.2632).
- [50] F. J. Dyson, “The S Matrix in Quantum Electrodynamics”, Phys. Rev., vol. 75, no. 11, pp. 1736–1755, Jun. 1949, DOI: [10.1103/PhysRev.75.1736](https://doi.org/10.1103/PhysRev.75.1736).
- [51] F. J. Dyson, “The Radiation Theories of Tomonaga, Schwinger, and Feynman,” Phys. Rev., vol. 75, no. 3, pp. 486–502, Feb. 1949, DOI: [10.1103/PhysRev.75.486](https://doi.org/10.1103/PhysRev.75.486).

- [52] J. Schwinger, "On Quantum-Electrodynamics and the Magnetic Moment of the Electron", Phys. Rev., vol. 73, no. 4, pp. 416–417, Feb. 1948, DOI: [10.1103/PhysRev.73.416](https://doi.org/10.1103/PhysRev.73.416).
- [53] J. Schwinger, "Quantum Electrodynamics. I. A Covariant Formulation," Phys. Rev., vol. 74, no. 10, pp. 1439–1461, Nov. 1948, DOI: [10.1103/PhysRev.74.1439](https://doi.org/10.1103/PhysRev.74.1439).
- [54] R. P. Feynman, "Mathematical Formulation of the Quantum Theory of Electromagnetic Interaction," Phys. Rev., vol. 80, no. 3, pp. 440–457, Nov. 1950, DOI: [10.1103/PhysRev.80.440](https://doi.org/10.1103/PhysRev.80.440).
- [55] R. P. Feynman, "Space-Time Approach to Quantum Electrodynamics," Phys. Rev., vol. 76, no. 6, pp. 769–789, Sep. 1949, DOI: [10.1103/PhysRev.76.769](https://doi.org/10.1103/PhysRev.76.769).
- [56] R. P. Feynman, "The Theory of Positrons", Phys. Rev., vol. 76, no. 6, pp. 749–759, Sep. 1949, DOI: [10.1103/PhysRev.76.749](https://doi.org/10.1103/PhysRev.76.749).
- [57] S. Tomonaga, "On a Relativistically Invariant Formulation of the Quantum Theory of Wave Fields", Prog. Theor. Phys., vol. 1, no. 2, pp. 27–42, Aug. 1946, DOI: [10.1143/PTP.1.27](https://doi.org/10.1143/PTP.1.27).
- [58] V. Mathieu, N. Kochelev, and V. Vento, "The Physics of Glueballs", Int. J. Mod. Phys. E, vol. 18, no. 01, pp. 1–49, Jan. 2009, DOI: [10.1142/S0218301309012124](https://doi.org/10.1142/S0218301309012124).
- [59] S. Aid et al., "A study of the fragmentation of quarks in e t- p collisions at HERA," Nucl. Phys. B, vol. 445, no. 1, pp. 3–21, Jul. 1995, DOI: [10.1016/0550-3213\(95\)91599-H](https://doi.org/10.1016/0550-3213(95)91599-H).
- [60] E. H. Saidi, "Introduction to the Standard Model of Electro-Weak Interactions," LPHE-MS, Faculty of Sciences, Mohamed V University, Rabat, Morocco, 2017.
- [61] D. J. Antrim, "Sweet Little Nothings; or, Searching for a Pair of Stops, a Pair of Higgs Bosons, and a Pair of New Small Wheels for the Upgrade of the Forward Muon System of the ATLAS Detector at CERN," 2019, Accessed: Oct. 13, 2020. [Online]. Available: <https://inspirehep.net/literature/1791945>.
- [62] M. A. Loualidi, "Introduction au Modèle Standard Minimal", 2020.
- [63] M. A. Loualidi, "Contribution à l'étude de masses et mélange des neutrinos au-delà de modèle standard avec symétries de familles," Faculty of Sciences, Mohammed V University, Rabat, Morocco, 2018.
- [64] J. Woithe, G. J. Wiener, and F. F. V. der Veken, "Let's have a coffee with the Standard Model of particle physics", Phys. Educ., vol. 52, no. 3, p. 034001, Mar. 2017, DOI: [10.1088/1361-6552/aa5b25](https://doi.org/10.1088/1361-6552/aa5b25).
- [65] S. Weinberg, The quantum theory of fields. Cambridge; New York: Cambridge University Press, 1995.
- [66] E. W. Weisstein, "Einstein Summation." <https://mathworld.wolfram.com/EinsteinSummation.html> (accessed Oct. 13, 2020).
- [67] M. A. Loualidi and M. Miskaoui, "One-loop Type II Seesaw Neutrino Model with Stable Dark Matter Candidates", ArXiv E-Prints, vol. 2003, p. arXiv:2003.11434, Mar. 2020, Accessed: Oct. 13, 2020. [Online]. Available: <http://adsabs.harvard.edu/abs/2020arXiv200311434L>.
- [68] A. D. Sakharov, "Violation of CP invariance, C asymmetry, and baryon asymmetry of the universe", Sov. Phys. Uspekhi, vol. 34, no. 5, pp. 392–393, May 1991, DOI: [10.1070/PU1991v03n05ABEH002497](https://doi.org/10.1070/PU1991v03n05ABEH002497).
- [69] F. Cain, "Are there antimatter galaxies?", Universe Today, <https://phys.org/news/2016-06-antimatter-galaxies.html> (accessed Oct. 13, 2020).

- [70] F. Jegerlehner, "The Hierarchy Problem and the Cosmological Constant Problem Revisited", Found. Phys., vol. 49, no. 9, pp. 915–971, Sep. 2019, DOI: [10.1007/s10701-019-00262-2](https://doi.org/10.1007/s10701-019-00262-2).
- [71] V. Trimble, "Existence and Nature of Dark Matter in the Universe", Annu. Rev. Astron. Astrophys., vol. 25, no. 1, pp. 425–472, Sep. 1987, DOI: [10.1146/annurev.aa.25.090187.002233](https://doi.org/10.1146/annurev.aa.25.090187.002233).
- [72] Planck Collaboration et al., "Planck 2013 results. I. Overview of products and scientific results", Astron. Astrophys., vol. 571, p. A1, Nov. 2014, DOI: [10.1051/0004-6361/201321529](https://doi.org/10.1051/0004-6361/201321529).
- [73] G. G. Ross, Grand unified theories. Menlo Park: Benjamin/Cummings Publ. Co., 1984.
- [74] D. Rickles, A Brief History of String Theory: From Dual Models to M-Theory. Berlin Heidelberg: Springer-Verlag, 2014.
- [75] David London and Jonathan L. Rosner, "Extra gauge bosons in  $E_6$ ", Phys. Rev. Part. Fields, vol. 34, no. 5, pp. 1530–1546, Sep. 1986, v: [10.1103/physrevd.34.1530](https://doi.org/10.1103/physrevd.34.1530).
- [76] H. Georgi and S. L. Glashow, "Unity of All Elementary-Particle Forces", Phys. Rev. Lett., vol. 32, no. 8, pp. 438–441, Feb. 1974, DOI: [10.1103/PhysRevLett.32.438](https://doi.org/10.1103/PhysRevLett.32.438).
- [77] R. W. Robinett and J. L. Rosner, "Minimally extended electroweak gauge theories in  $SO(10)$  and  $E_6$ ", AIP Conf. Proc., vol. 99, no. 1, pp. 193–201, Jun. 1983, DOI: [10.1063/1.34010](https://doi.org/10.1063/1.34010).
- [78] T. Fukuyama, A. Ilakovac, T. Kikuchi, S. Meljanac, and N. Okada, " $SO(10)$  Group Theory for the Unified Model Building", J. Math. Phys., vol. 46, no. 3, p. 033505, Mar. 2005, DOI: [10.1063/1.1847709](https://doi.org/10.1063/1.1847709).
- [79] W. Grimus, "Introduction to left-right symmetric models", Apr. 1993, Accessed: Nov. 16, 2020. [Online]. Available: <https://inspirehep.net/literature/353567>.
- [80] N. A. Asbah, "Search for the Production of a Standard Model Higgs Boson in Association with Top-Quarks and Decaying into a Pair of Bottom-Quarks with 13 TeV ATLAS Data.", 2018. Accessed: Oct. 13, 2020. [Online]. Available: <https://cds.cern.ch/record/2320703/?ln=en>.
- [81] A. C. Henrichs, Top Quark Pair Production. Cham: Springer International Publishing, 2014.
- [82] B. Peter, "Top Quark Pair Production at the LHC", thesis, der RWTH Aachen University, 2012.
- [83] P. Nason, S. Dawson, and R. K. Ellis, "The total cross-section for the production of heavy quarks in hadronic collisions," Nucl. Phys. B, vol. 303, no. 4, pp. 607–633, Jul. 1988, DOI: [10.1016/0550-3213\(88\)90422-1](https://doi.org/10.1016/0550-3213(88)90422-1).
- [84] S. Moch and P. Uwer, "Theoretical status and prospects for top-quark pair production at hadron colliders", Phys. Rev. D, vol. 78, no. 3, p. 034003, Aug. 2008, DOI: [10.1103/PhysRevD.78.034003](https://doi.org/10.1103/PhysRevD.78.034003).
- [85] U. Langenfeld, S. Moch, and P. Uwer, "New results for  $t\bar{t}$  production at hadron colliders", ArXiv09072527 Hep-Ph, Jul. 2009, Accessed: Oct. 21, 2020. [Online]. Available: <http://arxiv.org/abs/0907.2527>.
- [86] N. Kidonakis, "Next-to-next-to-leading soft-gluon corrections for the top quark cross section and transverse momentum distribution", Phys. Rev. D, vol. 82, no. 11, p. 114030, Dec. 2010, DOI: [10.1103/PhysRevD.82.114030](https://doi.org/10.1103/PhysRevD.82.114030).
- [87] V. Ahrens, A. Ferroglio, M. Neubert, B. D. Pecjak, and L. L. Yang, "Precision predictions for the  $t\bar{t}$  production cross-section at hadron colliders", Phys. Lett. B, vol. 703, no. 2, pp. 135–141, Sep. 2011, DOI: [10.1016/j.physletb.2011.07.058](https://doi.org/10.1016/j.physletb.2011.07.058).
- [88] M. Beneke, P. Falgari, S. Klein, and C. Schwinn, "Hadronic top-quark pair production with NNLL threshold resummation", Nucl. Phys. B, vol. 855, no. 3, pp. 695–741, Feb. 2012, DOI: [10.1016/j.nuclphysb.2011.10.021](https://doi.org/10.1016/j.nuclphysb.2011.10.021).

- [89] M. Cacciari, M. Czakon, M. L. Mangano, A. Mitov, and P. Nason, “Top-pair production at hadron colliders with next-to-next-to-leading logarithmic soft-gluon resummation”, Phys. Lett. B, vol. 710, no. 4–5, pp. 612–622, Apr. 2012, [DOI: 10.1016/j.physletb.2012.03.013](#).
- [90] CDF Collaboration, “Measurement of the  $t\bar{t}$  production cross-section in  $p\bar{p}$  collisions at  $\sqrt{s} = 1.8$  TeV”, Phys. Rev. D, vol. 67, no. 11, p. 119901, Jun. 2003, [DOI: 10.1103/PhysRevD.67.119901](#).
- [91] DØ Collaboration, “ $t\bar{t}$  production cross-section in  $p\bar{p}$  collisions at  $\sqrt{s} = 1.8$  TeV”, Phys. Rev. D, vol. 67, no. 1, p. 012004, Jan. 2003, [DOI: 10.1103/PhysRevD.67.012004](#).
- [92] CDF Collaboration and DØ Collaboration, “Combination of measurements of the top-quark pair production cross-section from the Tevatron Collider”, Phys. Rev. D, vol. 89, no. 7, p. 072001, Apr. 2014, [DOI: 10.1103/PhysRevD.89.072001](#).
- [93] CDF Collaboration, “Measurement of the top-quark pair production cross-section in events with two leptons and bottom-quark jets using the full CDF data set”, Phys. Rev. D, vol. 88, no. 9, p. 091103, Nov. 2013, [DOI: 10.1103/PhysRevD.88.091103](#).
- [94] DØ Collaboration, “Measurement of the inclusive  $t\bar{t}$  production cross-section in  $p\bar{p}$  collisions at  $\sqrt{s} = 1.96$  TeV and determination of the top quark pole mass,” Phys. Rev. D, vol. 94, no. 9, p. 092004, Nov. 2016, [DOI: 10.1103/PhysRevD.94.092004](#).
- [95] CMS Collaboration, “Measurement of the  $t\bar{t}$  production cross-section, the top quark mass, and the strong coupling constant using dilepton events in pp collisions at  $\sqrt{s} = 13$  TeV”, Eur. Phys. J. C, vol. 79, no. 5, p. 368, May 2019, [DOI: 10.1140/epjc/s10052-019-6863-8](#).
- [96] ATLAS Collaboration, “Measurement of the  $t\bar{t}$  production cross-section using  $e\mu$  events with b-tagged jets in pp collisions at  $\sqrt{s} = 13$  TeV with the ATLAS detector”, Phys. Lett. B, vol. 772, p. 879, Sep. 2017, [DOI: 10.1016/j.physletb.2017.09.027](#).
- [97] CMS Collaboration, “Measurement of the  $t\bar{t}$  production cross-section in the dilepton channel in pp collisions at  $\sqrt{s} = 8$  TeV”, J. High Energy Phys., vol. 2014, no. 2, p. 24, Feb. 2014, [DOI: 10.1007/JHEP02\(2014\)024](#).
- [98] ATLAS Collaboration, “Measurement of the  $t\bar{t}$  production cross-section using  $e\mu$  events with b-tagged jets in pp collisions at  $\sqrt{s} = 7$  and 8 TeV with the ATLAS detector”, Eur. Phys. J. C, vol. 76, no. 11, p. 642, Nov. 2016, [DOI: 10.1140/epjc/s10052-016-4501-2](#).
- [99] LHCb collaboration et al., “First observation of top quark production in the forward region”, Phys. Rev. Lett., vol. 115, no. 11, p. 112001, Sep. 2015, [DOI: 10.1103/PhysRevLett.115.112001](#).
- [100] M. Czakon, P. Fiedler, and A. Mitov, “The total top quark pair production cross-section at hadron colliders through  $\mathcal{O}(\alpha_s^4)$ ”, Phys. Rev. Lett., vol. 110, no. 25, p. 252004, Jun. 2013, [DOI: 10.1103/PhysRevLett.110.252004](#).
- [101] P. D. Group et al., “Review of Particle Physics”, Prog. Theor. Exp. Phys., vol. 2020, no. 8, Aug. 2020, [doi: 10.1093/ptep/ptaa104](#).
- [102] ATLAS Collaboration, “Evidence for  $t\bar{t}t\bar{t}$  production in the multilepton final state in proton-proton collisions at  $\sqrt{s} = 13$  TeV with the ATLAS detector,” ArXiv200714858 Hep-Ex, Jul. 2020, Accessed: Oct. 20, 2020. [Online]. Available: <http://arxiv.org/abs/2007.14858>.
- [103] R. Frederix, D. Pagani, and M. Zaro, “Large NLO corrections in  $t\bar{t}W^\pm$  and  $t\bar{t}t\bar{t}$  hadroproduction from supposedly subleading EW contributions”, J. High Energy Phys., vol. 2018, no. 2, p. 31, Feb. 2018, [DOI: 10.1007/JHEP02\(2018\)031](#).
- [104] ATLAS Collaboration, “ATLAS finds evidence of spectacular four-top quark production”, *ATLAS Experiment at CERN*, May 26, 2020. <https://atlas.cern/uploads/physics-briefing/evidence-four-top-quark-production> (accessed Oct. 21, 2020).

- [105] G. C. Branco, P. M. Ferreira, L. Lavoura, M. N. Rebelo, M. Sher, and J. P. Silva, “Theory and phenomenology of two-Higgs-doublet models”, Phys. Rep., vol. 516, no. 1–2, pp. 1–102, Jul. 2012, DOI: [10.1016/j.physrep.2012.02.002](https://doi.org/10.1016/j.physrep.2012.02.002).
- [106] S. Gori, I.-W. Kim, N. R. Shah, and K. M. Zurek, “Closing the Wedge: Search Strategies for Extended Higgs Sectors with Heavy Flavor Final States”, Phys. Rev. D, vol. 93, no. 7, p. 075038, Apr. 2016, DOI: [10.1103/PhysRevD.93.075038](https://doi.org/10.1103/PhysRevD.93.075038).
- [107] P. S. Bhupal Dev and A. Pilaftsis, “Maximally symmetric two Higgs doublet model with natural standard model alignment”, J. High Energy Phys., vol. 2015, no. 11, p. 147, Nov. 2015, DOI: [10.1007/JHEP11\(2015\)147](https://doi.org/10.1007/JHEP11(2015)147).
- [108] R. N. Mohapatra and J. C. Pati, “A Natural Left-Right Symmetry”, Phys. Rev. D, vol. 11, p. 2558, 1975, DOI: [10.1103/PhysRevD.11.2558](https://doi.org/10.1103/PhysRevD.11.2558).
- [109] J. H. Kim, K. Kong, S. J. Lee, and G. Mohlabeng, “Probing TeV scale Top-Philic Resonances with Boosted Top-Tagging at the High Luminosity LHC”, Phys. Rev. D, vol. 94, no. 3, p. 035023, Aug. 2016, DOI: [10.1103/PhysRevD.94.035023](https://doi.org/10.1103/PhysRevD.94.035023).
- [110] Z.-L. Guo, B.-C. Li, and H.-W. Dong, “Transverse momentum and pseudorapidity dependence of particle production in Xe-Xe collision at 5.44 TeV”, ArXiv190603920 Hep-Ph Physicsnucl-Th, Jun. 2019, Accessed: Oct. 25, 2020. [Online]. Available: <http://arxiv.org/abs/1906.03920>.
- [111] F. Deliot, N. Hadley, S. Parke, and T. Schwarz, “Properties of the Top Quark”, Annu. Rev. Nucl. Part. Sci., vol. 64, no. 1, pp. 363–381, Oct. 2014, DOI: [10.1146/annurev-nucl-102313-025655](https://doi.org/10.1146/annurev-nucl-102313-025655).
- [112] T. A. Collaboration et al., “The ATLAS Experiment at the CERN Large Hadron Collider”, J. Instrum., vol. 3, no. 08, pp. S08003–S08003, Aug. 2008, DOI: [10.1088/1748-0221/3/08/S08003](https://doi.org/10.1088/1748-0221/3/08/S08003).
- [113] T. C. Collaboration et al., “The CMS experiment at the CERN LHC”, J. Instrum., vol. 3, no. 08, pp. S08004–S08004, Aug. 2008, DOI: [10.1088/1748-0221/3/08/S08004](https://doi.org/10.1088/1748-0221/3/08/S08004).
- [114] T. A. Collaboration et al., “The ALICE experiment at the CERN LHC”, J. Instrum., vol. 3, no. 08, pp. S08002–S08002, Aug. 2008, DOI: [10.1088/1748-0221/3/08/S08002](https://doi.org/10.1088/1748-0221/3/08/S08002).
- [115] T. Lhc. Collaboration et al., “The LHCb Detector at the LHC”, J. Instrum., vol. 3, no. 08, pp. S08005–S08005, Aug. 2008, DOI: [10.1088/1748-0221/3/08/S08005](https://doi.org/10.1088/1748-0221/3/08/S08005).
- [116] T. Lhc. Collaboration et al., “The LHCf detector at the CERN Large Hadron Collider”, J. Instrum., vol. 3, no. 08, pp. S08006–S08006, Aug. 2008, DOI: [10.1088/1748-0221/3/08/S08006](https://doi.org/10.1088/1748-0221/3/08/S08006).
- [117] T. T. Collaboration et al., “The TOTEM Experiment at the CERN Large Hadron Collider”, J. Instrum., vol. 3, no. 08, pp. S08007–S08007, Aug. 2008, DOI: [10.1088/1748-0221/3/08/S08007](https://doi.org/10.1088/1748-0221/3/08/S08007).
- [118] V. A. M. and, “The MoEDAL experiment at the LHC: status and results”, J. Phys. Conf. Ser., vol. 873, p. 012010, Jul. 2017, DOI: [10.1088/1742-6596/873/1/012010](https://doi.org/10.1088/1742-6596/873/1/012010).
- [119] P. Abbon et al., “The COMPASS experiment at CERN”, Nucl. Instrum. Methods Phys. Res. Sect. Accel. Spectrometers Detect. Assoc. Equip., vol. 577, no. 3, pp. 455–518, Jul. 2007, DOI: [10.1016/j.nima.2007.03.026](https://doi.org/10.1016/j.nima.2007.03.026).
- [120] F. G. and, “The NA62 experiment at CERN”, J. Phys. Conf. Ser., vol. 873, p. 012015, Jul. 2017, DOI: [10.1088/1742-6596/873/1/012015](https://doi.org/10.1088/1742-6596/873/1/012015).
- [121] “The NA61/SHINE Collaboration”, J. Phys. G Nucl. Part. Phys., vol. 36, no. 6, p. 069807, May 2009, DOI: [10.1088/0954-3899/36/6/069807](https://doi.org/10.1088/0954-3899/36/6/069807).
- [122] F. Stagni, A. Tsaregorodtsev, L. Arrabito, A. Sailer, T. Hara, and X. Z. and, “DIRAC in Large Particle Physics Experiments,” J. Phys. Conf. Ser., vol. 898, p. 092020, Oct. 2017, DOI: [10.1088/1742-6596/898/9/092020](https://doi.org/10.1088/1742-6596/898/9/092020).

- [123] I. C. Tietje, "Low-energy antimatter experiments at the antiproton decelerator at CERN: Testing CPT invariance and the WEP", *J. Phys. Conf. Ser.*, vol. 1071, p. 012021, Aug. 2018, [DOI: 10.1088/1742-6596/1071/1/012021](#).
- [124] R. Catherall et al., "The ISOLDE facility", *J. Phys. G Nucl. Part. Phys.*, vol. 44, no. 9, p. 094002, Aug. 2017, [DOI: 10.1088/1361-6471/aa7eba](#).
- [125] E. Chiaveri et al., "The CERN n-TOF Facility: Neutron Beams Performances for Cross Section Measurements", *Nucl. Data Sheets*, vol. 119, pp. 1–4, May 2014, [DOI: 10.1016/j.nds.2014.08.003](#).
- [126] J. Casaus, "The AMS-02 experiment on the ISS", *J. Phys. Conf. Ser.*, vol. 171, p. 012045, Jun. 2009, [DOI: 10.1088/1742-6596/171/1/012045](#).
- [127] L. Evans and P. Bryant, "LHC Machine", *J. Instrum.*, vol. 3, no. 08, pp. S08001–S08001, Aug. 2008, [DOI: 10.1088/1748-0221/3/08/S08001](#).
- [128] K. Jakobs, "CERN and the ATLAS Experiment", p. 58, 2020.
- [129] H. Werner and M. Bruno, "Concept of luminosity", CERN, 2007.
- [130] A. T. Abouelfadl, "Measurements of Higgs boson production cross sections in the diphoton channel with the full ATLAS Run-2 data and constraints on anomalous Higgs boson interactions", p. 276.
- [131] M. Aaboud et al., "Performance of the ATLAS track reconstruction algorithms in dense environments in LHC Run 2," *Eur. Phys. J. C*, vol. 77, no. 10, p. 673, Oct. 2017, [DOI: 10.1140/epjc/s10052-017-5225-7](#).
- [132] Thesis Images, "magnetSystems.png (1824x1224)", <http://www.jetgoodson.com/images/thesisImages/magnetSystems.png> (accessed Oct. 19, 2020).
- [133] The ATLAS collaboration, "ATLAS Collaboration, Early Inner Detector Tracking Performance in the 2015 data at  $\sqrt{s} = 13$  TeV", Tech Rep ATL-PHYS-PUB-2015-051 CERN Geneva Dec 2015, 2015, [Online]. Available: <https://cds.cern.ch/record/2110140>.
- [134] T. Cornelissen, M. Elsing, S. Fleischmann, W. Liebig, E. Moyse, and A. Salzburger, "Concepts, Design and Implementation of the ATLAS New Tracking (NEWT)", Oct. 2012, Accessed: Nov. 01, 2020. [Online]. Available: <https://inspirehep.net/literature/1197243>.
- [135] "The Optimization of ATLAS Track Reconstruction in Dense Environments," May 2020, Accessed: Nov. 01, 2020. [Online]. Available: <https://inspirehep.net/literature/1795379>.
- [136] G. Piacquadio, K. Prokofiev, and A. Wildauer, "Primary vertex reconstruction in the ATLAS experiment at LHC", *J. Phys. Conf. Ser.*, vol. 119, no. 3, p. 032033, Jul. 2008, [DOI: 10.1088/1742-6596/119/3/032033](#).
- [137] Z. A. Meadows, "A Search for New Resonances Decaying into a Weak Vector Boson and a Higgs Boson in Hadronic Final States with the ATLAS Detector at the Large Hadron Collider", p. 209.
- [138] "Vertex Reconstruction Performance of the ATLAS Detector at  $\sqrt{s} = 13$  TeV", May 2020, Accessed: Nov. 02, 2020. [Online]. Available: <https://inspirehep.net/literature/1795362>.
- [139] ATLAS Experiment, public results, "ATLAS Stand-Alone Event Display, Atlas Public, TWiki" <https://twiki.cern.ch/twiki/bin/view/AtlasPublic/EventDisplayStandAlone> (accessed Nov. 02, 2020).
- [140] ATLAS Collaboration, "Performance of the ATLAS Inner Detector Track and Vertex Reconstruction in the High Pile-Up LHC Environment", Nov. 2012, Accessed: Nov. 02, 2020. [Online]. Available: <https://inspirehep.net/literature/1204277>.

- [141] ATLAS Collaboration, “Electron and photon performance measurements with the ATLAS detector using the 2015-2017 LHC proton-proton collision data”, J. Instrum., vol. 14, no. 12, pp. P12006–P12006, Dec. 2019, [DOI: 10.1088/1748-0221/14/12/P12006](https://doi.org/10.1088/1748-0221/14/12/P12006).
- [142] ATLAS Collaboration, “Muon reconstruction performance of the ATLAS detector in proton-proton collision data at  $\sqrt{s} = 13$  TeV”, Eur. Phys. J. C, vol. 76, no. 5, p. 292, May 2016, [DOI: 10.1140/epjc/s10052-016-4120-y](https://doi.org/10.1140/epjc/s10052-016-4120-y).
- [143] ATLAS Collaboration, “Search for high-mass dilepton resonances in  $pp$  collisions at  $\sqrt{s} = 8$  TeV with the ATLAS detector”, Phys. Rev. D, vol. 90, no. 5, p. 052005, Sep. 2014, [DOI: 10.1103/PhysRevD.90.052005](https://doi.org/10.1103/PhysRevD.90.052005).
- [144] ATLAS Collaboration, “Search for new particles in events with one lepton and missing transverse momentum in  $pp$  collisions at  $\sqrt{s} = 8$  TeV with the ATLAS detector”, J. High Energy Phys., vol. 2014, no. 9, p. 37, Sep. 2014, [DOI: 10.1007/JHEP09\(2014\)037](https://doi.org/10.1007/JHEP09(2014)037).
- [145] G. Aad et al., “Topological cell clustering in the ATLAS calorimeters and its performance in LHC Run 1”, Eur. Phys. J. C, vol. 77, no. 7, p. 490, Jul. 2017, [DOI: 10.1140/epjc/s10052-017-5004-5](https://doi.org/10.1140/epjc/s10052-017-5004-5).
- [146] ATLAS Collaboration, “Performance of pile-up mitigation techniques for jets in  $pp$  collisions at  $\sqrt{s} = 8$  TeV using the ATLAS detector”, Eur. Phys. J. C, vol. 76, no. 11, p. 581, Nov. 2016, [DOI: 10.1140/epjc/s10052-016-4395-z](https://doi.org/10.1140/epjc/s10052-016-4395-z).
- [147] W. Balunas, “A Search for Nothing: Dark Matter and Invisible Decays of the Higgs Boson at the ATLAS Detector”, p. 159.
- [148] M. Cacciari, G. P. Salam, and G. Soyez, “The anti- $k_t$  jet clustering algorithm”, J. High Energy Phys., vol. 2008, no. 04, pp. 063–063, Apr. 2008, [DOI: 10.1088/1126-6708/2008/04/063](https://doi.org/10.1088/1126-6708/2008/04/063).
- [149] ATLAS Collaboration, “Performance of the ATLAS Secondary Vertex b-tagging Algorithm in 900 GeV Collision Data”, Nov. 2012, Accessed: Nov. 09, 2020. [Online]. Available: <https://inspirehep.net/literature/1203985>.
- [150] ATLAS Collaboration, “Commissioning of the ATLAS high-performance b-tagging algorithms in the 7 TeV collision data”, Nov. 2012, Accessed: Nov. 09, 2020. [Online]. Available: <https://inspirehep.net/literature/1204180>.
- [151] G. Piacquadio and C. Weiser, “A new inclusive secondary vertex algorithm for b-jet tagging in ATLAS”, J. Phys. Conf. Ser., vol. 119, no. 3, p. 032032, Jul. 2008, [DOI: 10.1088/1742-6596/119/3/032032](https://doi.org/10.1088/1742-6596/119/3/032032).
- [152] ATLAS Collaboration, “Optimisation of the ATLAS  $b$ -tagging performance for the 2016 LHC Run”, INSPIRE, <https://inspirehep.net/literature/1795335> (accessed Nov. 09, 2020).
- [153] ATLAS Protected, “TopxAODStartGuideR21, Atlas Protected”, TWiki. [https://twiki.cern.ch/twiki/bin/view/AtlasProtected/TopxAODStartGuideR21#5.4.Object\\_selection](https://twiki.cern.ch/twiki/bin/view/AtlasProtected/TopxAODStartGuideR21#5.4.Object_selection) (accessed Nov. 12, 2020).
- [154] ATLAS Athena, “ConfigurationSettings.cxx”, GitLab. <https://gitlab.cern.ch/atlas/athena/blob/21.2/PhysicsAnalysis/TopPhys/xAOD/TopConfiguration/Root/ConfigurationSettings.cxx> (accessed Nov. 12, 2020).
- [155] ATLAS Experiment, “ATLAS Metadata Interface”, <https://ami.in2p3.fr/app/?subapp=tagsShow> (accessed Nov. 12, 2020).